2012

Evaluation of bridge component design and construction techniques: A look at integral abutment bridge precast approach slabs and post grouted drilled shafts

Anna Marie Nadermann
Iowa State University

Evaluation of bridge component design and construction techniques: A look at integral abutment bridge precast approach slabs and post grouted drilled shafts

by

Anna M. Nadermann

A thesis submitted to the graduate faculty

In partial fulfillment of the requirements for the degree of

MASTER OF SCIENCE

Major: Civil Engineering (Structural Engineering)

Program of Study Committee:
Jeramy C. Ashlock, Co-major Professor
Brent M. Phares, Co-major Professor
Jennifer Shane

Iowa State University

Ames, Iowa

2012

This work is dedicated to

my parents, Charles and Nola

TABLE OF CONTENTS

LIST OF TABLES

LIST OF FIGURES

LIST OF SYMBOLS

Symbol	Description	Unit
a	Constant	—
A	Sample cross-section area	in
b	Constant	—
d_{85}	Grout parameter, diameter corresponding to 85% finer by mass	mm
d_{90}	Grout parameter, diameter corresponding to 90% finer by mass	mm
d_{95}	Grout parameter, diameter corresponding to 95% finer by mass	mm
D_{10}	Soil parameter, diameter corresponding to 10% finer by mass	mm
D_{15}	Soil parameter, diameter corresponding to 15% finer by mass	mm
D	Drilled shaft diameter	in
D_b	Drilled shaft base diameter	in
D_i	Drilled shaft diameter corresponding to ith level	in
D_r	Relative Density	%
E	Young's modulas	ksi
FC	Fines content	%
F_r	Reduction factor	—
GPI	Grouting pressure index	—
GP_{max}	Maximum grouting pressure	psi
K	Constant	—
k	Stiffness	kips/in
k_1, k_2	Regression coefficients	—
L_i	Length of ith section of drilled shaft	ft
N	SPT blow count	—
N_c	Corrected SPT blow count	—
N_g	Groutability index	—
$q_{grouted}$	Grouted unit end bearing resistance	tsf
q_p	Unit end bearing resistance	tsf
q_{pr}	Reduced unit end bearing resistance	tsf
q_s	Unit side shear resistance	tsf

q_{si}	Unit side shear resistance at the ith level	tsf
Q_p	Ultimate end bearing resistance	kip
$Q_{p\text{-}grouted}$	Grouted ultimate end bearing resistance	kip
Q_s	Ultimate side shear resistance	kip
P	Applied load at surface	kip
ΔP	Incremental load	kip
S_u	Undrained shear strength of cohesive soil	tsf
TCM	Tip capacity multiplier	—
w/c	Water-to-cement ratio of grout	%
z	Depth below ground surface	ft
α	Adhesion factor	—
β	Skin friction coefficient	—
Δε	Incremental strain	in/in
σ'_{vo}	Overburden stress	tsf
ϕ	Soil friction angle	°
SPT	Standard penetration test	—
CPT	Cone penetration test	—
AASHTO	American Association of State Highway and Transportation Officials	—
LRFD	Load and resistance factor design	—
ASD	Allowable stress design	—

ABSTRACT

The bump at the end of the bridge and the high cost of deep embedded drilled shafts have long been recognized by many bridge owners. This research aims to mediate the bump at the end of the bridge and to validate the use of post grouting to increase drilled shaft capacity. Performance monitoring and full scale test programs were used to evaluate these technical issues.

The bump at the end of the bridge is typically due to settlement of the approach soils and cracking of the approach pavements. The settlement and cracking in integral abutment bridges are typically dealt with by connecting the approach slab to the integral abutment bridge. Two integral abutment bridges with integrally connected precast approach slabs were evaluated using long-term monitoring systems to study their structural performance and determine the range of forces that should be considered when designing such approach slabs. This study has identified design and construction considerations for integrally connected precast approach slabs. The approach slab study revealed the source and magnitude of forces to be considered in the design and construction of approach slabs integrally connected to integral abutment bridges. Consideration of these forces in the design and construction of such approach slabs could potentially lead to reduced maintenance costs associated with the bump at the end of the bridge.

The required deep embedment length of drilled shafts is due to the inability to fully mobilize the end bearing resistance of the shaft before reaching service displacement criteria. Post grouting of drilled shafts can be used to effectively increase the end bearing capacity within service displacement limits, often times allowing the drilled shaft to be shortened without sacrificing capacity. Through a load test program and long-term performance monitoring of production shafts, the increase in capacity and performance of post grouted drilled shafts were investigated. This study has identified design and construction considerations for post grouted drilled shafts. The post grouted drilled shaft study verified the use of post grouting as a technique for increasing the end bearing resistance of drilled shafts and also identified design and construction considerations for post grouted drilled shafts. Increasing the end bearing resistance of drilled shafts through the use of post grouting can

effectively allow the shafts to be shortened without losing capacity or exceeding service displacement criteria; potentially leading to reduced costs for bridge projects.

CHAPTER 1.

INTRODUCTION

This chapter presents the industry and technical problems addressed in these projects, the research goals and objectives, and a discussion of the significance of this research. The final section of this chapter describes the organization of this thesis.

INDUSTRY PROBLEMS

Following is a discussion of two problems which are experienced by many bridge owners and other users of deep foundations. The impact of these concerns is also discussed.

Industry Concerns

Integral Abutment Bridges – The Bump at the End of the Bridge

The bridge industry concern investigated in this research is the bump at the end of the bridge which is common to approach slab pavement at Integral Abutment (I-A) bridges. According to a study by Bigelow et al. (2008), this is a problem common to many bridge owners. Connecting approach slab pavements to I-A bridges is a technique used by many bridge owners to move the bump from the approach slab/abutment interface to the approach slab/mainline pavement interface. This research investigates the forces that are present in such a configuration which may contribute to bump forming.

Post Grouting of Drilled Shafts

In addition to investigating I-A bridge approach slabs, this research investigates the increase in the capacity of drilled shafts by the use of post grouting. Often times conditions such as vibration limits, lateral strength requirements, and scour require the use of drilled shafts rather than driven piles as an alternative for deep foundations. Although drilled shafts are typically considered to be a costly solution, post grouting is a technique used around the world to increase the cost effectiveness of drilled shafts.

Impact on industry

This research investigates techniques that can be used by bridge owners and other users of deep foundations to reduce costs. Although the bump at the end of the bridge is not a significant safety issue, it does present a costly maintenance issue and negative public

perception. The use of post grouting can potentially increase the capacity of drilled shafts, thereby enabling cost savings by the use of shorter drilled shafts.

TECHNICAL PROBLEM

The technical problems associated with the industry concerns previously discussed are discussed below.

Integral Abutment Bridges – The Bump at the End of the Bridge

According to Lenke (2006), the bump at the end of the bridge is typically attributed to settlement (and differential settlement) of backfill soil under the approach slab, deterioration of the corbel or paving notch, and joint design and maintenance. A common solution to these problems associated with I-A bridges is to attach the approach slab to the bridge abutment, effectively moving the expansion joint away from the approach slab/abutment interface and closer to the approach slab/mainline pavement interface where soil settlement is less of a concern and maintenance is presumably easier. This study investigates the forces that develop from this configuration and the effective design of this type of system.

Post Grouting of Drilled Shafts

Drilled shafts tipped in granular soil rely primarily on skin friction due to the large displacement generally required to fully mobilize the end bearing capacity. Typically, end bearing is not mobilized before service load displacement criteria are exceeded. Post grouting of drilled shafts is a mechanism used to pre-compact or compress the soil directly below the tip of a drilled shaft as a means of increasing the mobilized end bearing before displacement criteria are exceeded, this effectively increasing the ultimate capacity of a drilled shaft. The research presented herein aims to fill the gap of long-term performance monitoring of post grouted drilled shafts with the intent to better understand the effects of post grouting on test shafts loaded to failure as well as production shafts under service loads.

GOAL OF THE RESEARCH

The following are goals of the research presented herein:

1. Mediate the bump at the end of the bridge.
2. Validate the use of post grouting to increase drilled shaft capacity.

OBJECTIVES

Through performance monitoring and test programs, the technical problems associated with the bump at the end of the bridge and the general inability to rely on the end bearing capacity of drilled shafts tipped in granular soil were evaluated. Two integral abutment bridges with integrally connected approach slabs were evaluated with the use of long-term monitoring systems to study their structural performance and determine the range of forces that should be considered when designing such approach slabs. Through a load test program and long-term performance monitoring of production shafts, the increase in capacity and performance of post grouted drilled shafts were investigated.

SIGNIFICANCE OF THE RESEARCH

This research has the ability to reduce maintenance costs for bridge owners and reduce material costs for construction of deep foundations. Understanding the forces that develop in approach slabs tied to integral abutments can lead to approach slab designs that reduce or even eliminate the bump at the end of the bridge. For deep foundations, validating the increase in the capacity of post grouted drilled shafts over that of ungrouted drilled shafts and understanding the long-term performance of post grouted drilled shafts can lead to the use of shorter drilled shafts. Increasing the capacity of drilled shafts using post grouting can lead to the shortening of the drilled shafts which will reduce the cost of labor materials such as concrete and steel.

THESIS ORGANIZATION

This thesis includes three papers to be submitted for publication in scholarly journals. The chapters listed here follow this introduction chapter:

- Background: A review of relevant literature and previous research.
- Performance of Precast Approach Slabs Integral with Integral Abutment Bridges: An evaluation of the forces in approach slabs tied to I-A bridges.
- Forensic Investigation of a Load-Tested Post Grouted Drilled Shaft: An evaluation of a post grouted drilled shaft test program.
- Performance of Post Grouted Drilled Shafts: An evaluation of the influence of construction loads and service loads on post grouted drilled shafts.

- Conclusions: Research findings and benefits derived from those findings.

CHAPTER 1. WORKS CITED

Bigelow, J., Faris, A., Greimann, L., Phares, B. 2008. Instrumentation and Monitoring of Integral Bridge Abutment-to-Approach Slab Connection. IHRB Projects TR-530 & TR-539, Iowa DOT Projects 05-197 & 05-219. Ames, IA, Institute for Transportation.

Lenke, L. 2006. Settlement Issues – Bridge Approach Slabs (Final Report Phase 1). Transportation Engineering Research Program (TERP). Albuquerque, NM. Department of Civil Engineering.

Mullins, G., Dapp, S., Frederick, E. and Wagner, V., 2001. Post Grouting Drilled Shaft Tips, Phase I. Florida Department of Transportation, Report FDOT BC165 v1.

CHAPTER 2. BACKGROUND/LITERATURE REVEIW

This chapter presents two kinds of background for the project; a review of relevant literature and a summary of present practices. The purpose of this chapter is to provide an overview showing how this research relates to current theory and practice.

RELEVANT RESEARCH AND LITERATURE

Major Contributions to Integral Abutment Bridges

Traditionally, bridge structures have used components such as expansion joints, roller supports, and expansion bearings to accommodate movements related to thermal expansion and contraction strains, creep, and shrinkage. According to Kunin (1999), I-A bridges are becoming an increasingly popular alternative among bridge owners. I-A bridges are designed without expansion joints and designed for all supports to accommodate thermal, and other movements (Mistry 2005). There are many benefits derived from the use of I-A bridges (Kunin 1999) including:

- Lower cost (both initial construction costs and long-term maintenance costs)
- Decreased deterioration from de-icing chemicals and snowplows
- Decreased impact loads
- Improved ride quality
- Simplified construction, and
- Improved structural resistance to seismic events.

Although there are many benefits of I-A bridges, approach slab pavements at I-A bridges are susceptible to settlement and cracking, which according to Horvath (2000) is manifested as the “bump at the end of the bridge.” The bump at the end of the bridge does not present a significant safety problem but it is an expensive maintenance issue. Lenke (2006) attributes the formation of the bump to the following factors:

- settlement of backfill under the approach slab,
- deterioration of the corbel or paving notch,
- joint design, and
- lack of joint maintenance.

It is believed that the joint design of I-A bridges may worsen the bump, and a common solution is to attach the approach slab to the bridge abutment. Attaching the approach slab to the bridge abutment moves the expansion joint from the approach slab/abutment interface to a position closer to the approach slab/mainline pavement interface. Soil settlement is less of a concern near the approach slab/mainline pavement interface and maintenance is presumed to be easier at the location as well.

Present Practice for Integral Abutment Bridges

Based on a review of literature including surveys of bridge owners, the present practice in most of the United States, areas in Canada, and parts of Europe, is to connect the approach slab to integral abutment bridges. According to a study by Bigelow et al. (2008), use of this configuration moved the bump from the end of the bridge to the pavement end of the approach slab. However, cracking at the bridge end of the approach slab was reported with the use of a horizontal connection, rather than a diagonal connection.

Major Contributions to Post Grouted Drilled Shafts

This section contains a brief background on drilled shafts, an overview on drilled shaft design capacity, a background on post grouted drilled shafts and the components of post grouting, and an overview of drilled shaft design capacity.

Drilled Shafts Background

Drilled shafts have evolved from a specialty foundation for situations where vibrations could not be tolerated or where shallow foundations were insufficient, to more widely used foundations due to the requirements for increased lateral strength of bridge foundations (Mullins et al. 2006). Foundations for water crossing bridges are also impacted by scour, which requires an increased depth for pile foundations whereas drilled shaft length is minimally affected by scour.

To insure a structurally sound shaft, the stability of the excavation must be maintained prior to and during placement of the concrete. The method of construction as well as the properties of the concrete can affect the capacity of the shaft. The various methods of construction adopted to address site-specific conditions include the following:

- Dry vs. wet construction,

- Cased vs. uncased shaft construction
- Tremie placed or free-fall placed concrete.

Inherently stable soil formations such as stiff clay or rock without ground water are needed to perform dry construction. Wet construction should be used when groundwater is present and likely to enter the excavation. Wet construction involves the use of a slurry or drilling mud in the excavation to maintain pressure on the walls o the excavation. Mineral, synthetic, and natural slurry types can be used for wet construction. The length of time the slurry is left in the excavation as well as the slurry type can affect the capacity of the shaft.

A relatively thin-walled steel pipe casing, can also be used to maintain stability of the excavation walls. Casing is intended to be used when slurries are ineffective, or when the top elevation of the shaft must be higher than the surface of free standing bodies of water. Casings can be driven, vibrated, jetted or oscillated into position prior to excavation. The capacity of the shaft can also be affected by the installation and removal of temporary casings.

Free-fall concrete placement can be used with dry construction, although there may be restrictions by regulatory agencies against its use due to separation aggregates leading to poor quality shafts. Wet construction requires the use of tremie placed concrete which eliminates the possibility of segregation of the concrete and/or mixing with the in situ slurry.

Whether the allowable strength design (ASD) or load and resistance factor design (LFRD) design approach is used, the concept of usable capacity as a function of ultimate capacity must be addressed. To this end, a permissible displacement limit must be established. The usable capacity is then determined for the specified displacement limit. Design of drilled shafts therefore requires the displacement criteria be superimposed onto load carrying capability, even when using the LRFD design method.

The load carrying capacity of drilled shafts is derived from a combination of side shear and end bearing. The permissible displacement criteria generally allow the side shear to be assumed 100% usable but the end bearing may not be 100% usable. Therefore, the concept of mobilized end bearing (the capacity developed at a given displacement) is utilized.

The usable capacity or effective ultimate capacity is used rather than the ultimate capacity derived from either ASD or LRFD design methods. The effective ultimate capacity is a displacement-restricted usable capacity.

Drilled Shaft Design Capacity

Drilled shaft capacity is derived from both side shear resistance and end bearing resistance. Various design methods are available for determining the capacity of drilled shafts including the use of SPT data, CPT data, rock core data, and load test data. Because the research project presented in this document used SPT data, the methods of determining drilled shaft capacity based on SPT data are presented here in.

The ultimate side shear capacity, *Qs*, is the summation of the unit side shear developed over the length of the shaft using the following equation:

$$Q_s = \pi \sum_{i=1}^{n} q_{si} L_i D_i, \tag{2.1}$$

where q_{si} is the estimated unit side shear for the i^{th} soil layer, L_i is the thickness of the i^{th} soil layer, and D_i is the diameter of the shaft in the i^{th} soil layer. For calculation of q_{si}, Mullins et al. (2004) recommends the use of O'Neill and Hassan's (1994) Modified Beta Method. Estimates of the unit side shear resistance developed between the perimeter of a drilled shaft and adjacent sandy soils, are presented in Table 1.

The unit side shear resistance developed between the perimeter of a drilled shaft and clay soils is a function of the adhesion factor α and undrained shear strength S_u;

$$q_s = \alpha S_u, \tag{2.2}$$

The ultimate end bearing capacity, Q_p, is represented by:

$$Q_p = \frac{\pi}{4} D^2 q_p, \tag{2.3}$$

where q_p is the estimated unit end bearing resistance and D is the shaft diameter at the base of the shaft. Estimates of the unit end bearing resistance can be found in Table 2 for shafts of diameter less than 4.17 ft. If the shaft diameter, D, is greater than 4.17 ft, the end bearing resistance should be reduced to

$$q_{pr} = 4.17 q_p / D, \tag{2.4}$$

The unit end bearing developed at the base of a drilled shaft tipped in clay soils and having a diameter less than 75 inches is represented by (AASHTO, 1998)

Table 1. Drilled Shaft Side Shear Design Methods for Sandy Soils (adapted from AASHTO, 1998)

Source	Side Shear Resistance, q_s (tsf)
Touma and Reese (1974)	$q_s = K\sigma'_{vo}\tan\phi < 2.5$ tsf where K = 0.7 for $D_b \leq 25$ ft K = 0.6 for 25 ft < $D_b \leq 40$ ft K = 0.5 for $D_b > 40$ ft
Meyerhof (1976)	$q_s = N/100$
Quiros and Reese (1977)	$q_s = 0.026N < 2.0$ tsf
Reese and Wright (1977)	$q_s = N/34$, for $N \leq 53$ $q_s = (N - 53) / 450 + 1.6$, for $53 < N \leq 100$ $q_s \leq 1.7$
Reese and O'Neill (1988) *Beta Method*	$q_s = \beta\sigma'_{vo} < 2.0$ tsf, for $0.25 \leq \beta \leq 1.2$ where $\beta = 1.5 - 0.135z^{0.5}$, z in ft
O'Neill and Hassan (1994) *Modified Beta Method*	$q_s = \beta\sigma'_{vo} < 2.0$ tsf, for $0.25 \leq \beta \leq 1.2$ where $\beta = N/15(1.5 - 0.135z^{0.5})$ for $N \leq 15$ $\beta = 1.5 - 0.135z^{0.5}$ for $N > 15$

D_b is the drilled shaft base diameter.
N is the uncorrected SPT blow count

$$q_p = N_c S_u \leq 40 \text{ tsf} \tag{2.5}$$

where

$$N_c = \begin{cases} 6\left[1 + 0.2\left(\frac{Z}{D}\right)\right] \leq 9, & S_u < 0.25\ tsf \\ 4\left[1 + 0.2\left(\frac{Z}{D}\right)\right] \leq 9, & S_u > 0.25\ tsf \end{cases} \tag{2.6}$$

and Z/D is the ratio of the drilled shaft depth to the drilled shaft diameter. AASHTO (1998) recommends a reduction factor as, shown below, be used for drilled shafts greater than 75 inches in diameter;

$$q_{pr} = q_p F_r, \tag{2.7}$$

where

$$F_r = 2.5/(12aD_p + 2.5b) \leq 1.0 \tag{2.8}$$

The parameters *a* and *b* in Equation 2.8 are functions of the depth to load ratio and the undrained shear strength, respectively;

$$a = 0.0071 + 0.0021\frac{Z}{P} \leq 0.015 \quad (2.9)$$

$$b = 0.45(2S_u)^{0.5} \; for \; 0.5 \leq b \leq 1.5 \quad (2.10)$$

Table 2. Drilled Shaft End Bearing Design Methods for Sandy Soils (adapted from AASHTO, 1998)

Source	**End Bearing Resistance, q_p (tsf)**	
Touma and Reese (1974)	Loose Sand, Medium Dense Sand, Very Dense Sand, where k = 1 for D_p < 1.67 ft k = 0.67D_p for $D_p \geq$ 1.67 ft Method applicable for shaft embedment in sand bearing layer D_b > 10D	q_p = 0.0 q_p = 16/k q_p = 40/k
Meyerhof (1976)	$q_p = (2N_{corr}D_b)/(15D_p)$ $q_p < (4/3)N_{corr}$ for sand $q_p < N_{corr}$ for non-plastic silts	
Reese and Wright (1977)	q_p = 2/3N for N ≤ 60 q_p = 40 for N > 60	
Reese and O'Neill (1988)	q_p = 0.6N for N ≤ 75 q_p = 45 for N > 75	

D_b is the drilled shaft base diameter.
$N_{corr} = 0.77\, log\left(\frac{20}{\sigma_v'}\right) N$

Post Grouted Drilled Shaft Background

Since the 1980's, post grouting has been routinely used in many parts of the world (Mullins et al. 2001). Post grouting is a two step process consisting of (1) installing grout pipes during cage preparation, and (2) injecting high pressure grout beneath the tip of the shaft after the concrete in the shaft has cured. Historically, post grouting drilled shafts in cohesionless soils has usually increased the end bearing capacity.

For sands, there is typically a direct correlation between volume of cement grout injected and the ultimate load increase. Loose to medium dense sands generally give the highest

increases in capacity. Both permeation grouting and compaction grouting are applicable to loose to medium dense sands and dense sand. However, dense sands may yield less significant improvements with permeation grouting relative to compaction grouting. Compaction grouting can be used with silty sands, although it is more effective in clean sands.

In sites where the soil is likely to be stratified, lensed, or highly permeable, staged grouting may be effective in confining the grout to a smaller region around the shaft tip. With staged grouting, an initial volume of grout is allowed to set before subsequent stages are completed. Allowing the previous stage of grout to set and develop some strength before adding more grout will fill possible escape routes for the next stage of grouting. With staged grouting, the tip improvement is limited by the shaft side shear available for the grouting pressure to react against. According to Mullins et al. (2001), the sleeve-port grouting apparatus design works well for staged grouting, while the flat-jack design does not.

Grouting Techniques

Grouting techniques vary with the mechanism for dispensing grout beneath the shaft tip. Two basic systems are used for distribution of the grout: (1) simple compaction grouting (sleeve-port), and (2) mechanical grouting system (flat-jack). Mullins et al. (2001) discuss three forms of grout distribution; (1) Stem (Orifice), (2) Sleeve-Port (Tube-a-Manchette), and (3) Flat-Jack (Pre-Load Cells).

Due to the simplicity of the stem form of post grouting, this form of grout distribution is only used as a remediation technique for substandard shafts with inadequate capacity. This grouting apparatus consists of a pressure conduit (such as a pipe or cored hole through an existing shaft). Such a conduit terminates at the desired grouting location.

Sleeve-port systems consist of a simple network of u-shaped perforated pipes encased in rubber sleeves at the base of the shaft connected to grout tubes to the top of the shaft. The rubber membrane is intended to prevent blockage during shaft construction and act as a check-valve to prevent back flow of grout up the tubes following grouting. There are several variations to the sleeve-port. Another complication with the sleeve-port apparatus is that the grout pressure is unable to break the encapsulation in cases where the excavation depth is lower than the sleeve-port elevation. Mullins et al. (2001) recommends the use of a floating

sleeve-port or the use of flexible grout hoses for instances where the cage length and excavation may not be consistent or where the top of steel set is critical.

The flat-jack method uses one steel plate with a neoprene membrane beneath. An impermeable liner covers the plates to prevent concrete blockage of the injection ports during construction and to ensure the grout does not permeate into the surrounding soil.

Grout Mixes

The success of post-grouting drilled shaft tips is highly dependent upon the grout mixture. Grouting properties and procedures can vary widely including the following: grout mixers, grout pumps, access lines, grout mixing, grout physical properties, and grout constituents.

The equipment and mechanisms used in grouting have many variations. Grout mixers are classified into three groups: high-quality, less efficient and lower quality. The classification of mixer to be used is a function of the grout pressure and the size of the access lines. A wide variety of grout pumps are available. Grout pumps vary in method (continuous pumping or cyclic pumping), maximum pressure, and the type of grout constituents used.

The size of the access line should also be considered in determining the grouting procedures. Reduction in the size of the access lines can cause grout build up due to water segregation from the paste. This type of buildup can block the flow through the pump and should be avoided (Mullins et al. 2001).

The requirements of the fresh and hardened properties of the grout will vary among projects. The fresh properties of a grout mix are the flowability, pumpability, viscosity, and the colloidal nature of the grout. Pumpability of a grout is a function of pump type, pressure to be achieved, access line dimensions, and time of pumping a single mix. The hardened properties of grout that need to be considered are the compressive strength, leaching or segregation, creep and bleeding (a quasi-hardened property). The required compressive strength of the grout should far exceed soil strength for post-grouting of drilled shafts.

Grout Constituents

Grout mixes are comprised of water, cement, aggregates, and admixtures. Tap water is generally used in grout mixes. According to Mullins et al. (2001) Type I/II Portland Cement

with admixtures is typically used in post grouting processes. In general, only fine aggregates are used in grout mixes. Fine aggregates are typically comprised of crushed or natural sands.

Admixtures can affect many of the fresh and hardened properties as well as the set times and initial shrinkage. Admixtures have two general classifications: mineral and chemical admixtures. Mineral admixtures include fly-ash, blast furnace slag, and metakaolin. Mineral admixtures will improve the flow and pumpability, and lessen the bleed water by increasing the amount of fines in a grout mix. Although mineral admixtures are beneficial to the grout mix properties, these benefits may not outweigh the added costs involved.

Chemical admixtures include water reducers, retarders, accelerators, air entrainers, de-air entrainers, latexes, finishing agents, shrinkage reduction agents, corrosion inhibitors and many other chemicals which can be used to alter the properties of a grout mix. Water reducers, retarders, and air entrainers are generally used with grout mixes that will be pumped.

Post Grouted Drilled Shaft Design Capacity

The empirical design method for post grouted drilled shafts in sands, developed by Mullins et al. (2006) is based on studies involving full-scale Statnamic load tests. In the empirical method, the unit end bearing capacity of a post grouted drilled shaft is related to the unit ungrouted end bearing capacity through the tip capacity multiplier (*TCM*);

$$q_{grouted} = (TCM)q_p \tag{2.11}$$

where the empirical tip capacity multiplier (*TCM*) is given by

$$TCM = 0.713 \cdot GPI \cdot \%D^{0.364} + \frac{\%D}{0.4 \cdot \%D + 3} \tag{2.12}$$

In Equation 2.12, the grouting pressure index (*GPI*), is the ratio of the maximum grouting pressure (GP_{max}) to the ungrouted end bearing capacity (q_p) at 5%D displacement and *%D* is the chosen allowable tip displacement expressed as a percentage of the shaft diameter.

Present Practice for Post Grouted Drilled Shafts

Based on a review of literature, the use of post grouted drilled shafts is typically accompanied by load test programs. Although the review of literature revealed the use of post grouted drilled shafts world-wide, little information was found on long-term performance monitoring of post grouted drilled shafts.

CONTEXT FOR THESE PROJECTS

This section discusses the purpose of the projects presented in this thesis. Although many bridge owners are connecting their approach slabs to their I-A bridges, a rigorous review of the literature revealed that little has been done to determine the forces that develop in approach slabs tied to I-A bridges. The I-A bridge study presented herein attempts to bridge this knowledge gap.

As discussed previously, post grouting of drilled shafts is being used around the world, though little work has been published on long-term performance monitoring of post grouted drilled shafts. Also, there has been little published on the investigation of failed attempts at post grouting of drilled shafts. The post grouted drilled shaft study presented herein extends the existing database of load test information available on improvement of drilled shaft capacity via post grouting, examines the inability to post grout a test shaft, and provides new data on the long-term performance of post grouted production drilled shafts.

CHAPTER 2. WORKS CITED

American Association of State Highway and Transportation Officials (AASHTO). 1998. AASHTO LRFD Bridge Design Specification. Customary U.S. Units Second Edition.

Akbulut, S. and A. Saglamer. 2002. Estimating the groutability of granular soils: a new approach. *Tunneling and Underground Space Technology*. Volume 17. Issue 4. Pages 371-380, ISSN 0886-7798, DOI: 10.1016/S08867798(02)0040-8.

Bigelow, J., Faris, A., Greimann, L., Phares, B. 2008. Instrumentation and Monitoring of Integral Bridge Abutment-to-Approach Slab Connection. IHRB Projects TR-530 & TR-539, Iowa DOT Projects 05-197 & 05-219. Ames, IA, Institute for Transportation.

Burwell, EB. 1958. Cement and clay grouting of foundations. Practice of the corps of engineering. ASCE, Soil Mechanics and Foundation Division, Vol 84, No. SM1 Paper 1551.

Dapp, S.D., Muchard, M., and Brown, D.A., 2010. "Experiences with Base Grouted drilled Shafts in the Southeastern United States," Proc. of 10th International Conference on Deep Foundations, Amsterdam, Netherlands.

Mistry, V.. 2005. Integral Abutment and Jointless Bridges. Federal Highway Administration (FHWA) Conference.

Horvath, J. 2000. Integral-Abutment Bridges: Problems and Innovative Solutions Using EPS Geofoam and Other Geosynthetics. Manhattan College Research Report No. CE/GE-00-2. Bronx, New York.

Incecik, M. and Ceren, I. 1958. Cement grouting model tests. Bulletin of The Technical University of Istanbul, 48(2): 305-317.

Kunin, J., Alampalli, S. 1999. Integral Abutment Bridges: Current Practice in the United States and Canada. Transportation research and Development Bureau, New York State Department of Transportation. Federal Highway Administration (FHWA) Special Report 132.

Lenke, L. 2006. Settlement Issues – Bridge Approach Slabs (Final Report Phase 1). Transportation Engineering Research Program (TERP). Albuquerque, NM. Department of Civil Engineering.

Mullins, G., Dapp, S., Frederick, E. and Wagner, V., 2001. Post Grouting Drilled Shaft Tips, Phase I. Florida Department of Transportation, Report FDOT BC165 v1.

Mullins, G., Winters, D., and Dapp, S. 2006. Predicting End Bearing Capacity of Post-Grouted Drilled Shaft in Cohesionless Soils. *Journal of Geotechnical and Geoenvironmental Engineering, ASCE.* Volume 132. Issue 4. Pages 478-487, ISSN 1090-0241, DOI: 10.1016/(ASCE)1090-0241(2006)132:4(478).

O'Neill, M.W. and Hassan, K.M., 1994. "Drilled Shafts: Effects of Construction on Performance and Design Criteria." Proceedings of the International Conference on Design and Construction of Deep Foundations, December 1994, Vol. 1, pp. 137-187.

CHAPTER 3. PERFORMANCE OF PRECAST APPROACH SLABS INTEGRAL WITH INTEGRAL ABUTMENT BRIDGES

A paper to be submitted to the Journal of Bridge Engineering

Anna Nadermann, Brent Phares, Lowell Greimann

Abstract

Approach slab pavement at integral abutment bridges is prone to settlement and cracking, as has been long recognized by many bridge owners. A common solution to these problems is to attach the approach slab to the bridge abutment. In this study, the behavior of such approach slabs was investigated by implementing health monitoring systems on approach slabs, interpreting the data obtained during 12-month monitoring periods, and conducting periodic visual inspections at two bridge sites. Based on the information obtained, the following general conclusions were made. (1) The connection between the approach slabs and the bridges appear to function well with no observed distress at these locations and no relative movements measured between the two components. (2) The measured strains in the approach slabs indicate that significant forces exist at the expansion joints between the approach slab and pavement, which should be taken into consideration when designing both the approach slab and the bridge. (3) Although measures were taken to reduce frictional forces on the slabs, notable friction was measured.

Introduction

The Iowa Department of Transportation (Iowa DOT) and other bridge owners have long recognized that approach slab pavements at integral abutment (I-A) bridges are prone to settlement and cracking, which is manifested as the “bump at the end of the bridge” (Horvath 2000). The bump is not a significant safety problem; rather, it is an expensive maintenance issue. Further, public perception is negatively affected by the presence of the bump. The formation of the bump is typically attributed to settlement of backfill soil under the approach slab and deterioration of the corbel or paving notch (Lenke 2006). Lenke also lists joint design and maintenance as a contributing factor in the development of the bump. Although it

is recognized that I-A bridges have many highly desirable attributes, the joint design may be worsening the bump. A common solution to the observed problems is to attach the approach slab to the bridge abutment, which moves the expansion joint, typically found at the approach slab/abutment interface, to a location further from the bridge where soil settlement is less of a concern and maintenance is presumably easier.

As part of the Iowa DOT's quest to improve the long-term performance of their bridges, several projects were initiated to investigate a new detail for attaching approach slabs to integral abutment bridges. One of the goals of these projects was to understand the performance of the connection detail and the magnitude of the forces developed in the approach slab as it moved with expansion and contraction of the I-A bridge. This paper summarizes the results of parts of two larger studies. Specifically, the behavior of attached approach slabs at two bridge sites in Iowa will be discussed with a primary focus on the forces that develop in the slab.

State-of-Practice

The most obvious general benefit derived from using I-A bridges is cost, both initial construction costs and long-term maintenance costs. Kunin (1999) lists additional specific benefits of I-A bridges including reduced deterioration from de-icing chemicals and snowplows, decreased impact loads, improved ride quality, simplified construction, and improved structural resistance to seismic events.

The bump that can develop at I-A bridges is typically due to differential settlement of the bridge abutment and approach pavement, i.e., soil structure interaction (Horvath 2000). Bigelow et al. (2008) attributes the differential settlement to one of the following: (1) insufficient compaction of soil or poor backfill properties, (2) void development due to erosion, or (3) displacement due to pavement growth. Generally, void development occurs within the first year after construction. Annual expansion and contraction of I-A bridges due to thermal variations generally causes further compaction of the fill material creating void space under the approach slab (Horvath 2000). Water naturally collects in these voids which can cause soil erosion, further increasing the size of the void.

Approach slabs are intended, among other things, to minimize the effects of differential settlement and to provide a smooth transition to and from the mainline pavement and the

bridge. Connecting the approach slab to the bridge further improves the minimization of differential settlement. In general, the slab can be connected to the bridge in one of two ways:

- Extending the deck reinforcing into the approach slab (horizontal – see Figure 1a) or
- Using reinforcing steel to connect the slab to the corbel or abutment (diagonal – see Figure 1b).

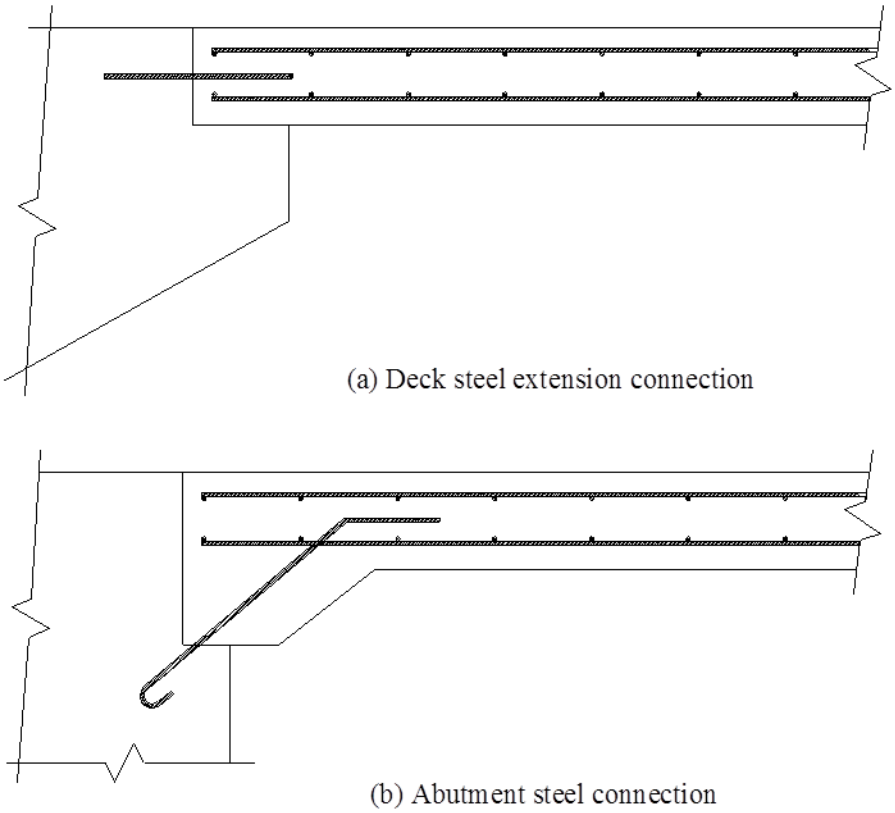

Figure 1. Typical connection of approach slab to bridge; (a) Deck steel extension connection and (b) Abutment steel connection

Bigelow et al. (2008) conducted a survey of the DOTs of the north central states to assess various aspects of bridge ride-ability. Table 1 is a partial summary of the survey. In general, it was reported that an approach slab connected to the bridge moved the bump from the end of the bridge to the pavement end of the approach slab where it was felt that it could be more easily maintained. Generally, cracking at the bridge end of the approach slab was reported when a horizontal connection was used. Minnesota originally used a horizontal connection and experienced cracking; after changing to a diagonal connection, no cracks were reported.

Table 3. Summary of DOT Survey Responses

State	Connection Type	Performance
Illinois	Horizontal	Transverse cracking problem
Kansas	Horizontal	Reasonably well
Minnesota	Diagonal	No problems reported
Missouri	Horizontal	No answer
Nebraska	Diagonal	Management is pleased
North Dakota	Horizontal	Very well
South Dakota	Horizontal	Pretty Well

Objective and Approach

As mentioned previously, two projects were initiated by the Iowa DOT to evaluate the performance of integral abutment bridges with integrally connected approach slabs and to determine the range of forces that should be considered when designing such slabs. Bridges in O'Brien County, IA (2 twin side-by-side bridges) and Bremer County, IA with integrally connected approach slabs were instrumented with long-term monitoring systems to study their structural performance over several seasons.

Bridge Descriptions

O'Brien County Bridges

Two new side-by-side bridges on the new Iowa Highway 60 bypass of Sheldon, IA in O'Brien County (O'Brien County Bridge) were the first bridges in Iowa to tie the approach slab to an I-A abutment bridge. One bridge utilized a cast-in-place approach slab system while the other utilized a precast approach slab system. The O'Brien County bridges are twin three-span-continuous prestressed concrete girder bridges, 303 ft x 40 ft, with a right-hand-ahead 30 degree skew angle. The end spans are 90 ft - 9 in. and the interior span measures 121 ft - 6 in. The bridges are inclined with a change in elevation from the North abutment to the South abutment of approximately 1 ft – 2-1/2 in. With the exception of the approach slab type (precast or cast-in-place) the two O'Brien County bridges were identical. For consistency in making comparisons with the Bremer County Bridge, only the precast approach slab is discussed herein.

The precast approach consists of eight panels that are nominally 12 in. thick. Six panels are rectangular panels 20 ft long by 14 ft wide. The remaining two panels are trapezoidal

panels 14 ft wide with a 30 degree skew at the bridge end. The approach slab is connected to the bridge by a vertical anchor bar drilled and grouted into the cast-in-place paving notch. At the other end of the approach slab an IADOT standard EF expansion joint (a slip dowel-type joint) was used. A friction reducing polyethylene sheeting was used under the approach slab.

Bremer County Bridge

Two new bridges were constructed on US-63 over County Road C-50 (Fayette St.) in Denver, IA in Bremer County (Bremer County Bridge). The typical precast approach slab system used for the Bremer County Bridge is shown in Figure 2a. The northbound bridge is a three-span precast concrete girder bridge, 161 ft x 40 ft, with a right-hand-ahead 2°29’52” skew angle. The bridge is inclined with a change in elevation from the South abutment to the North abutment of approximately 9 ½ in.

Unlike the O’Brien County Bridge, the Bremer County bridge approach slab uses both precast and cast-in-place shoulder sections (see Figure 2a). Each approach slab consists of eight precast prestressed panels that are nominally 12 in. thick, except at the abutment where the thickness was reduced to 9.5 in. to match the paving notches (see Figure 2b). The four panels at the pavement end of the approach are rectangular and doweled to the pavement (E joint). The four panels at the bridge end of the approach are trapezoidal with a skew to match the bridge. The approach slab is connected to the bridge by an angled dowel bar as depicted in Figure 2b. A friction reducing polyethylene sheeting was used under the approach slab.

Instrumentation

Both the O’Brien and Bremer County bridges were instrumented with long-term monitoring systems consisting of a data logger and vibrating wire sensors. Each bridge was monitored for approximately one year with data collected and stored once an hour. Although other sensors were used to monitor other areas of the bridges, the principal sensors of interest herein are strain gages embedded in the approach slab and crackmeters. At the O’Brien County Bridge sixteen strain gages were embedded in the approach slab. Two gages were placed in each of the eight panels and oriented and aligned such that they created four lines of four sensors measuring strains in the direction of the roadway. Additionally,

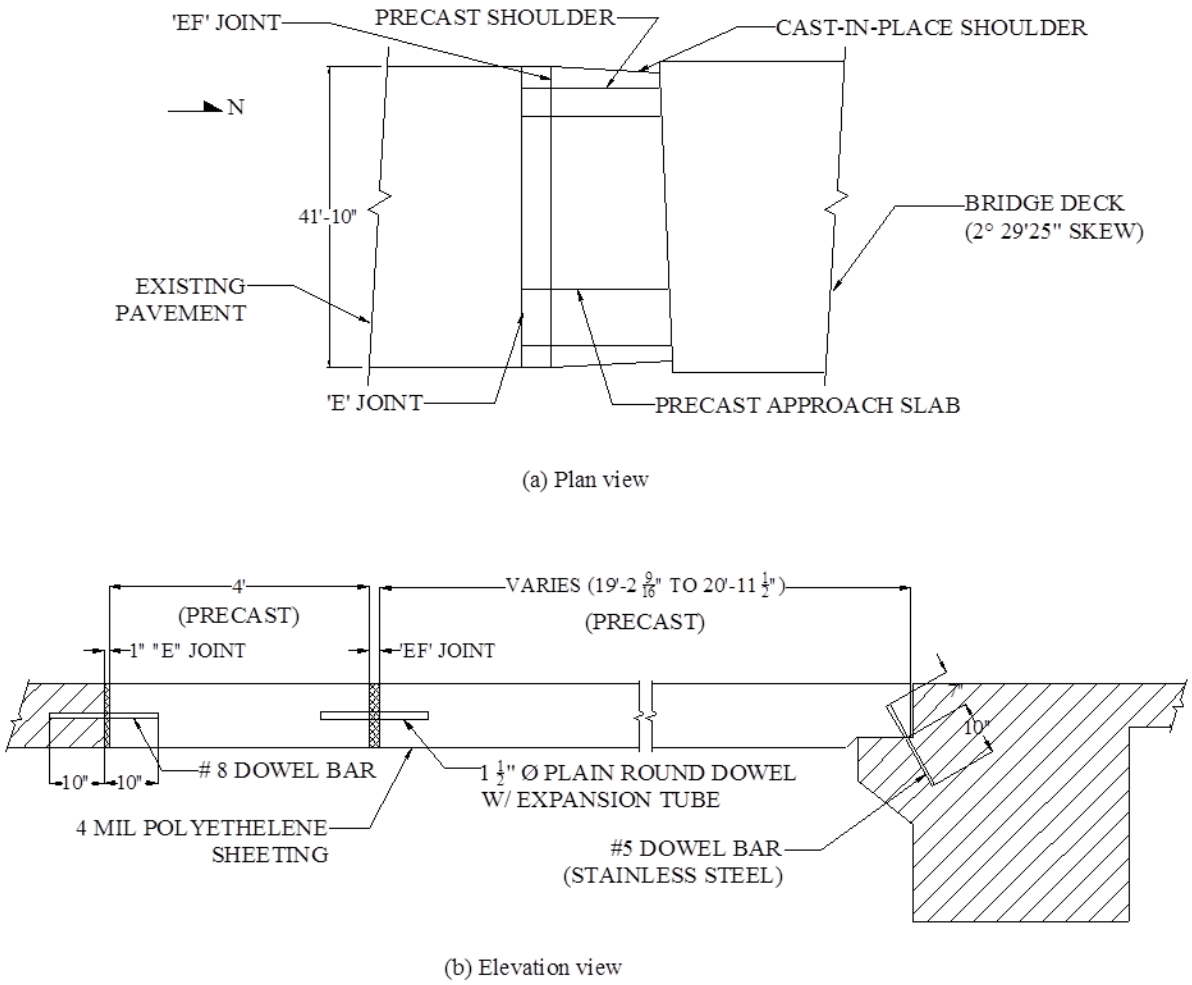

Figure 2. Precast approach slab; (a) Plan view and (b) Elevation view of precast approach slab [Bremer]

crackmeters were installed at each panel-to-panel joint; at the approach-to-bridge interface and at the approach-to-pavement interface (a total of ten crackmeters). Due to construction restrictions, a modified instrumentation scheme was utilized at the Bremer County Bridge as shown in Figure 3 (24 strain gages in four lines and eight crack meters). Note that the same basic behaviors were measured (e.g., four lines of longitudinally oriented strain gages and joint openings) at each bridge.

Results

In the following section the results of the experimental investigation are summarized with specific attention paid to those results which pertain to the forces on the approach pavement.

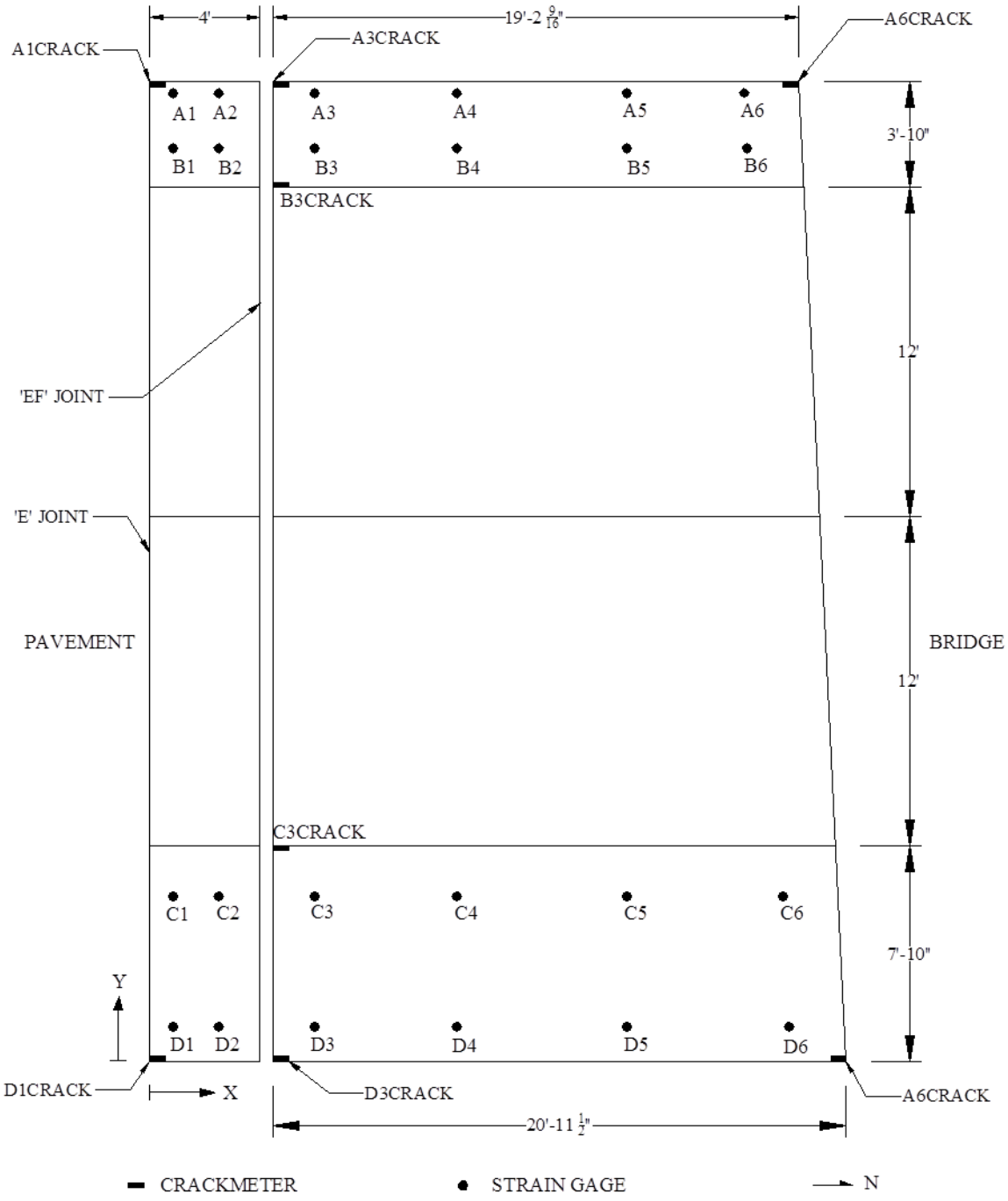

Figure 3. Instrumentation layout in precast approach slab [Bremer]

Note that at times reference is made to “hot”, “average”, and “cold” days. These days occurred on July 21, 2009, April 18, 2009, and January 5, 2010, respectively, and represent the general behavior during cold, temperate and hot periods at the Bremer County site. For

comparison and reference herein, similar “cold”, “average”, and “hot” dates were considered for the O’Brien County site.

Load Strain

The load-related strain (i.e. corrected for thermal strain effects) time histories for select Bremer County bridge sensors are shown in Figure 4; the load strain time history is similar for the O’Brien County Bridge and is not shown here in the interest of brevity. Note that “load strain” is the load-related strain due to loads resulting from restrained thermal expansion and contraction. The load strain does not include unrestrained strain resulting from temperature changes.

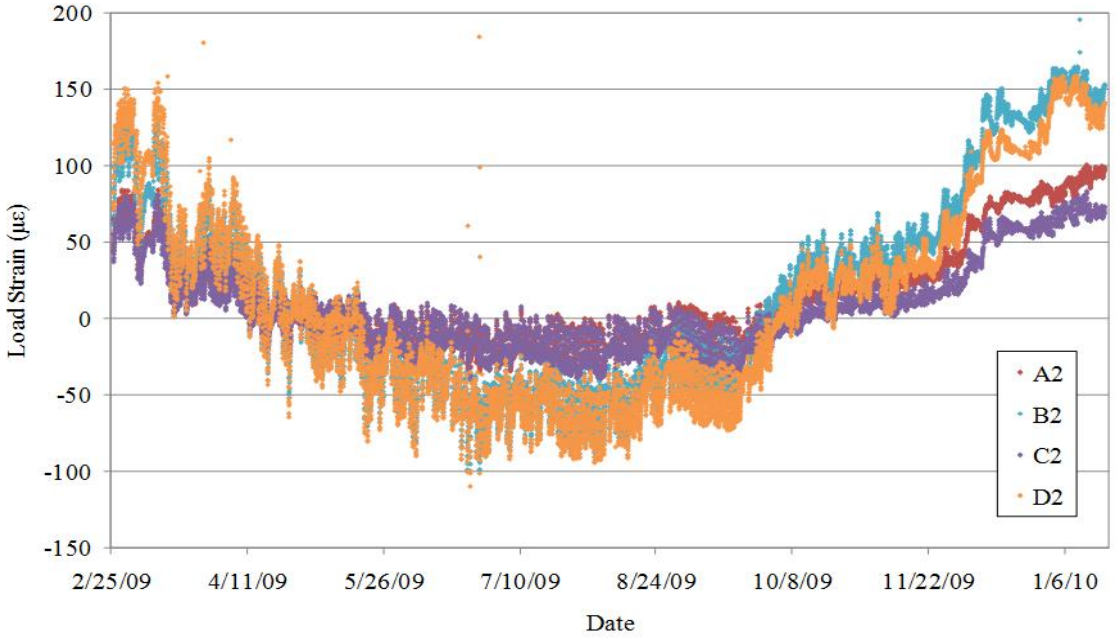

Figure 4. Load strain in approach slab over time [Bremer]

The difference in strains measured along the four lines of gages (A, B, C, and D) show that load strains vary transversely. This indicates that the slab restraint varied transversely – potentially due to the slight skew. In general, as the temperature decreases, the load strain within the slab increases (i.e. the load strain moves toward tension (positive) in winter months and toward compression in summer months). This consistent behavior (both in lateral and longitudinal position) indicates that forces are being developed in the slab as a result of joint behavior “lock-up” and/or bottom-of-slab frictional force development. As the approach slab cools it contracts away from the expansion Type EF joint and as the approach slab

warms it expands into the Type EF joint. A properly operating joint and frictionless resting surface would result in the development of no force in the approach slab. Quite to the contrary it can be observed (and will be further discussed in the following sections) that frictional forces and joint forces are being developed.

The load strain at the O'Brien County Bridge was generally observed to be uniform both longitudinally and transversely. Figure 5 shows how the load strain at the Bremer County Bridge varies longitudinally on the cold and the hot days along the D line of gages (Figure 4). The load strain is relative to the "average" day (i.e. the load strain is shown as zero for the "average" day). The figure shows the locations of the EF joint and the abutment joint as well as the linear regression line on the cold day extrapolated to the abutment joint. The slope of the regression line is a direct measure of the frictional resistance being encountered by the slab. Although length limitations prohibit showing graphically, the data indicate that during different seasons the slope of the line changes from negative (as shown in Figure 5) to positive. This represents a change in the direction of the frictional force as will be discussed further.

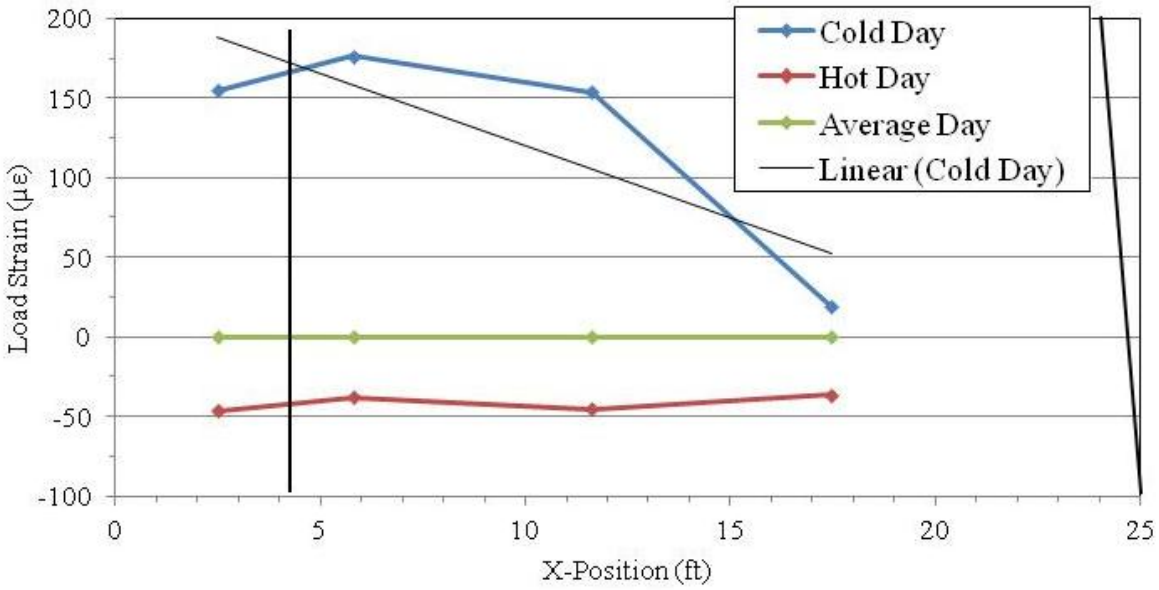

Figure 5. Load strain along D-line of approach slab [Bremer]

Although not shown here in the interest of brevity, the linear regression lines, on the cold day, for gage lines A, B and D have slopes of differing magnitudes but in the same direction (i.e., the load strain is decreasing longitudinally toward the abutment) indicating that the

frictional resistance is not uniform across the width. Interestingly, the linear regression line, on a typical cold day, for gage line C slopes in the opposite direction (i.e., the load strain is increasing toward the abutment) as the gage lines A, B, and D. This behavior could possibly be explained by the location of line C being nearer to the center of the approach slab mass. Additional instrumentation near the centerline of the approach slabs may have revealed a gradient and explained the behavior difference. The load strain at the Bremer County Bridge also varies transversely, varying more on cold days (see Figure 4 for variations in lines A, B, C and D) than on hot days. This larger variation in load strain across and along the approach slab during winter months indicates that the slab is experiencing stresses during the winter months which are not present during the summer months. These stresses may be the result of the water freezing either the expansion joint or soil beneath the slab. Likely, this would result in the formation of bottom of slab "lugs" that significantly resisted slab movement.

Force

Figures 6 and 7 show the forces at the expansion and abutment joints of the O'Brien County and Bremer County Bridges, respectively. At both sites, a cyclical pattern emerges with the winter and summer having the maximum and minimum force, respectively, while the spring and fall are transition periods. As can be seen, the slab forces tend toward compression in the summer and tension in the winter. Upon closer inspection of the data, daily cyclic patterns emerge as well. Both bridges had a range of forces of approximately 200 kips/ft.

At the O'Brien County site, the forces at the expansion joint and at the abutment were generally of similar magnitude and coincided throughout the time. This would indicate that the primary source of force generation in the slab might be the expansion joint.
However, at the Bremer County site, the force at the expansion joint and the abutment begin to deviate during the winter months – a behavior discussed previously and likely related to freezing water under the slab. In this case, during the cold months the largest force generating mechanism was likely friction on the slab bottom.

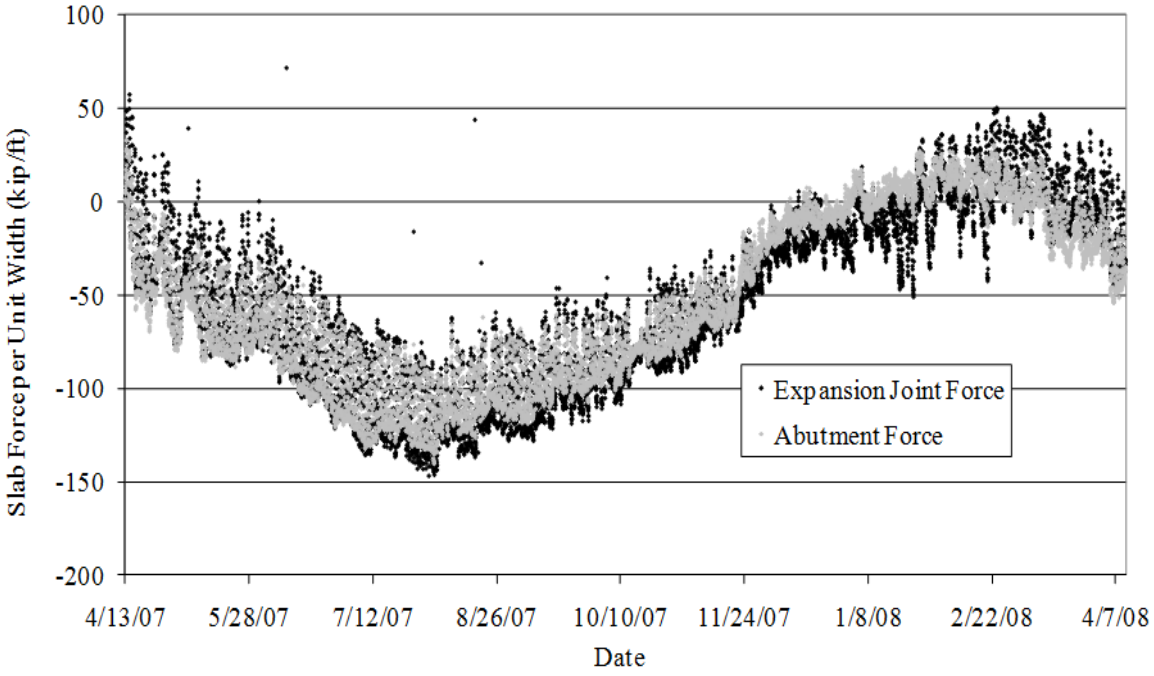

Figure 6. Average slab force across EF and abutment joints [O'Brien]

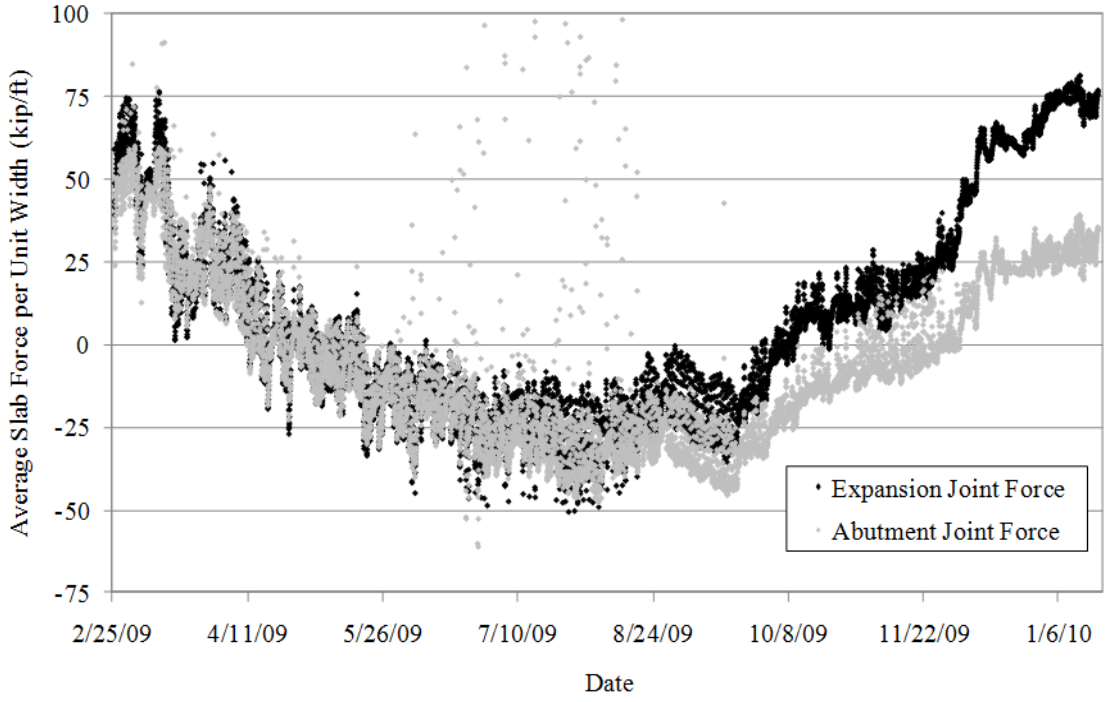

Figure 7. Average slab force across EF and abutment joints [Bremer]

Friction

Figures 8 and 9 show the friction coefficient with time for the O'Brien County and Bremer County bridges, respectively (a positive coefficient of friction indicates movement of the approach slab toward the abutment and negative coefficient indicates movement toward the expansion joint). The coefficient of friction for the O'Brien County Bridge had an approximate range of -1.9 to 1.9. Coefficients of friction greater than 1 indicate that the interface between the approach slab and the supporting soil was very rough. Field observations during construction indicate that the large horizontal forces at the O'Brien County site are due to construction problems related to grouting operations.

For the Bremer County Bridge the coefficient of friction apparently reached nearly 20 during the winter months, when the force in the EF and abutment joint varies most as shown in Figure 7 and discussed previously. This increase in the coefficient of friction during the winter months indicates the approach slab needs to overcome a much larger force during winter months than in summer months. The apparently large coefficient of friction in the Bremer County Bridge may be caused by the approach slab and supporting soil freezing as a unit. This may have created the previously mentioned "lug" effect that created active soil

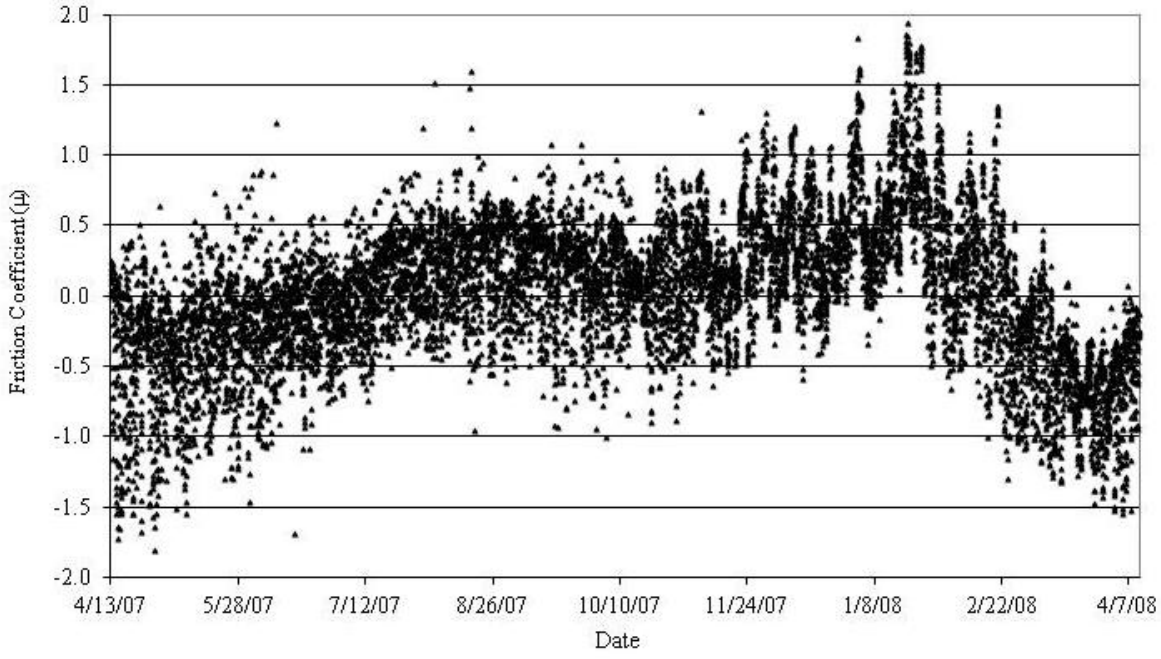

Figure 8. Bottom of slab friction over time – northbound bridge [O'Brien]

pressure at the face of the "lug". During the summer months the coefficient of friction had similar ranges for both locations and was slightly larger at the Bremer County Bridge, which may be related to the type of soils at the site.

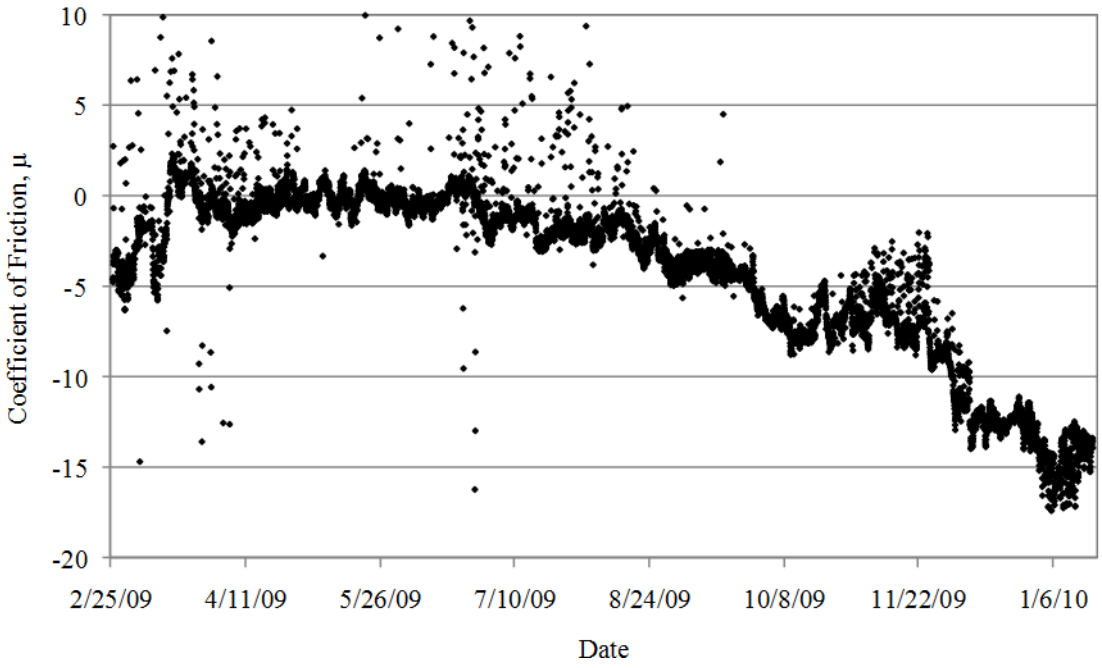

Figure 9. Coefficient of friction over time [Bremer]

Joint Movements

For the O'Brien County bridge the crackmeters not located at the expansion joint showed less than 0.03 in. of relative movement during the test period. The crackmeter located at the expansion joint between the approach slab and pavement had a relative movement range of over 0.90 in. Figure 10 shows how the O'Brien County Bridge joint opening varies with temperature. On the Bremer County Bridge the crackmeters located along the abutment joint and pavement joint had relative movements of less than 0.02 in. The crackmeters located at the expansion joint also had a total range of 0.90 in. Figure 11 shows the Bremer County bridge expansion joint opening versus temperature.

The data shown in Figures 10 and 11 corroborate the behaviors measured with the strain gages and discussed previously (e.g., the approach slab moving away from the expansion joint in winter and towards it in summer). Further, when viewed with time there is an apparent cyclic nature to the data. This cyclic nature can also be partially observed if one

accepts that temperature variation with time is, over long periods of time, generally consistent. Figure 12 shows that the compressive force in the slab increases as the expansion

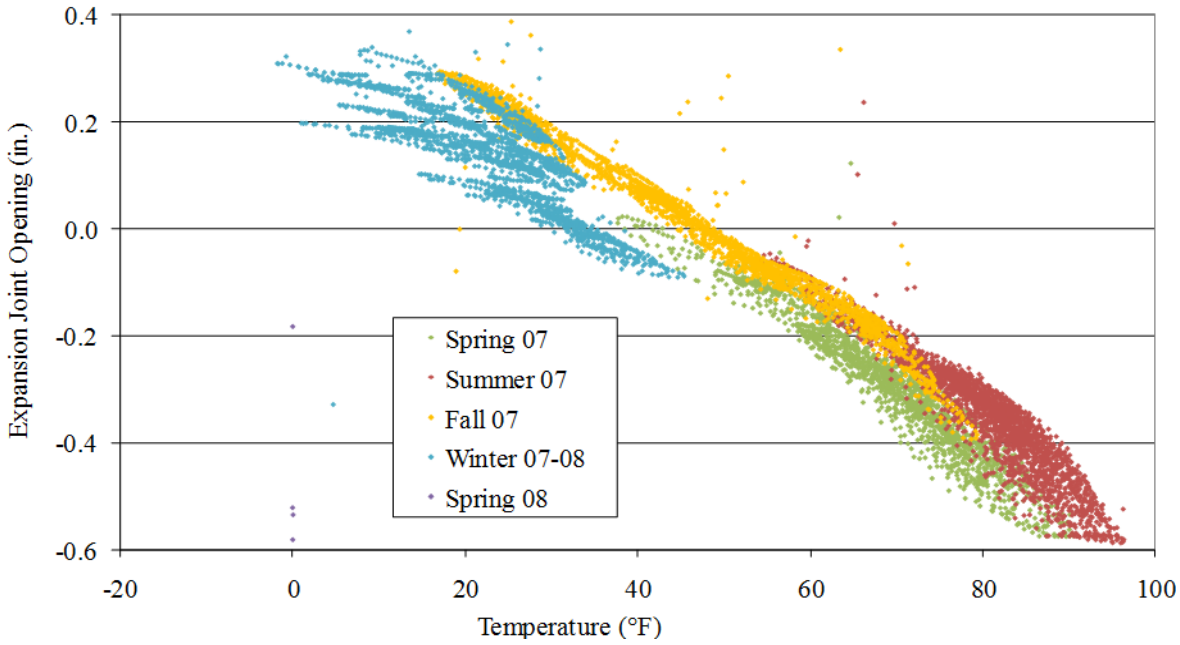

Figure 10. Expansion joint movement relative to average slab temperature [O'Brien]

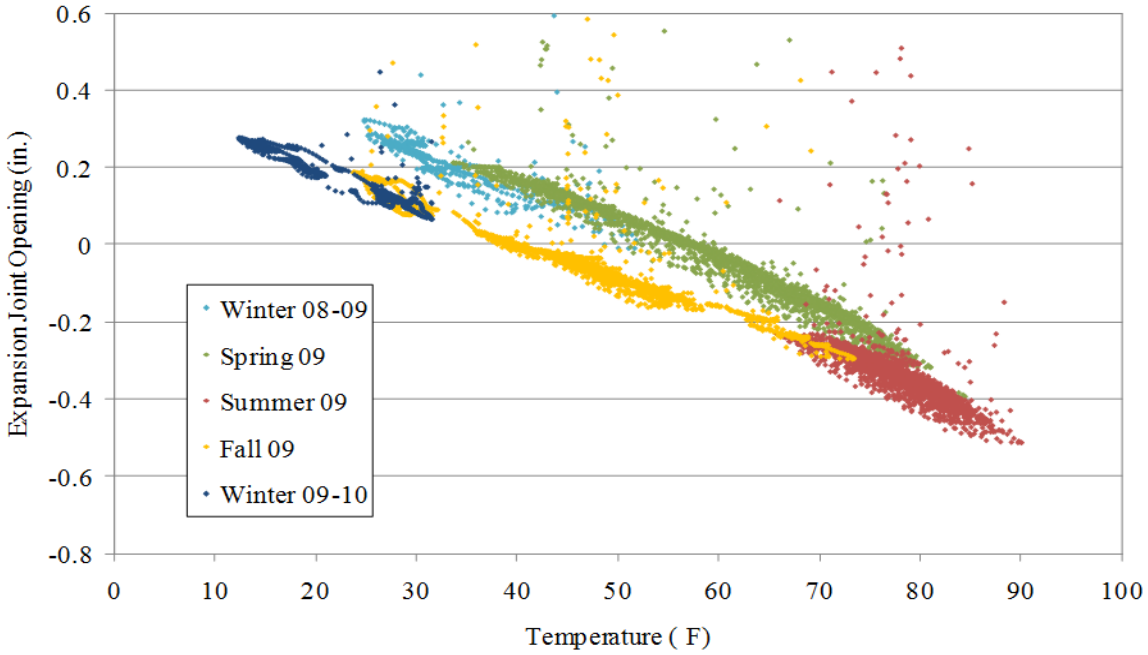

Figure 11. Expansion joint movements relative to average slab temperature [Bremer]

joint contracts for the O'Brien County Bridge. This same relationship is seen in Figure 13 for the Bremer County Bridge. Figure 13 also shows that the force varies transversely. The larger

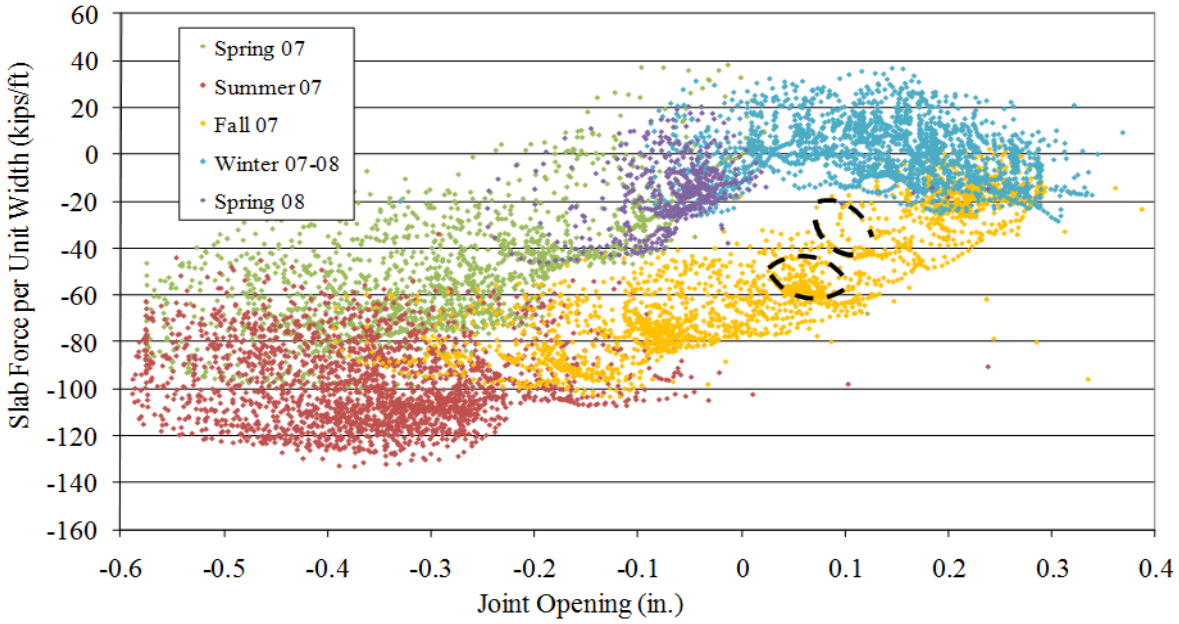

Figure 12. Slab force per unit width relative to expansion joint movement [O'Brien]

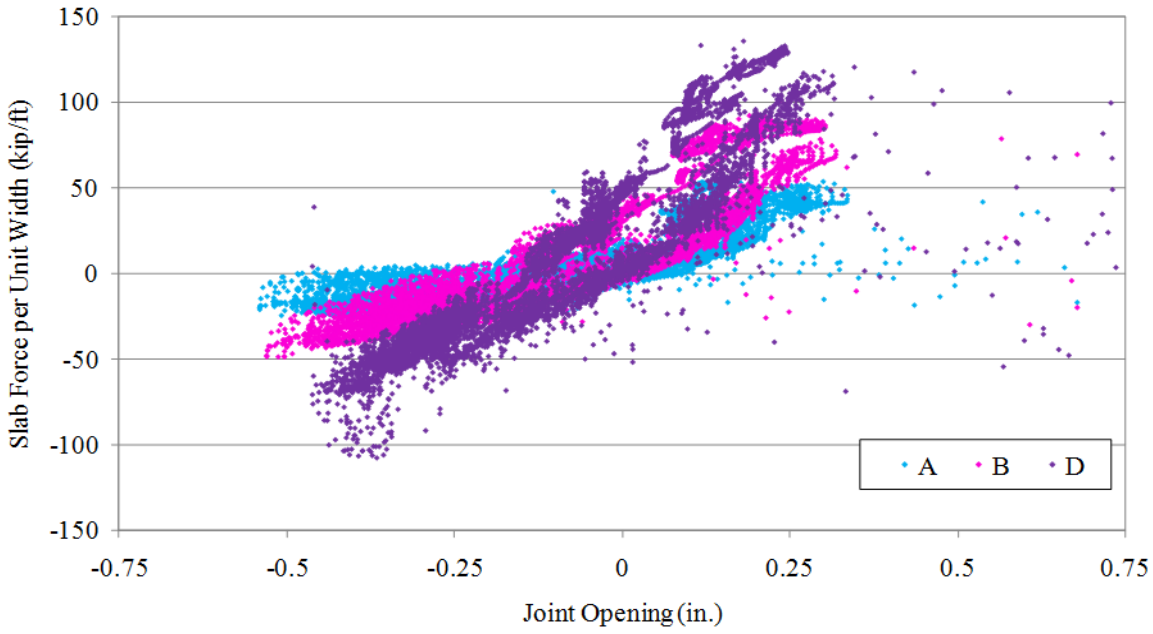

Figure 13. Slab force per unit width relative to expansion joint movement [Bremer]

slope of the force at the expansion joint along line D of the slab for the Bremer County Bridge indicates the slab force behaves differently here from the force in other areas of the slab and, again, illustrates the transverse variation of the slab forces at the Bremer County site.

The responses shown in Figure 12 generally follow an annual cyclic and/or short term cyclic pattern. The annual cyclic pattern had summer responses at one extreme, a transition through the fall to the other extreme response in the winter, followed by a transition in the spring back to the summer responses. Short term cycles (as indicated by the dashed lines which can be typically observed) were evident for both approach slabs and are likely caused by friction ratcheting. Friction ratcheting is a cyclic build-up of stress to overcome friction. During short term (daily) cyclic stresses build up in the slab that are not large enough to overcome the friction at the bottom of the slab before being released. During this short term build up and release of stresses the abutment is pushed by the expanding and contracting approach slab. This means that forces are being developed on both sides of the abutment – from the approach slab on one side and from the superstructure on the other. Not only is the expansion and contraction of the bridge superstructure acting on the abutment, there is also a force from the approach slab due to this build up and release of stresses. However, as temperatures continue their seasonal trend, the buildup of stresses becomes large enough to eventually overcome the slab friction and the slab slides to a new position where the short term cycles begin again without sliding.

Visual Inspection

During the monitoring periods the bridges at both locations were visually inspected. Cracks were observed in the approach slab of the O'Brien County Bridge at about 34 ft from the abutment joint. This crack was half the width of the approach slab extending from the East shoulder to the center longitudinal joint. No cracks were present in the precast approach slab panels or the cast-in-place shoulders of the Bremer County Bridge. In general it was felt that visible distress (however minor) could not be attributed to the fact that the approach slab had been integrally connected to the bridge.

Conclusions and Recommendations

In an effort to reduce the bump experience at the end of bridges, the Iowa DOT is interested in integrally connecting the approach slabs to their I-A bridges. To investigate the performance of such a detail, year-long monitoring of two I-A bridges with precast approach slabs was conducted. The monitoring consisted of instrumenting the precast approach slab systems with strain gages and crack meters at two bridge sites. The data were interpreted and periodic visual inspections were conducted. The following conclusions were developed based on the findings of this study:

- The integral connection between the approach slabs and the bridge appear to function well with no observed distress and little relative longitudinal movement.
- The measured strains in the approach slabs indicate that a notable force exists at the expansion joint. This force approached a range of approximately 200 kips/ft in this work.
- Notable frictional forces exist at the bottom of the approach slab.
- The minor visible distress could not be attributed to the fact that the approach slab is integrally connected to the bridge.

Based on the conclusions drawn from the data collected, the following recommendations for current practice and future studies should be considered when designing and constructing I-A bridges:

- Prevention of the “bump at the end of the bridge” should be considered a design goal for all approach slabs.
- The force which develops at the expansion joint should be taken into consideration when designing both the approach slab and the bridge. A more robust abutment may transfer less of the expansion/contraction force to the approach slab and more to the abutment foundation, resulting in less force at the expansion joint. A second alternative would be to reduce or even eliminate the interaction of the abutment and soil with the use of a mechanically stabilized earth wall placed between the abutment and earth fill.
- The roughness of the supporting soil should be taken into consideration during the design process as well.

- As good engineering practice dictates, these recommendations should undergo a comprehensive testing program and be validated with further studies. Future studies should also ensure that approach slabs are instrumented throughout their entire width in order to determine if a gradient exists in the forces across the slab.

CHAPTER 3. WORKS CITED

Bigelow, J., Faris, A., Greimann, L., Phares, B. 2008. Instrumentation and Monitoring of Integral Bridge Abutment-to-Approach Slab Connection. IHRB Projects TR-530 & TR-539, Iowa DOT Projects 05-197 & 05-219. Ames, IA, Institute for Transportation.

Horvath, J. 2000. Integral-Abutment Bridges: Problems and Innovative Solutions Using EPS Geofoam and Other Geosynthetics. Manhattan College Research Report No. CE/GE-00-2. Bronx, New York.

Kunin, J., Alampalli, S. 1999. Integral Abutment Bridges: Current Practice in the United States and Canada. Transportation research and Development Bureau, New York State Department of Transportation. Federal Highway Administration (FHWA) Special Report 132.

Lenke, L. 2006. Settlement Issues – Bridge Approach Slabs (Final Report Phase 1). Transportation Engineering Research Program (TERP). Albuquerque, NM. Department of Civil Engineering.

CHAPTER 4. FORENSIC INVESTIGATION OF A LOAD-TESTED POST GROUTED DRILLED SHAFT

A paper to be submitted to ASCE Journal of Geotechnical and Geoenvironmental Engineering

Anna Nadermann, Jeramy Ashlock, Brent Phares

Introduction

Post-grouting of drilled shafts has been employed around the globe for approximately 5 decades, and has recently experienced increased usage in the U.S. Alternately referred to as tip grouting or base grouting, the technique involves pressure grouting to preload the soil below the shaft tip. The perceived advantages of post-grouting are (1) increased mobilization of end bearing capacity within service displacement limits by compressing loose or relaxed soils and construction debris, (2) quality assurance through verification of shaft capacity based on the achieved grouting pressure, and (3) cost savings by enabling shafts in sandy soils to be shortened due to the increased usable end bearing. The 2010 replacement of the Broadway (US 6) Viaduct in Council Bluffs, IA was the first Iowa Department of Transportation project to implement post-grouting of drilled shafts. The viaduct is 1,537 ft in length between centerlines of the abutment bearings and includes 11 piers and a total of 53 production post-grouted drilled shafts.

Nearly all design methods for drilled shafts rely primarily on the side shear component and utilize only a fraction of the end bearing because of the large displacements required to fully mobilize the ultimate end bearing capacity. A design technique being used worldwide to regain some of this end bearing is pressure grouting (i.e. post grouting or base grouting) the shaft (Mullins et al. 2006). Such a process allows the soil below the shaft tip to be pre-compressed before the shaft is loaded. The technique requires a grout distribution system to enable high-pressure injection of grout below the base of the shaft after the concrete has cured. Pressure to which the grout can be pumped is dependent upon the available side shear so as to prevent failure during the grouting process.

Two load test programs featuring grouted and ungrouted shafts were carried out for the Broadway Viaduct site to evaluate the capacity increase due to post-grouting, assess the cost effectiveness and suitability of the technique, and determine parameters for use in design. The first load test program (LTP1) was performed in 2008 and included Statnamic load tests of one 55 ft long ungrouted control shaft and two grouted shafts 55 and 65 ft in length. The test shafts featured tube-a-manchette (sleeve port) grout distribution systems and were installed with a center to center spacing of 40 ft in an equilateral triangle pattern. The grout tubes became partially plugged during grouting and the resulting unit ultimate end bearing values determined by Statnamic testing were lower than predicted. Based on the Statnamic test results, it was estimated that grout pressure acted on only 50% of the pressure plate area (CH2MHill, 2008). In an effort to answer questions raised by LPT1 and provide useful parameters for design, a second load test program (LTP2) was performed adjacent to the Broadway Viaduct in 2010. LTP2 featured Osterberg cell (O-cell) load tests of one 75 ft ungrouted control shaft and one 75 ft grouted shaft with a flat-jacking grout distribution system. Additionally, four Geokon model 4850 stress cells were installed in the grout distribution plate to verify whether the grout pressure acted over the entire shaft area. Both test shafts were fitted with a series of strain gages for monitoring during load testing and for later analysis of the post grouting and load testing.

A substantial volume of grout was pumped below the tip of the post-grouted shaft in three stages, yet only a fraction of the target grouting pressure was achieved. Relative to the ungrouted control, the grouted shaft exhibited a greater initial stiffness but no increase in ultimate end-bearing capacity. This paper details the site conditions, grouting program, load test results and the findings of a groutability study and forensic investigation conducted in an effort to determine the spatial distribution of the grout and explain the poor performance of the post-grouted shaft in LTP2.

Site Description

LTP2 consisted of two test shafts referred to as TS3 (ungrouted) and TS4 (grouted). Subsurface investigation at the centerlines of the two shafts indicated that the soil consisted primarily of fine sand with silt over a layer of silty clay between 18.5 and 23.5 ft, underlain by loose to dense fine sand with traces of gray fat clay, gravel and lignite below 63 ft. The

water table was located at a depth of approximately 20 ft. The test shafts were 75 ft. long with a 66 in. diameter to a depth of about 11 ft. and 60 in. diameter for the remainder of the shaft. The bottoms of the O-cells were located at a depth of 60 ft to balance failure between end-bearing and upward shearing modes.

Background

This section focuses on the sequence of events for LTP2. The capacity of the drilled shafts is discussed followed by the post grouting procedures and the load test. Finally, the production shaft post grouting is discussed.

Capacity of Ungrouted and Grouted Drilled Shafts

The capacity of the shafts was calculated using the AASHTO design method (AASHTO 1998), in which the unit side resistance is represented in clayey soils by

$$q_s = \alpha S_u \tag{4.1}$$

and in sandy soils by

$$q_s = \beta \sigma'_{vo} \tag{4.2}$$

where α is an adhesion factor, S_u is the mean undrained shear strength, β is a load transfer coefficient and σ'_{vo} is the vertical effective stress. The unit end bearing is related empirically to the SPT blow count by

$$q_p \text{ (ksf)} = 1.2N \tag{4.3}$$

where N is representative of the soil within two diameters below the shaft tip and q_p is in ksf. The load transfer coefficient is taken as

$$\beta = \begin{cases} \frac{N}{15}\left(1.5 - 0.135\sqrt{z}\right), & N < 15 \\ 1.5 - 0.135\sqrt{z}, & N \geq 15 \end{cases} \tag{4.4}$$

Using Equations 4.1 – 4.4, the total side resistance and ungrouted end bearing capacities of TS4 were determined to be Q_s = 1723 kips and Q_p = 342 kips, respectively, for a total capacity of 2065 kips. The ungrouted total side resistance and ungrouted end bearing capacities of TS3 were determined to be Q_s = 1112 kips and Q_p = 330 kips, respectively, for a total capacity of 1442 kips. These capacities do not include a factor of safety and ignore the top five feet of the shaft as recommended by the AASHTO design method.

Mullins et al. (2006) developed an empirical design method for post grouted drilled shafts in sands based on studies involving full-scale Statnamic tests. In the method, the ratio of the maximum grouting pressure (GP_{max}) to the ungrouted end bearing capacity (q_p) at 5%D displacement is referred to as the grouting pressure index (GPI). The maximum grouting pressure is calculated as that which would mobilize the ultimate side shear capacity in uplift using an appropriate factor of safety. The unit end bearing capacity of a post grouted drilled shaft is then related to the unit ungrouted end bearing capacity through the tip capacity multiplier (TCM) as shown here:

$$q_{grouted} = (TCM)q_p \tag{4.5}$$

where the empirical tip capacity multiplier (TCM) given in Mullins et al. (2006) is

$$TCM = 0.713 \cdot GPI \cdot \%D^{0.364} + \frac{\%D}{0.4 \cdot \%D + 3} \tag{4.6}$$

and %D is the chosen allowable tip displacement expressed as a percentage of the shaft diameter. According to that study, post grouting of shafts tipped in formations other than sand (i.e. clays, silts, and rock) can also prove beneficial. For instance, side shear and end bearing can be engaged simultaneously for pressure grouted shafts tipped in rock. More recently, a modification of the TCM of Eq. 4.6 was demonstrated by Dapp et al. (2010) to more closely match observations from nine O-cell tests of 7.5 ft diameter 200 ft long post-grouted drilled shafts at the Audubon Bridge in Louisiana.

Using the calculated side shear resistance for TS4 of 1723 kips, the GP_{max} was calculated to be 609 psi, with a factor of safety FS = 1. This grouting pressure coupled with the calculated ungrouted end bearing of 342 kips leads to a GPI of 4.8. Stipulating a displacement limit of one inch, by Eq. 4.6, the TCM for TS4 is 4.9. Using Eq. 4.5 then provides a grouted capacity for TS4 of $Q_{p\text{-}grouted}$ = 1635 kips

Post Grouting Procedure

Prior to the post grouting of TS4; the integrity of the test shafts was investigated. A SoniCaliper test and a Cross-hole Sonic Logger (CSL) test were performed. Both tests indicated there were no anomalies in the test shafts.

The post grouting procedure was carried out by Applied Foundation Testing and was observed by the authors. The grout distribution apparatus used for TS4 was a flat jack grout

distribution plate. Ash Grove Type I/II Portland Cement and water were used for a neat cement grout with a starting water/cement ratio of 0.50. This ratio was incrementally decreased to a minimum of 0.42 in the second and third grouting stages. Based on the results of LTP1 (see Farouz et al., 2010) the target grout pressure was 650 psi with a maximum permissible displacement of 0.25 in. and a minimum grout volume of 3.0 ft^3 pumped below the toe of the drilled shaft. However, after pumping more than 34 ft^3 of grout below the shaft, the grout pressure did not build as expected and staged grouting was implemented. A total of three stages were used without approaching the target grout pressure. The staged grouting followed the procedure outlined in Mullins (2004). Table 4 lists a summary of the results for all three stages. The maximum sustained grout pressure was 140 psi and the final volume of grout placed was 156 ft^3 (5.7 yd^3), which is equivalent to a 6.7 ft diameter sphere, or a cylinder of diameter equal to the shaft with a height of 7.9 ft. For reference, a grout pressure of 660 psi was achieved in LTP1 with a grout volume equivalent to a cylinder of only 1 ft height.

Table 4. Test Shaft Post Grouting Results

Stage	Maximum Grout Pressure (psi)	Upward Shaft Displacement (in.)	Net Grout Volume Placed ($ft.^3$)
1	90	0.031	34.3
2	140	0.026	98.1
3	90	0.019	23.1

TS3 and TS4 were instrumented with a total of 22 Geokon Model 4911 vibrating wire rebar strain gages at the depths listed in Table 5 (LoadTest, 2010) for analysis purposes as well for monitoring during load testing. AFT provided the authors with the data obtained during grouting, the data was corrected according to the strain gage manuals including temperature effects. Further analysis, by the authors, of the strain data during the post grouting process revealed the shaft was in bending about the North-South axis and the East-West axis during all three stages of grouting.

During first stage of grouting there was almost negligible bending in both directions at the tip of the shaft. The bending moments about the North-South axis, according to the right-handed coordinate system, were negative while the bending moments about the East-West

axis were positive during the first stage of grouting. The largest bending forces during the first stage were predominately about the North-South axis

Table 5. Strain Gage Locations

Strain Gage Level	Distance Below Top of Shaft (ft.)	Number of Strain Gages per Level
1	73.3	4
2	65.3	3
3	55.3	3
4	45.3	3
5	35.3	3
6	25.3	3
7	10.3	3

and occurred just below and just above the O-cell which was located at a depth of 60 ft. The bending forces began to diminish along the length of the shaft above the O-cell during the first stage of grouting. Bending in the first stage of grouting was in a consistent direction over the length of the shaft and over the duration of time. During the second stage of grouting the bending forces were of similar magnitude in both directions but the strains did not diminish with distance above the O-cell. Also unlike the first stage, during the second stage of grouting the direction of bending was inconsistent over the length of the shaft and over the duration of grouting. The bending forces were much more erratic and complex during the second stage of grouting as compared with the first stage. Bending about the North-South axis during the third stage of grouting was similar that of the first stage of grouting, with the largest bending forces concentrated near the O-cell and diminishing with distance from the O-cell. The bending forces about the East-West axis during the third stage were consistent with time similar to the first stage, though the bending forces with depth were not similar to the first stage. During the third stage of grouting the largest bending forces occurred about the East-West axis and nearest to the ground surface rather than nearest the O-cell.

Load Testing

Each test shaft was equipped with a 24 inch diameter, 3,000 kip Osterberg cell (O-cell) installed at a depth of 60 ft. Standard load test instrumentation also included three displacement transducers to measure expansion between the top and bottom O-cell plates,

two telltales to measure shaft compression, and two automated digital survey levels to measure the top of shaft displacement.

A comparison of the load-displacement curves for the two test shafts is shown in Figure 14. As seen in the figure, the grouted TS4 exhibited an initially stiffer response both above and below the O-cell, and a more sudden, plunging failure of the lower portion at a smaller ultimate capacity than the ungrouted TS3. The maximum bi-directional load for the ungrouted shaft was 1,308 kips inducing displacements of 0.81 in. upward and 4.65 in. downward above and below the O-cell, respectively. For the grouted shaft, however, the maximum applied load was 1,221 kips with displacements of 0.37 in. upward and 5.30 in. downward. The failure of TS4 is indicative of a plunging mode indicating no increase in tip capacity from grouting. The greater stiffness may be a result of a slight increase in shaft area near the tip due to grout traveling up the sides (see Fernandez et al. 2007).

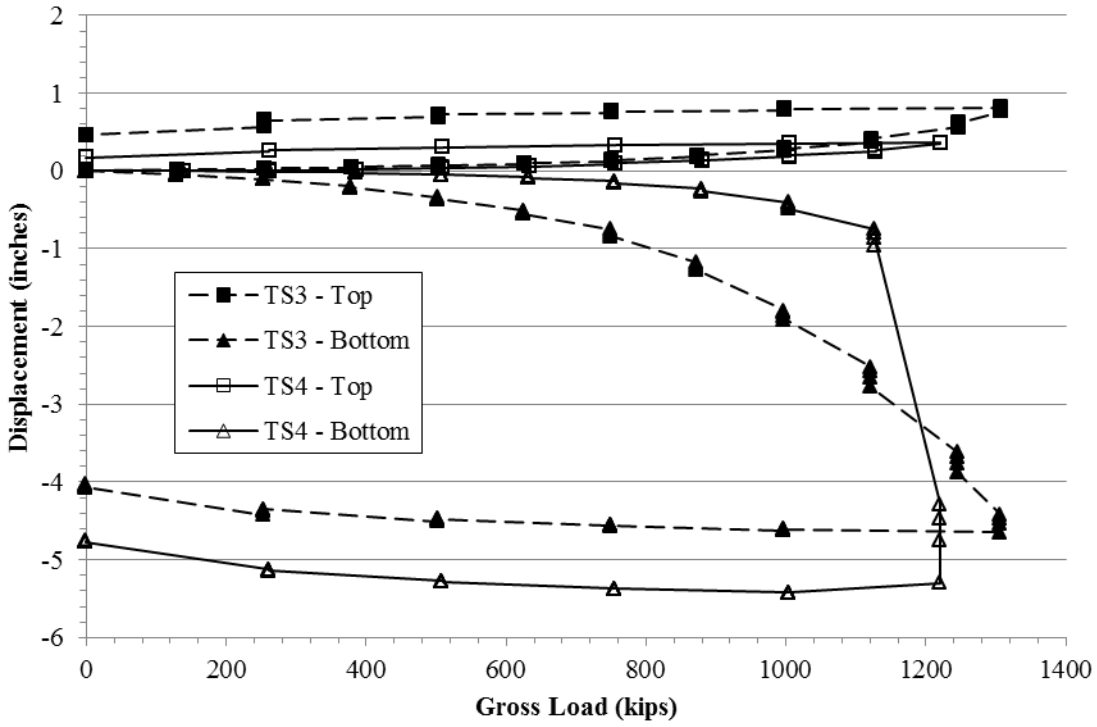

Figure 14. Comparison of load with displacement for TS3 and TS4

An increased stiffness can also be attributed to the influence of skin friction stress reversal as described in Ruiz et al. (2009), although this is less likely because the grout pressure was not locked-in for this shaft. The difference in grouted and un-grouted stiffness is quantified in

Figure 15, which contains the incremental secant stiffness of the soil-shaft systems during each load step. As shown in the figure, the initial stiffness of TS4 is nearly nine times greater than the ungrouted TS3. Table 6 indicates the mobilized net unit side shear of the shafts at the maximum applied load as calculated by LoadTest and the authors.

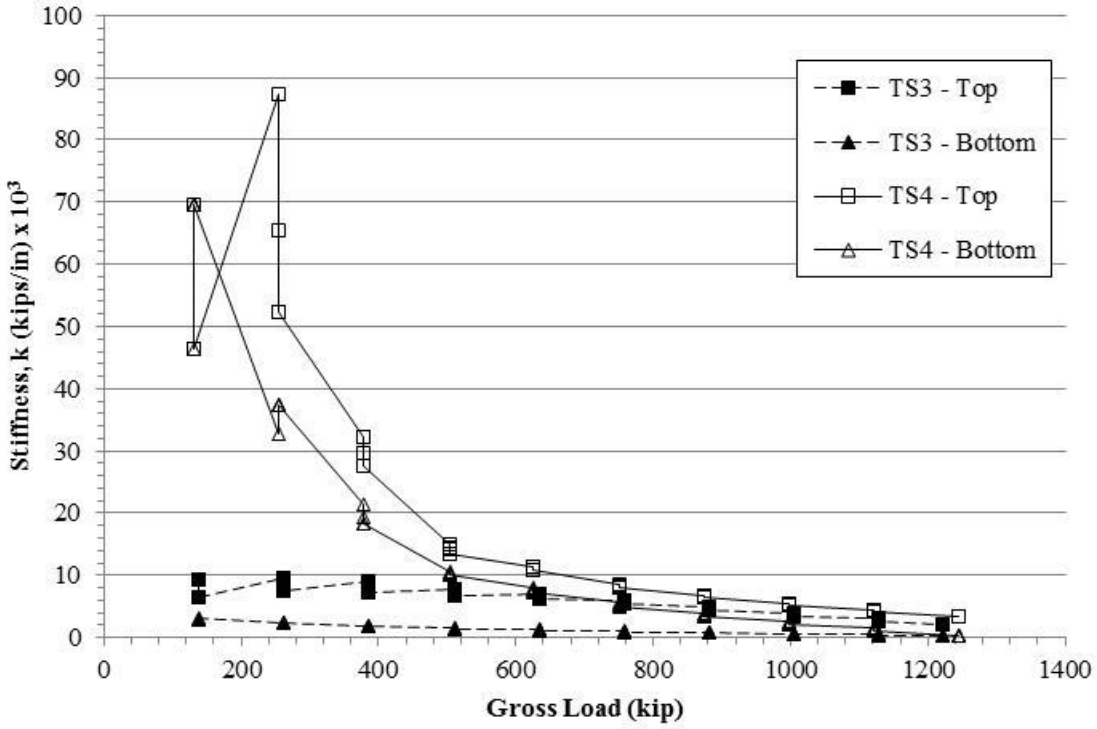

Figure 15. Comparison of shaft stiffness for TS3 and TS4

The difference in reported net unit side shear values can be attributed to the difference in reported buoyant weight of the shaft above the O-cell. The net load, defined as the force applied by the O-cell minus the buoyant weight of the shaft above the O-cell, is used to determine the net unit side shear above the O-cell. The buoyant weights above the O-cell as reported by LoadTest for TS3 and TS4 were 139 kips and 142 kips, respectively. The authors determined the buoyant weight above the O-cell of TS3 and TS4 to be 139 kips for both shafts, leading to the slightly different values of net unit side shear with depth. This discrepancy in buoyant weight could likely be due to use of water table elevations differing by approximately 2.5 feet, which is within the range of variation for the various boring logs from the project. However, the water table elevations used by the authors were consistent with those given in the LoadTest reports.

To calculate the maximum end bearing load of the shafts, the net unit side shear measured between Level 2 and Level 1 strain gages was also assumed to act between Level 1 and the shaft tip. The net side shear force acting on each shaft section was subtracted from the maximum O-cell load to determine the resultant axial force in the shaft at strain gage

Table 6. Mobilized Net Unit Side Shear as Reported by LoadTest (2010) and the Authors

	LoadTest				Authors	
	TS3 (ungrouted)		TS4 (grouted)		TS3 (ungrouted)	TS4 (grouted)
Zone	Load Direction & Disp. (in.)	Net Unit Side Shear (ksf)	Load Direction & Disp (in.)	Net Unit Side Shear (ksf)	Net Unit Side Shear (ksf)	Net Unit Side Shear (ksf)
Top - Level 7	↑ 0.80	0.20	↑ 0.35	0.21	0.21	0.21
Level 7 - Level 6	↑ 0.80	0.31	↑ 0.35	0.55	0.33	0.62
Level 6 - Level 5	↑ 0.80	1.85	↑ 0.35	0.89	1.92	0.93
Level 5 - Level 4	↑ 0.81	1.37	↑ 0.36	1.30	1.41	1.35
Level 4 - Level 3	↑ 0.81	1.25	↑ 0.36	0.81	1.25	0.83
Level 3 - O-cell	↑ 0.81	4.29	↑ 0.36	5.31	4.45	5.40
O-cell - Level 2	↓ 4.65	3.82	↓ 5.30	5.93	3.85	5.97
Level 2 - Level 1	↓ 4.65	1.29	↓ 5.30	0.11	1.31	0.10

elevations as well as the end bearing. Using the nominal diameter of 60 in., the authors determined the end bearing load to be 805 kips for the ungrouted TS3 and 736 kips for the grouted TS4, corresponding to end bearing pressures of 41.0 ksf and 37.5 ksf , respectively. The end bearing loads and pressures determined by the authors agree with those reported by LoadTest. The end bearing capacity of the grouted shaft is 9% lower than that of the ungrouted shaft, indicating that post-grouting of TS4 did not improve the end bearing capacity. This lack of improvement is likely due to the inability to reach the design grouting pressure. As a result, three mechanisms believed to contribute to capacity improvement; namely preloading the soil below the shaft tip, stress reversal of the skin-friction, and increased bearing area by formation of a grout bulb were not realized (see Fernandez et al. 2007, Ruiz and Pando 2009).

Prior to the construction of TS3 and TS4, confirmation borings were completed in an attempt to have the most accurate soil profiles possible for the shafts. The SPT results of these borings indicated TS3 and TS4 to be tipped in fine to coarse sand with traces of sandy clay and gravel. Within three shaft diameters above TS3 and TS4 the average SPT blow

counts were 9.3 and 12.7, respectively. Within three shaft diameters below TS3 and TS4 the average SPT blow count was 13.7 and 16.0. The SPT results indicates that both TS3 and TS4 were tipped in similar material, thus the lack of improvement for the post grouting of TS4 cannot be attributed to the shafts being tipped in dissimilar material.

Post Grouting of Production Shafts

The intent of LTP2 was to allow all production shafts on the project to be shortened based on the increase in mobilized end-bearing observed for TS4. Although grouting of TS4 was unsuccessful, grouting of the production shafts was still performed as planned while forgoing any shortening of the shafts. The results of the post grouting of the production shafts can be found in Table 7, the results of the test shafts are included for comparison purposes.

Table 7. Post Grouting Results for All Drilled Shafts

Drilled Shaft	Drilled Shaft Diam. (ft)	As-built Drilled Shaft Embed. Length (ft)	Post Grouted	Measured Ultimate Capacity (kip)	Measured Unit Ultimate End Bearing (ksf)	Measured Ultimate End Bearing (kip)	Measured Ultimate Side Resistance (kip)
TS3*	5	75	No	1513	41	805	708
TS4*	5	75	Yes	1340	37	736	604
P1N	5	50	Yes	1534	42	820	714
P1Shaft1	5	50	Yes	2439	65	1272	1167
P2N	5	70	Yes	2235	60	1188	1048
P2S	5	70	Yes	2733	73	1436	1296
P3N	5	65	Yes	2656	71	1394	1263
P3S	5	65	Yes	1673	46	902	771
P10Shaft1	5	70	Yes	3553	94	1846	1706
P11Shaft 2	5	55	Yes	2261	60	1188	1073
EAbutS1	5	50	Yes	1698	46	902	796
EAbutS2	5	50	Yes	1941	52	1024	918

*Test shaft

Post grouting the production shafts provided the benefit of verifying the mobilized end bearing and side shear of the production shafts at a specified maximum upward displacement of 0.25 in. For this purpose, the verified end bearing capacity of production shafts was determined as the maximum grouting pressure multiplied by the shaft tip area of 19.64 ft^2. The verified side shear capacity was calculated as the actual grouting force at the tip minus

the shaft buoyant weight. Using this procedure, Figure 16 shows the predicted end bearing, shear resistance and total capacities as they correlate to the measured values for the six production shafts which had grouting data available. There appears to be a stronger correlation in the predicted versus measured values for shear resistance than for the end bearing.

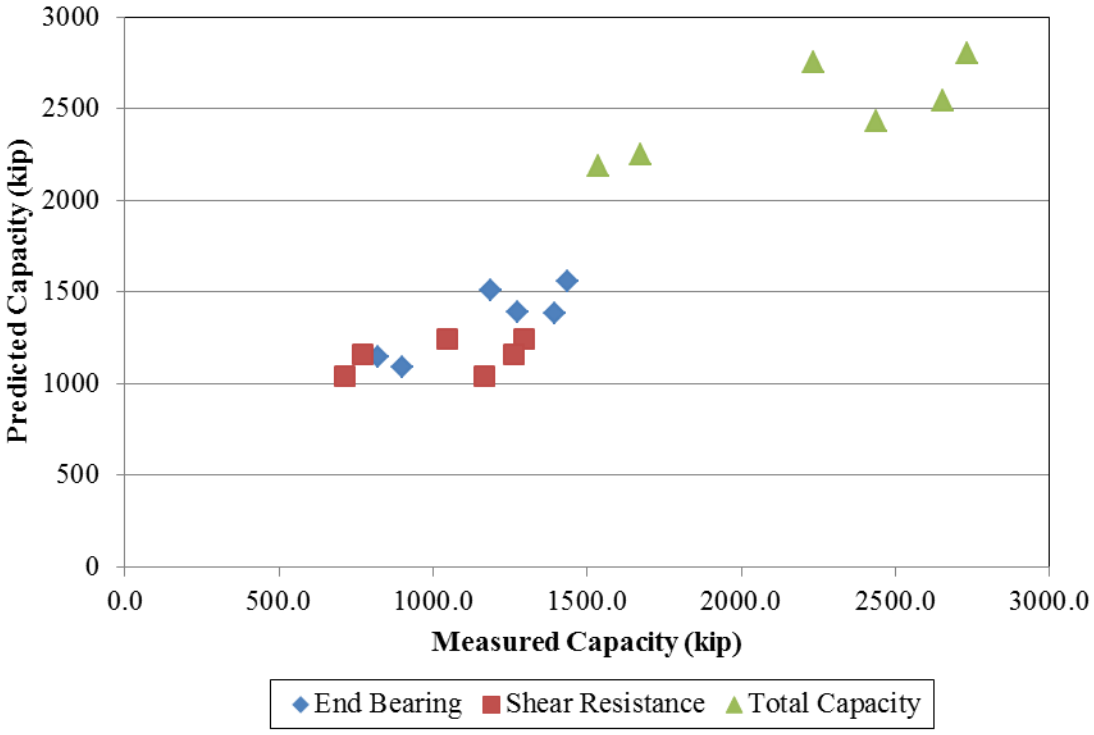

Figure 16. Predicted production shaft capacity versus measured production shaft capacity

Table 8 provides the ratio of predicted grouted capacity to measured grouted capacity of the production drilled shafts which were used in Figure 16. The predicted side shear capacity of production shafts was determined using the average unit side shear acting over three sections of TS4 during the O-cell test. The unit shear resistance values used were 0.25 ksf for the upper 20 ft, 2.0 ksf between 20 and 60 ft, and 2.2 ksf between 60 and 75 ft. Of the six production shafts analyzed, three had under predicted the grouted side resistance by up to 11%. The grouted side resistance of production shafts P2N and P3S closely matched their measured grouted side resistance. The remaining three shafts were over predicted by a range of 18% to 51%. The predicted end bearing capacities of P1N and P2N closely matched their

measured grouted end bearing, while the predicted end bearing capacities of P1Sh1, P2S, and P3N were over predicted by a range of 31% to 70%. The predicted end bearing capacity of

Table 8. Predicted Capacities of Production Shafts

Drilled Shaft	Predicted Ultimate Side Resistance (kip)	Predicted Ultimate End Bearing (kip)	Predicted Ultimate Total Capacity (kip)	Post Grouted	Predicted/ Measured Ultimate Side Resistance	Predicted/ Measured Ultimate End Bearing	Predicted/ Measured Total Capacity
P1N	1042	1144	2186	yes	89%	90%	90%
P1Sh1	1042	1392	2434	yes	146%	170%	159%
P2N	1240	1510	2750	yes	96%	105%	101%
P2S	1240	1560	2800	yes	118%	131%	125%
P3N	1160	1380	2540	yes	151%	153%	152%
P3S	1160	1092	2252	yes	92%	78%	85%

P3S was under predicted by 22%. The degree of over prediction was similar for both side resistance and end bearing capacities and therefore the over prediction of the total capacity of the shafts followed the same trend. The predicted total capacity of P2N was within 1% of the measured total capacity. The predicted total capacity of P1N and P3S were under predicted by up to 15% while the total capacity of the remaining three shafts was over predicted by a range of 25% to 59%.

The improvement of the capacity of the drilled shafts due to post grouting can be seen in Table 9.

Table 9. Improvement Due to Post Grouting of Production Shafts

Drilled Shaft	Ungrouted Predicted Ultimate Side Resistance (kip)	Ungrouted Predicted Ultimate End Bearing (kip)	Ungrouted Predicted Ultimate Total Capacity (kip)	Grouted/ Ungrouted Verified Side Resistance	Grouted/ Ungrouted Verified End Bearing	Grouted/ Ungrouted Total Capacity
P1N	1042	518	1560	112%	246%	156%
P1Sh1	1042	518	1560	69%	158%	98%
P2N	1240	448	1688	105%	321%	161%
P2S	1240	448	1688	84%	265%	133%
P3N	1160	448	1608	66%	201%	104%
P3S	1160	448	1608	109%	311%	165%

The predicted ungrouted side resistance was determined using the same unit shear resistance factors as were used above for the grouted calculations. The predicted ungrouted end bearing was determined using Eq. 4.3. The side resistance of the shafts saw little to no improvement from post grouting, although the post grouting did improve the end bearing, more than three times in some cases. The improvement of end bearing due to post grouting ranged from 58% to 221% over the predicted ungrouted end bearing. Five of the six productions shafts saw improvement in total capacity from post grouting. While production shaft P1Sh1 did not see improvement in total capacity and production shaft P3N saw a minimal 4% improvement in total capacity, the remaining four production shafts saw verified/minimum improvements ranging from 33% to 65%.

Forensic Investigation

A forensic investigation was undertaken to determine the reason for the lack of grout pressure buildup beneath TS4 despite staged grouting with a large grout take of 6 cubic yards, which led to poor performance in the load test. In contrast to the tube-a-manchette grout distribution system of LTP1, measurements from the stress cells during grouting indicated that grout pressure acted uniformly over the shaft tip with the flat-jacking system. However, the migration path of the rather large volume of grout is unclear. Possible migration paths include grout traveling vertically up the sides of the shaft, horizontally in a gravel seam or highly permeable layer, downward directly below the shaft, or possibly entering a large void. The experimental plan included five boreholes spaced around the perimeter of the shaft, in which SPT tests with sampling were performed at 5 ft intervals for the first 40 ft, and continuously between depths of 40 and 85 ft. Due to the predominantly sandy profile, mud rotary boring was used, with a 2-1/4 inch rotary bit and bentonite slurry. The continuous sampling and SPT testing were intended to identify the location of grout through increased blow counts and physical confirmation of the presence of grout in the samples. Figure 17 shows the blow counts for confirmation boreholes at the centerlines of TS3 and TS4 along with those in which grout was found in the forensic investigation boreholes. Over the 70 to 80 ft depth, which is the region in which layers of grout were found on the North and East sides of TS4, the forensic boreholes C1 and C2 exhibit slightly higher blow counts compared to the confirmation borehole of TS4. The forensic boreholes were

placed within 3 to 14 inches of the shaft perimeter in an attempt to achieve a balance between detection of a grout bulb near the shaft tip or a layer of grout formed by horizontal flow through a gravel seam.

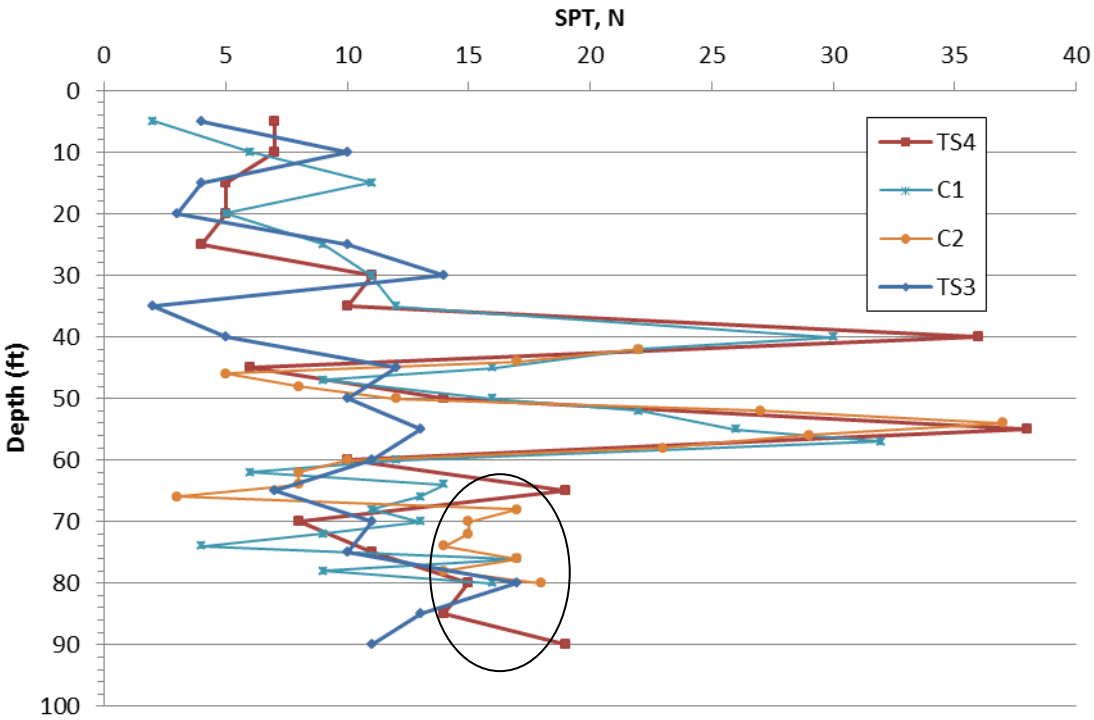

Figure 17. Comparison of blowcount before drilling and during forensic investigation

Groutability Study

Prior to field testing, the groutability of the soil was studied by analyzing samples taken from TS4 as well as three production shafts. Four methods for determining the groutability of a soil sample employing various soil and grouting parameters were examined. Each method uses a different relationship to determine a groutability index, N_g. Table 10 lists the soil parameters, grouting parameters, and relationships for each method.

Three of the methods consider only ratios of grain-sizes of soil and grout, which is primarily relevant for permeation grouting. A study by Akbulut and Saglamer (2002) further incorporated relative density (D_r) and finer content (FC, defined as percent passing a 0.6 mm sieve), grouting pressure (P), and grout water to cement (w/c) ratio, as each of these parameters also affects the groutability of a soil. However, it should be noted that the study was focused on permeation rather than compaction grouting, and had the following

limitations: (1) the finer content ranged from 0 to 6%, (2) the water-to-cement ratio was between 0.8 and 2.0, and (3) grouting pressure did not exceed 200 kPa (29 psi). Staged grouting as performed for TS4 is often designed to cause permeation grouting followed by compaction grouting. Permeation grouting can allow for easy creation of large grout bulbs, while compaction grouting can dramatically improve soil stiffness (Mullins et al. 2001). Both grouting methods can therefore create conditions known to improve the end-bearing of drilled shafts.

Table 10. Groutability Study Relationships

Method	Soil Parameters	Relationship	Comments
Akbulut & Saglamer	D_{10}, d_{90}, k_1, w/c, FC, k_2, P, D_r	$N_g = \frac{D_{10}}{d_{90}} + k_1 + \frac{w/c}{FC} + k_2 \frac{P}{D_r}$	If N>28 granular soil can be grouted. If N<28 granular soil cannot be grouted,
Burwell (1)	D_{15}, d_{85}	$N_g = \frac{D_{15}}{d_{85}}$	If N>25 grout can successfully be injected, but apply Burwell (2) as well. If N<11 grout cannot successfully be injected.
Burwell (2)	D_{10}, d_{95}	$N_g = \frac{D_{10}}{d_{95}}$	If N>11 grouting is possible. If N<5 grouting is not possible.
Incecik & Ceren	D_{10}, d_{90}	$N_g = \frac{D_{10}}{d_{90}}$	If N>10 grouting is possible.

where,

D_x = the diameter through which x% of total soil mass is passing

d_x = the diameter through which x% of total grout mass is passing

D_r = relative density

k_1 = constant based on test experiences, taken as 0.5 (Akbulut and Saglamer 2002)

k_2 = constant based on test experiences, taken as 0.5 (Akbulut and Saglamer 2002)

FC = finer content % of the total soil mass passing through 0.6 mm sieve

w/c = water-to-cement ratio

Three soil samples from production shafts (P3-S2, P2-S2, and E. Abut.) and two from TS4 (TS4 Light and TS4 Dark) were collected during excavation of the shaft tips. For comparison purposes, data collected from soil samples at the base of the post grouted shafts of LTP1 were also investigated. The LTP1 data from Test Shaft 1 (TS1S-13) and Test Shaft 2 (TS2S-14) were used. The soil and grouting parameters for each of the soil samples are listed in Table 11.

Table 11. Soil and Grouting Parameters (Actual Grouting Pressure)

Samples	Soil Parameters					Grouting Parameters					
	D_r	D_{10}	D_{15}	D_{85}	FC	w/c	P (psi)	P (kPa)	d_{95}	d_{90}	d_{85}
P3-S2	0.40	0.0087	0.0707	1.1004	0.81	0.44	319	2198	0.043	0.034	0.028
P2-S2	0.46	0.0723	0.1154	0.4142	0.89	0.43	508	3500	0.043	0.034	0.028
E. Abut.	0.48	0.0799	0.1195	0.4002	0.96	0.50	362	2494	0.043	0.034	0.028
Light	0.38	0.0821	0.1193	0.3397	0.99	0.46	107	737	0.043	0.034	0.028
Dark	0.33	0.0324	0.0954	1.3353	0.74	0.46	107	737	0.043	0.034	0.028
TS1S-13*	0.40	0.0852	0.1301	1.5996	0.63	0.48	662	4561	0.043	0.034	0.028
TS2S-14*	0.52	0.0886	0.1159	0.3362	0.93	0.48	662	4561	0.043	0.034	0.028

*Sample from LTP1

Groutability was analyzed using the design water/cement ratio of 0.5 and grouting pressure of 650 psi (4550 kPa) as well as the average actual w/c ratio and grouting pressures achieved, none of which reached the target of 650 psi. The results of the groutability analysis using design parameters are shown in Table 12.

Table 12. Design Groutability Index

Samples	Akbulut & Saglamer		Burwell (1)		Burwell (2)		Incecik & Ceren	
	N_g	Comments	N_g	Comments	N_g	Comments	N_g	Comments
P3-S2	113	Groutable	2.5	Not groutable	0.20	Not groutable	0.26	Not groutable
P2-S2	102	Groutable	4.1	Not groutable	1.7	Not groutable	2.1	Not groutable
E. Abut.	97	Groutable	4.3	Not groutable	1.9	Not groutable	2.4	Not groutable
Light	123	Groutable	4.3	Not groutable	1.9	Not groutable	2.4	Not groutable
Dark	139	Groutable	3.4	Not groutable	0.75	Not groutable	0.95	Not groutable
TS1S-13*	118	Groutable	4.7	Not groutable	2.0	Not groutable	2.5	Not groutable
TS2S-14*	91	Groutable	4.1	Not groutable	2.0	Not groutable	2.6	Not groutable

*Sample from LTP1

Although the parameters of this study fall outside the ranges from which the equation of Akbulut & Saglamer was developed, the method indicates that all of the samples are groutable using the design parameters, whereas the other indices based on grain-sizes alone indicate that the soils are not groutable (Table 12). Using the actual pressures recorded

during grouting, the method of Akbulut and Saglamer indicates that the production shafts are groutable while TS4 is not (see Table 13), which agrees with the observed results.

Table 13. Actual Groutability Index

Samples	Akbulut & Saglamer		Burwell (1)		Burwell (2)		Incecik & Ceren	
	N_g	Comments	N_g	Comments	N_g	Comments	N_g	Comments
P3-S2	55	Groutable	2.5	Not groutable	0.20	Not groutable	0.26	Not groutable
P2-S2	79	Groutable	4.1	Not groutable	1.7	Not groutable	2.1	Not groutable
E. Abut.	54	Groutable	4.3	Not groutable	1.9	Not groutable	2.4	Not groutable
TS4-Light	22	Not groutable	4.3	Not groutable	1.9	Not groutable	2.4	Not groutable
TS4-Dark	24	Not groutable	3.4	Not groutable	0.75	Not groutable	0.95	Not groutable

This is simply due to the low achieved grouting pressure for TS4 which the method would not have predicted. However, use of a groutability index which takes into account the grouting pressure and fines content among other parameters may prove useful for efficiently identifying ungroutable soils on future projects. The forensic investigation described herein was undertaken to help determine why the design grouting pressure could not be achieved for TS4.

Ultrasonic Imaging Tests

Previous studies of tip grouting have revealed that grout commonly migrates upwards a distance of a few shaft diameters, covering the shaft in 1 to 2 inches of grout (Mullins, 2006). In addition to the increased stiffness and capacity resulting from three effects of grouting mentioned above, the diameter of the shaft is also effectively increased in this zone (i.e. skin grouting), further increasing the contributions to stiffness and capacity from skin friction. Although the SPT sampling program as planned may have been capable of identifying a horizontal grout flow or bulb, it could not realistically detect 1-2 inches of grout migrating up the surface of the shaft at depths of 65-75 ft. Similarly, grout flowing downward below the shaft tip would not be detected by vertical exploratory borings. A number of geophysical methods were therefore considered for imaging the extent of grout traveling up the surface of the shaft and below its tip. Among the methods considered were gamma-gamma logging, and cross-hole sonic logging (CSL) between existing CSL tubes in the shaft and additional tubes grouted into the surrounding soil. However, consultation with engineering firms experienced in nondestructive evaluation indicated that none of the currently available nondestructive

testing methods possessed sufficient resolution to detect a 1-2 inch thick layer of grout around the shaft perimeter at the required depths. Imaging of the shaft and grout was therefore attempted using a new experimental high-resolution ultrasonic p-wave imaging probe developed at UCLA (Brandenberg and Coe 2010).

The ultrasonic probe consists of a 2 in. x 4 in. stainless steel case with a pointed tip (see Figure 18). The probe uses an ultrasonic p-wave reflection imaging system to delineate the surface of foundations in soil (Coe 2010). The probe contains two piezoelectric ultrasonic transducers, acting as source and receiver, a signal amplifier, and a high voltage pulser circuit. The probe is attached to standard CPT rods and typically pushed into soft soils by a CPT rig. A digital string potentiometer was mounted on the drill rig to trigger the pulses at 1 cm intervals. The ultrasonic probe data acquisition system includes National Instruments signal generation, data acquisition, and oscilloscope cards in a PXIe chassis and a personal computer equipped with LabVIEW software.

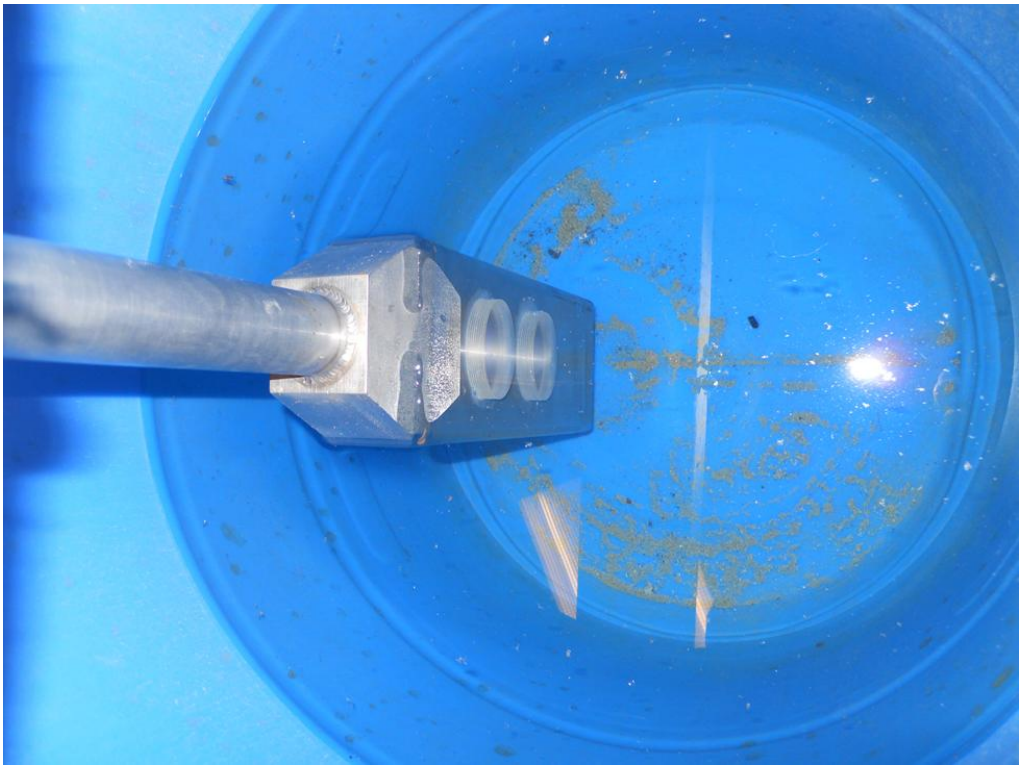

Figure 18. Ultrasound probe in 35 gallon drum of water

While the probe had previously been used to successfully image a foundation in soft bay mud (Brandenberg and Coe, 2010), the technique required modification for operation in the

fine sands at the Broadway Viaduct site. In particular, based on previous experience in the project area, the drillers indicated that the drill rig would not be able to push the probe and safely retrieve it because of the large resistance and collapsibility of the fine sands. To overcome these difficulties, two new approaches were devised for advancing the probe. The first approach involved drilling a 6.5 inch diameter borehole stabilized by bentonite drilling mud and polymer additives, then lowering the suspended probe into the pre-bored hole rather than forcing it into the sands. However, laboratory tests indicated that the ultrasonic p-wave was greatly attenuated by bentonite slurry, and the transducers were rendered unusable if polymer additives were used. The reduced effectiveness of the probe in the bentonite slurry may have been partially caused by a lack of complete saturation of sand in the lab despite vacuum saturation techniques. Therefore, it was decided to attempt this approach in the field as the sand was expected to be fully saturated in situ.

A second testing method was devised involving casing the same pre-bored hole with a 6 inch diameter PVC pipe, flushing the drilling mud from the pipe leaving it filled with water, then lowering the probe down the water-filled pipe. The delay lines of the ultrasonic transducers are optimized to work in water, and this approach would therefore minimize performance degradation associated with the suspended bentonite particles in the first approach. Laboratory tests indicated that the probe could image the inside of a 35 gallon drum filled with water, effectively "seeing through" the PVC pipe. However, the wall of the 6 inch diameter pipe caused multiple early reflections which combined with those from the target outside of the pipe. The early reflections were successfully minimized by attaching a horizontal circular divider plate between the source and receiver transducers in the gap between the probe and pipe, which also served as a centralizer for the probe body. The divider consisted of a sheet of rubber supported by an acrylic plate, and functioned as a wave-blocker for the unwanted early deflections.

Previous tests of the probe in sand by its developers revealed that complete saturation of the sand was necessary for useful signals, as the presence of small amounts of air resulted in scattering of the p-wave energy. While it is expected that saturation of the sand in the field should be near 100% given the age of the deposit and the depth below the water table, creating a fully saturated, large specimen in the laboratory required careful preparation. The

laboratory samples were therefore vacuum-saturated under a vacuum of 15 bar, while CO_2, was introduced into the bottom of the sample to displace air bubbles. The sample was then saturated from the bottom up using de-aired water. The results of the laboratory test of the ultrasound probe in a PVC cased borehole in a 35 gallon drum of saturated sand can be seen in Figure 19.

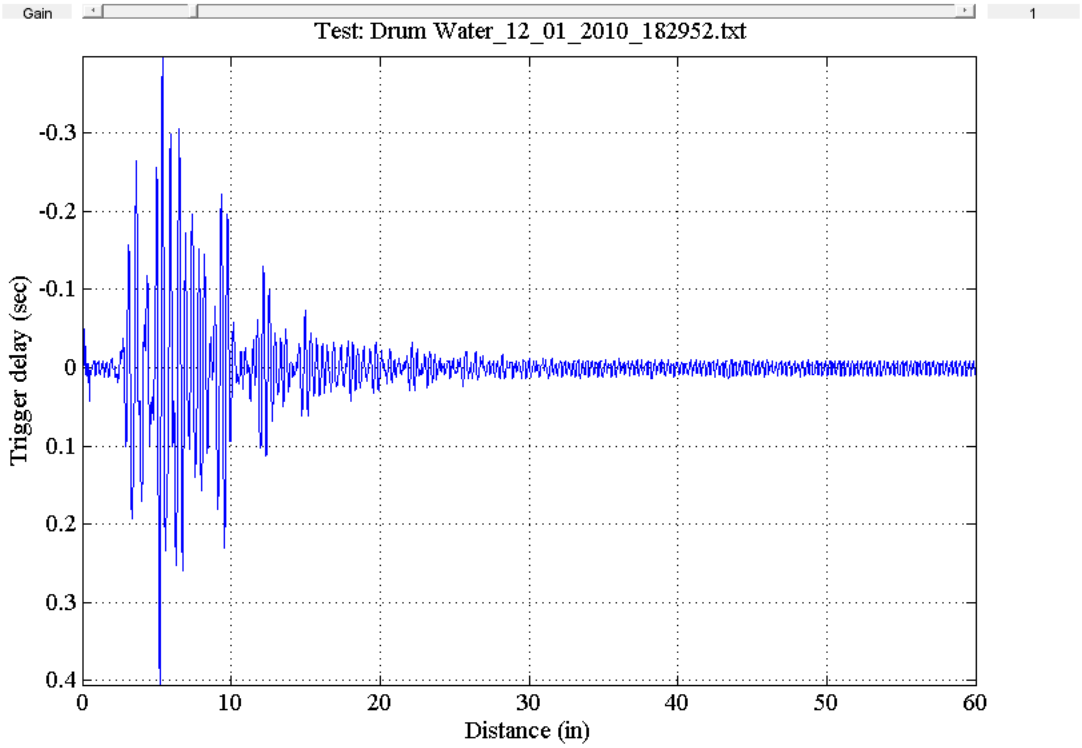

Figure 19. Signal plot with probe in 35 gallon drum of saturated sand with PVC

Continuous SPT Tests

Ultimately, five continuous sampling boreholes (C1 through C5) were placed around the diameter of TS4. The continuous sampling was started at 40 ft., as the grout would not likely have traveled this far up the side of the shaft. In general, continuous sampling continued to 5 ft. below the shaft base, a depth of 80 ft. The bore holes were located 8 to 10 in. from the perimeter of TS4 at the ground surface. Figure 20 shows the placement of the boreholes around TS4. According to the drillers, the water table was located at 18 ft. for boreholes C1, C2, and C3 while the water table was not reported for boreholes C4 and C5.

The first continuous sampling borehole, C1, revealed a layer of grout approximately 2 in. thick at a depth of 74 ft between a layer of fat clay with sand and a layer of gravel. A 3 in.

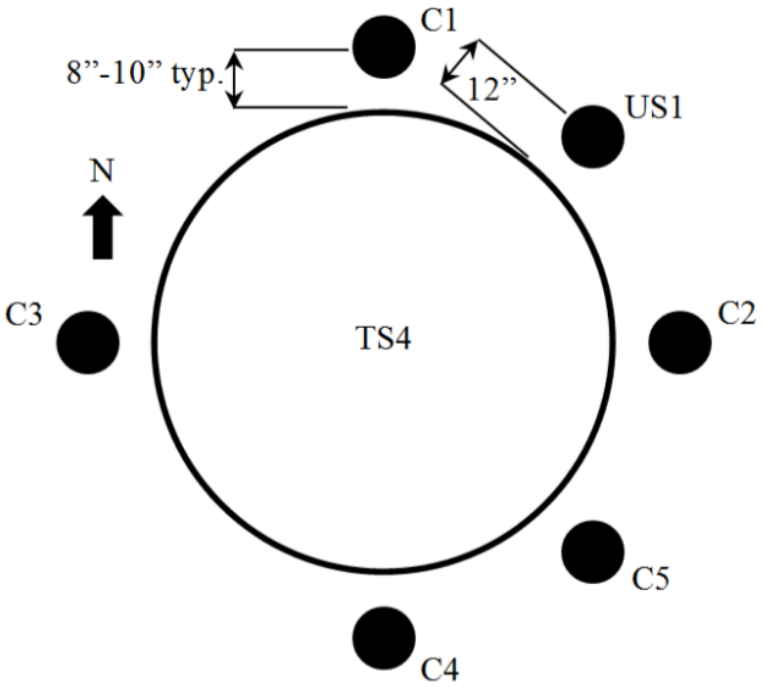

Figure 20. Forensic borehole locations around TS4

layer of grout was encountered at a depth of 74 ft in borehole C2 between layers of fat clay with sand. No grout was encountered in boreholes C3, C4, or C5. Borehole C4 revealed an apparent void from 58 to 62 ft. During drilling of borehole C4, the slurry mix entered the fractured CSL tubes at the O-cell location and began flowing out of the top of the CSL tubes at the shaft surface. Drilling could not be continued beyond this depth due to the loss of pressure. The apparent void was therefore likely cause by the fluid entering the O-cell and circulating to the surface. The loss of pressure caused the hole to collapse and drilling could not continue. Borehole C5 was drilled to a depth of 15 ft, below which the drilling rods were advanced with little resistance, even dropping in some regions, to a depth of 74 ft. No penetration tests were performed in borehole C5 above 74 ft due to the lack of penetration resistance, which is likely due to disturbance created by wash boring in the previous 4 boreholes. Three samples taken below 74 ft. indicated dense fine sands.

Results and Discussion

Groutability

Although some of the soils from the project site fell outside the range of parameters for which the groutability criteria in Akbulut & Saglamer (2002) were developed, the

groutability indices shown in Table 13 indicated that the soils in the vicinity of TS4 were less groutable than those at the production shafts. Although this is simply due to the lower achieved grouting pressure, the resulting groutability indices indicate that permeation grouting was unlikely and compaction grouting may have been occurring as intended. All of the production and test shafts were drilled with wet drill methods using bentonite slurry, and the soil samples were retrieved from the spoil piles during augering of the shafts. Therefore, the soil samples used in the groutability study may have contained fine particles from the drilling mud. This would increase the fines contents for the particle size distribution curves on which the groutability criteria depend, possibly altering conclusions regarding groutability. To examine this possibility, the results were verified by using particle size distribution curves for SPT samples taken during the drilling phase of LTP-1. These samples gave the same results as those obtained during construction of the production shafts, lending confidence to the other results.

Ultrasound

Preliminary field testing of the ultrasound probe indicated that the testing method would need to be modified for testing in fine sands. An important step in modeling the site conditions was to achieve full saturation of the fine sand in the laboratory. Full saturation of the sand would also improve the signal produced by the ultrasound probe as the transducers perform optimally in water, and air bubbles in partially saturated sands can cause a loss of wave energy due to scattering. The results of the laboratory tests indicate that the probe may require further development for use in fine sands. This investigation also demonstrated that the use of a wave blocker in conjunction with a water-filled, cased borehole may be a practical technique for using the ultrasonic probe in granular soils normally exhibiting borehole instability or collapse.

Based on the laboratory results, PVC cased holes were selected for the ultrasound probe at TS4. The same type of 6 in PVC pipe was used in the field as in the laboratory. Ten foot sections of PVC piping were connected using PVC couplers fastened with PVC glue and screws. The first ultrasound probed bore hole, US1, was installed approximately 12 in. from the edge of the shaft and 3.75 ft. from the center of the shaft (at ground surface), as shown in

Figure 20. US1 was installed to coincide with the direction of the major principal-axis of bending strains measured during grouting, to the northeast of the shaft. Table 14 shows the

Table 14. US1 Soil Profile

Depth (ft)	Comments
0-67	Sand/sandy clay
67-72	Stiff clay
72-73	Grout
73-74	Rock
74-80	Sand

soil profile encountered while drilling US1, which reveals a layer of grout approximately 12 in. thick at an approximate depth of 72 ft, sandwiched between a layer of fat clay (67-72 ft) and what was later revealed through SEM imaging to be lignin, or partially formed coal from 73 to 74 ft.

The 6 in PVC pipe was installed immediately after drilling but could not be advanced beyond a depth of 37 ft due to collapse of the borehole. The ultrasound probe was tested the next day after flushing the casing with water. Borehole US1 was then probed to the depth of the PVC casing and the cone tip on the probe allowed the probe to be pushed into the sand about one to two feet before the wave blocker bracket was damaged. Figure 21 shows the image produced from the ultrasound probe of borehole US1.

As seen in Figure 21, the probe produced reflections from the PVC casing but could not image the shaft through the fine sands. Therefore, the ultrasound imaging was then abandoned and the continuous sampling and SPT tests were used to continue the investigation.

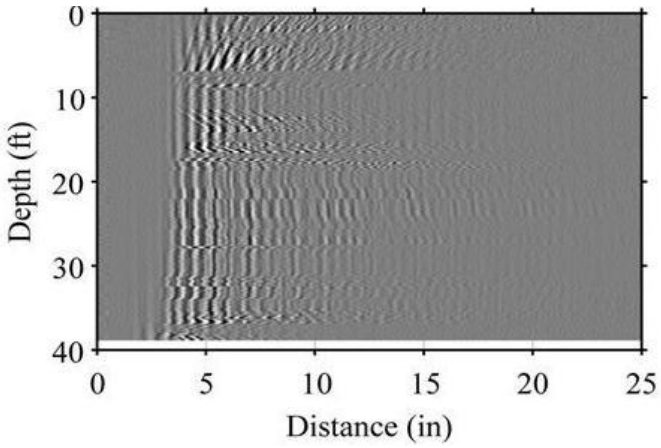

Figure 21. Ultrasound image from bore hole US1

Continuous SPT Data

Performing continuous SPT tests on the soil immediately surrounding TS4 revealed a minimal presence of grout. A six inch grout layer was found on the North side of the shaft and a three inch grout layer was found on the East side of the shaft, both at approximate depths of 74-75 ft, coinciding with the shaft tip. No grout was found on the South or West sides of the shafts.

Preceding the drilling of boreholes C4 and C5, there was extensive flooding of the Missouri River, within two miles of the project site, and water levels were still high during the drilling of these boreholes. High water levels in the area could mean a higher water table at the site. The change in pore water pressure associated with an increased water table may have disturbed the soil at borehole C5, although rotary mud drilling at the previous boreholes may have caused the lack of resistance starting at 15 ft and ending with the cavity around the O-cell depth. When drilling borehole C2 the drill bit and rod could have strayed from the course of vertical and moved toward the future location of borehole C5, possibly disturbing the soil and impacting the results of the drilling of borehole C5.

Conclusions

Post grouting can be used to verify the capacity of drilled shafts while post grouting for improved end bearing is sensitive to the soil conditions. Post grouting did not lead to any improvement in the end bearing capacity of the test shaft TS4, but production shafts on the Broadway Viaduct project exhibited an average 150% increase in end bearing capacity and 36% increase in total capacity.

A groutability study indicated that the soil at TS4 may have been groutable if the design grouting pressure of 650 psi could be achieved, but the soil was likely not groutable at the actual achieved grouting pressure of 140 psi. The groutability study also indicated that permeation grouting was unlikely and compaction grouting was likely occurring at TS4. However, there was also a possible rupture of the grout tubes as indicated by measured bending strains, and forensic SPT sampling indicated a possible 2-12 in. thick grout migration towards the northeast of TS4. Despite the large grout take and inability to reach grouting pressure at TS4, the grouting pressures for the production shafts were much closer to the design pressures, giving some quality assurance in the form of verified mobilized resistances.

CHAPTER 4. WORKS CITED

American Association of State Highway and Transportation Officials (AASHTO). 1998. AASHTO LRFD Bridge Design Specification. Customary U.S. Units Second Edition.

Applied Foundation Testing (AFT). 2010. Broadway Viaduct Bridge Replacement Post Grout Report.

Akbulut, S. and A. Saglamer. 2002. Estimating the groutability of granular soils: a new approach. *Tunneling and Underground Space Technology*. Volume 17. Issue 4. Pages 371-380, ISSN 0886-7798, DOI: 10.1016/S08867798(02)0040-8.

Burwell, EB. 1958. Cement and clay grouting of foundations. Practice of the corps of engineering. ASCE, Soil Mechanics and Foundation Division, Vol 84, No. SM1 Paper 1551.

CH2MHILL. 2007. Preliminary Geotechnical Recommendations for Broadway Bridge Viaduct Improvement Project Council Bluffs, Pottawattamie County, Iowa.

Coe, J. and S. Brandenberg, 2010. P-Wave Reflection Imaging of Submerge Soil Models Using Ultrasound. *Journal of Geotechnical and Geoenvironmental Engineering, ASCE.*

Dapp, S.D., Muchard, M., and Brown, D.A., 2010. "Experiences with Base Grouted drilled Shafts in the Southeastern United States," Proc. Of 10th International Conference on Deep Foundations, Amsterdam, Netherlands.

Farouz, E., Muchard, M., and Yang, K. 2010. Evaluation of Axial Capacity of Post Grouted Drilled Shafts, *Deep Foundations and In Situ Geotechnical Testing (GSP 205), Proc. GeoShanghai 2010*, ASCE, pp. 216-223.

Fernandez, A.L.,Pando, M.A., and King, P.G. 2007. Load Test Program to Validate Model for Post Grouted Drilled Shafts, *Contemporary Issues in Deep Foundations (GSP 158), Proc. Geo-Denver 2007*, 221, 32, ASCE, DOI:10.1061/40902(221)32.

Incecik, M. and Ceren, I. 1958. Cement grouting model tests. Bulletin of The Technical University of Istanbul, 48(2): 305-317.

LoadTest. 2010. Report on Drilled Shaft Load Testing (Osterberg Method). May 2010.

Mullins, G., Dapp, S., Frederick, E. and Wagner, V., 2001. Post Grouting Drilled Shaft Tips, Phase I. Florida Department of Transportation, Report FDOT BC165 v1.

Mullins, G. and Winters, D., 2004. Post Grouting Drilled Shaft Tips, Phase II. Florida Department of Transportation, Report FDOT BC165 v2.

Mullins, G., Winters, D., and Dapp, S. 2006. Predicting End Bearing Capacity of Post-Grouted Drilled Shaft in Cohesionless Soils. *Journal of Geotechnical and Geoenvironmental Engineering, ASCE.* Volume 132. Issue 4. Pages 478-487, ISSN 1090-0241, DOI: 10.1016/(ASCE)1090-0241(2006)132:4(478).

Ruiz, M.E. and Pando, M.A. 2009. Load Transfer Mechanisms of Tip Post-Grouted Drilled Shafts in Sand, Contemporary Topics in Deep Foundations – Proc. 2009 Int. Foundation Congress and Equipment Expo, GSP No. 185, pp. 23-30, Elsevier, ISSN 08950563, DOI 10.1061/41021(335)3

CHAPTER 5. PERFORMANCE OF POST GROUTED DRILLED SHAFTS: INFLUENCE OF CONSTRUCTION LOADS AND SERVICE LOADS ON POST GROUTED DRILLED SHAFTS

A paper to be submitted for publication

Anna Nadermann, Jeramy Ashlock, Brent Phares

Introduction

The 2010 replacement of the Broadway Viaduct (US 6) in Council Bluffs, Iowa presented an opportunity for the Iowa Department of Transportation (Iowa DOT) to utilize technologies which were either entirely new or fairly new to them. The Broadway Viaduct replacement was the first project in which the Iowa DOT implemented post grouting of drilled shafts and one of only a few Iowa DOT projects which utilized light weight foam concrete fill (LFCF) in the approaches.

The proximity of the Broadway Viaduct to historic and residential buildings eliminated the use of driven piles due to the potential for negative effects of the vibration associated with driving piles. An alternative of post grouted drilled shafts was selected. Generally, the design capacity of drilled shafts is derived primarily from the side shear component and utilizes only a fraction of the available end bearing due to the large displacements required to fully mobilize the ultimate end bearing capacity. According to Mullins et al. (2006), pressure grouting (i.e. post grouting or base grouting) is a technique being used worldwide to regain a portion of this end bearing. Full scale load tests were performed at the Broadway Viaduct project to verify the estimated grouted shaft capacity while incorporating effects of local soil conditions and construction procedures.

The bridge abutments on either end of the Broadway Viaduct rested on compressible soils, and overexcavation with light weight foamed concrete fill (LFCF) was used to prevent excessive settlement at the abutments. Light weight foam concrete fill material was used to achieve a zero net loading with a goal of eliminating settlement due to the fill. Minimization of settlements also decreased the construction time by eliminating pre-compaction of the base

soil at the abutment and also decreased cost by eliminating the need for soil improvement techniques.

The relative newness of the post grouting and LFCF technologies to the Iowa DOT presented an opportunity to monitor the construction and performance of post grouting and LFCF. Both technologies were monitored during the construction of their respective bridge components as well as during subsequent bridge construction phases. The post grouted drilled shafts and the LFCF abutment were also equipped for long term monitoring. In addition to the construction and long term monitoring, the bridge is scheduled to undergo a live load test with monitoring of the drilled shaft as well as the LFCF and MSE retaining wall.

Bridge Description

The Broadway Viaduct is 1,537 ft long and is supported on 11 piers with a total of 53 post-grouted drilled shafts. The Broadway Viaduct is a key artery and critical structure in Council Bluffs as the viaduct crosses the Indian Creek Conduit, several city streets, and the Burlington Northern/Illinois Central and Union Pacific railroads.

Objectives

The focus of this document will be the construction and long term monitoring of the post grouted drilled shafts. Specifically, the loads experienced by post grouted drilled shafts during bridge construction and during service will be determined and discussed. The measured loads during construction will also be compared to the theoretical loads expected. The evolution of the load transfer both seasonally and in the long term will be discussed. Also, the load transfer and load distribution during construction and in service will be compared to the minimum verified capacity of the drilled shafts determined from the post grouting parameters.

Data Collection

Following is the instrumentation plan and a description of the load test data, construction data, and service data.

Instrumentation

A long-term monitoring system was installed on the four shafts of Pier 10, consisting of a data logger and 48 vibrating wire sensors. The data logger was a Campbell Scientific model

CR1000 and the strain gages were Geokon Model 4911 Vibrating Wire Rebar Strain Meters (referred to as sister-bars). The bridge will be monitored for a minimum of one year, though at the time of publication about eight months of long term monitoring were complete. Each of the four shafts were fitted with three levels of sister-bar gages at the top, middle, and bottom of the shafts. Each level consisted of four sister-bar gages tied to the longitudinal steel reinforcing bars and spaced equidistant around the diameter of the shaft. The instrumentation plan for the Pier 10 drilled shafts is shown in Figure 22.

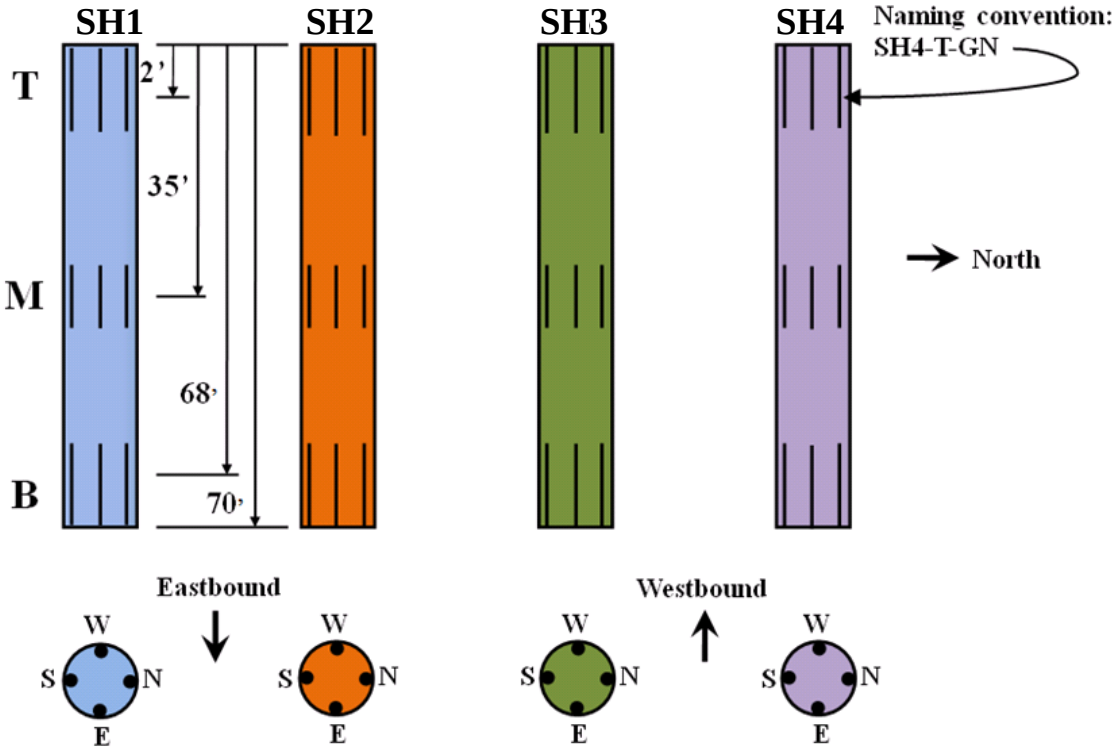

Figure 22. Pier 10 drilled shaft instrumentation plan

Figure 23 is a diagram or the gage locations for Shaft 1, the gages of Shafts 2-4 are placed in a similar manner. Following is a list of gages which were malfunctioning due to either the cable connecting the gage to the data logger being damaged or the gage itself being damaged:

- SH1-M-GN
- SH2-M-GN
- SH2-M-GS
- SH4-B-GN
- SH4-M-GN

Construction Data

The Broadway Viaduct was constructed in two phases. Phase I consisted of construction of the South half of the structure; the eastbound lanes and their supporting structure. Phase II consisted of the North half of the structure; the westbound lanes and their supporting structure. The construction data presented herein pertains almost entirely to the first stage of construction starting when Shafts 1 & 2 were constructed, through the construction of the Phase I bridge deck, as well as two construction readings taken during Phase II construction. All data recorded during construction was obtained by hand using a Geokon GK404 Readout Box.

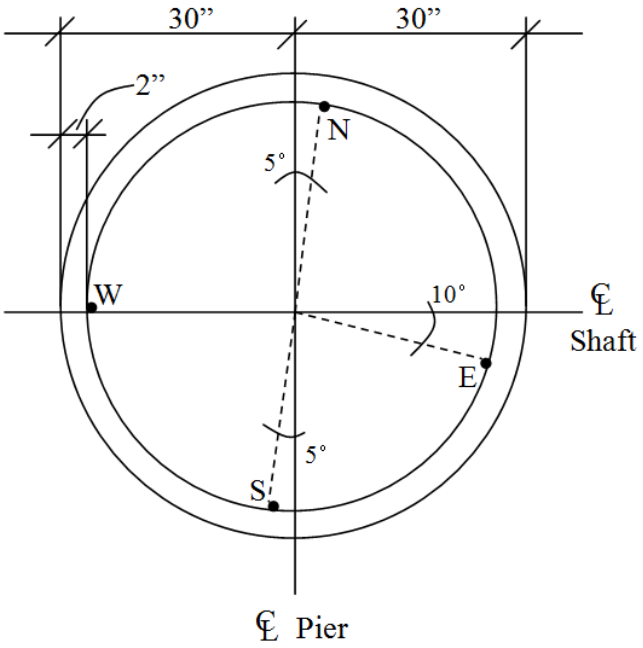

Figure 23. Plan view of instrumentation in Shaft 1

Shafts 1 and 2 were constructed on June 8 and 9, 2010, respectively. Although readings of the sister-bars were taken during construction of Shafts 1 and 2, the decision was made to disregard these readings because the concrete in the shafts was just placed and still wet. The next reading was taken on July 9, 2010 just before the column concrete was placed. At this time the shaft concrete had reached the 28 day strength and would therefore begin to act integrally with the rebar strainmeters. This reading, referred to as the Shaft concrete cured

reading, was therefore considered to be the first meaningful reference point for readings from the rebar strainmeters. Table 15 lists the dates of the readings along with the corresponding milestones in the construction of Pier 10.

Table 15. Construction Data Readings

Date	Milestone
July 9, 2010	Phase I – Shaft concrete cured (no load)
July, 21, 2010	Phase I – Column load
September 7, 2010	Phase I – Pier cap load
November 22, 2010	Phase I – Diaphragm and bridge deck load
February 22, 2011	Phase II – Miscellaneous formwork/construction equipment load (1)
April 11, 2011	Phase II – Miscellaneous formwork/construction equipment load (2)

Service Data

The service data, which includes Shafts 1-4, is referred to as the data collected after installing the CR 1000 data logger on August 17, 2011. The data logger registered a reading from each sensor every hour. The data logger was powered by a 12-volt battery charged by a solar panel mounted on the side of the bridge abutment. A faulty battery-solar panel system resulted in the data logger occasionally failing to take readings due to lack of power. The data at these times was filtered out which explains the gaps in data for the month of October 2011 and the beginning of December 2011.

Results and Discussion

Following is a discussion of the recorded data in terms of temperature, load-related strains, and load-related force. Observed bending and load-shedding behavior of the Pier 10 shafts are also discussed, and measured loads are compared to estimates of the construction loads.

Temperature

The temperature in the top level of gages is compared to the ambient temperature in Figure 24. The two sources of ambient temperature used for the comparison in Figure 24 are the Omaha, Nebraska Airport weather station (Weather Underground 2012) and the data logger installed at the bridge abutment. The Omaha, Nebraska Airport ambient temperature closely matches the data logger ambient temperature. The top gages of the Pier 10 Shafts generally follow the overall trend of the ambient temperature, although with a time-lag and little daily

variation. The lag in the top gages can be attributed to the insulation provided by the ground cover.

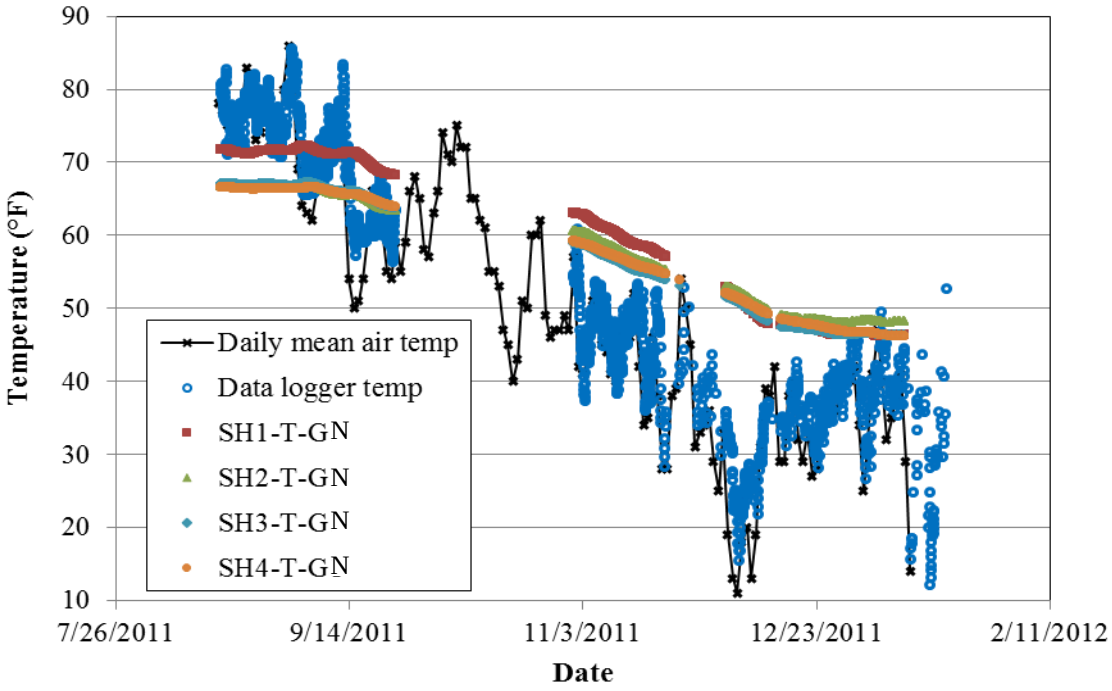

Figure 24. Comparison of ambient temperature to top of shaft temperature

The variation over time in the average temperature at each level of gages in Shaft 1 can be seen in Figure 25. The top level of gages follows a seasonal trend while the middle and bottom levels of gages remains constant at around 58°F. All four shafts follow similar trends for temperature although it should be noted that in summer months, Shaft 1 was consistently approximately 5°F warmer than the other shafts. The higher temperatures in Shaft 1 can likely be attributed to the southern sun exposure of Shaft 1, whereas the other shafts are shaded by the bridge deck.

Load Strain and Load Force

The axial load strain (note that here load strain refers to the strain caused by external loads, obtained by correcting for the concrete partially restraining the steel due to concrete's lower coefficient of thermal expansion) time history for the top, middle, and bottom level of gages of Shaft 1is shown in Figure 26. The axial load strain at each level was determined by averaging the functioning strain gages at each level. The load strain time histories for Shafts

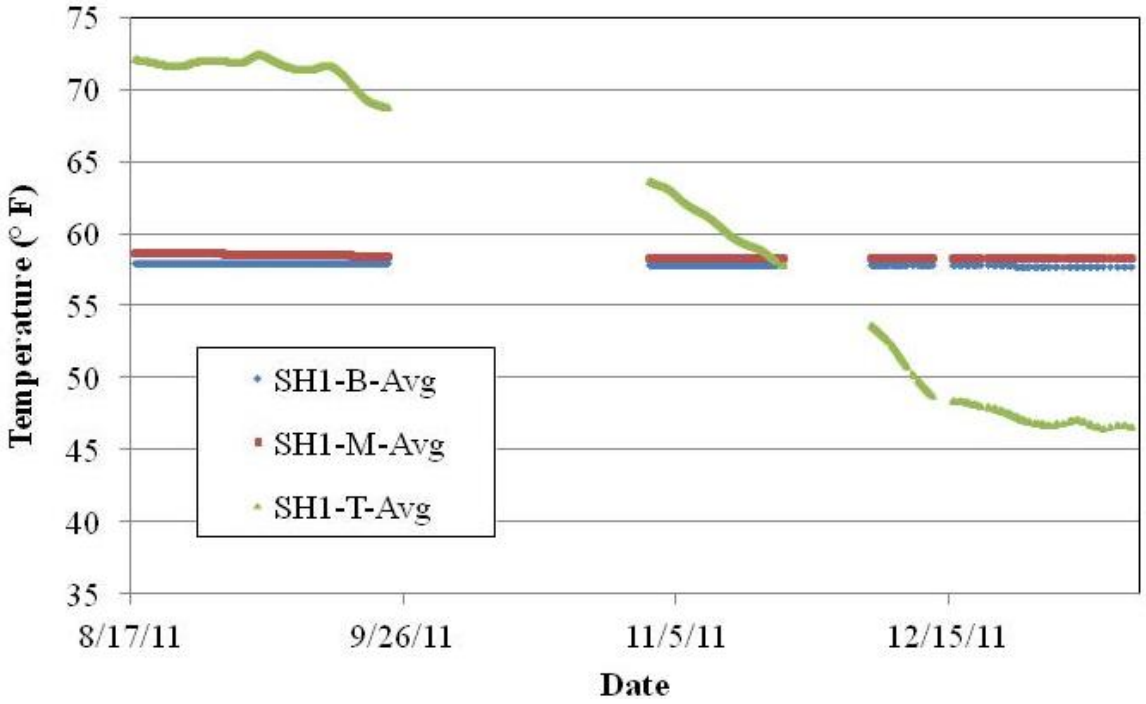

Figure 25. Variation in average temperature of bottom, middle, and top of Shaft 1

2-4 were similar to that of Shaft 1 and are therefore not shown in the interest of brevity. Figure 26 indicates that the top and middle level of gages were in compression while the bottom level of gages moved towards tension relative to the load measured on the reference data. The reduction in load, relative to the initial reading, in the bottom level of gages may be due to the grout bulb shrinking away from the base of the shaft and the soil's relaxation/consolidation. The axial strain in the top level of gages indicates a reduction in compressive load over time while the middle and bottom experience an increase in compression. Although the maximum axial load strain would be expected in the top level of gages, as the strain should dissipate with depth, Figure 26 reveals that the maximum axial load strain occurs in the middle level of gages. The top level of gages is at a distance of about two feet from the top of the drilled shaft where the overlap of reinforcing from the column steel is located. This larger steel area ratio increases the axial stiffness and therefore decreases the axial deformation near the top level of gages, compared to the middle and bottom sections of the drilled shaft.

The axial load force is a function of the axial load strain as indicated in Eq. 5.1. The axial force time history for the top, middle, and bottom level of gages of Shaft 1 is shown in Figure

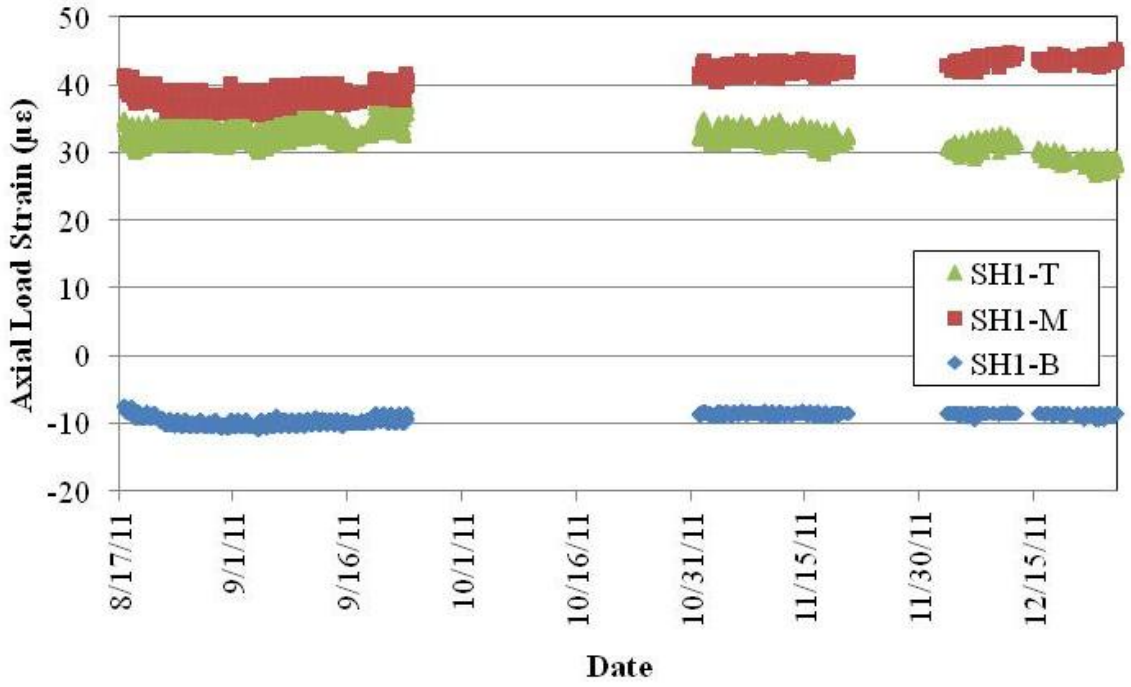

Figure 26. Time history of Shaft 1 load strain

27. The force in Shafts 2-4 are similar to that of Shaft 1 and are therefore not shown. As expected, the direction of load force and the change in load force with time is the same at each level as with load strain. However, the maximum load force does not follow the trend of the maximum load strain. The maximum load strain consistently occurred at the middle of the shafts, whereas the maximum load force alternately occurred in the top or middle of the shafts at different times. The differences in the relative trends for the top and middle of the shafts in Figures 26 and 27 can be attributed to the higher steel ratio and axial stiffness at the top, where the incremental axial force is calculates as

$$\Delta P = \Delta\varepsilon(E_s A_s + E_c A_c) \qquad 5.1$$

where $\Delta\varepsilon$ = measured incremetal strain,

A = the cross sectional area, and

E = Young's modulus

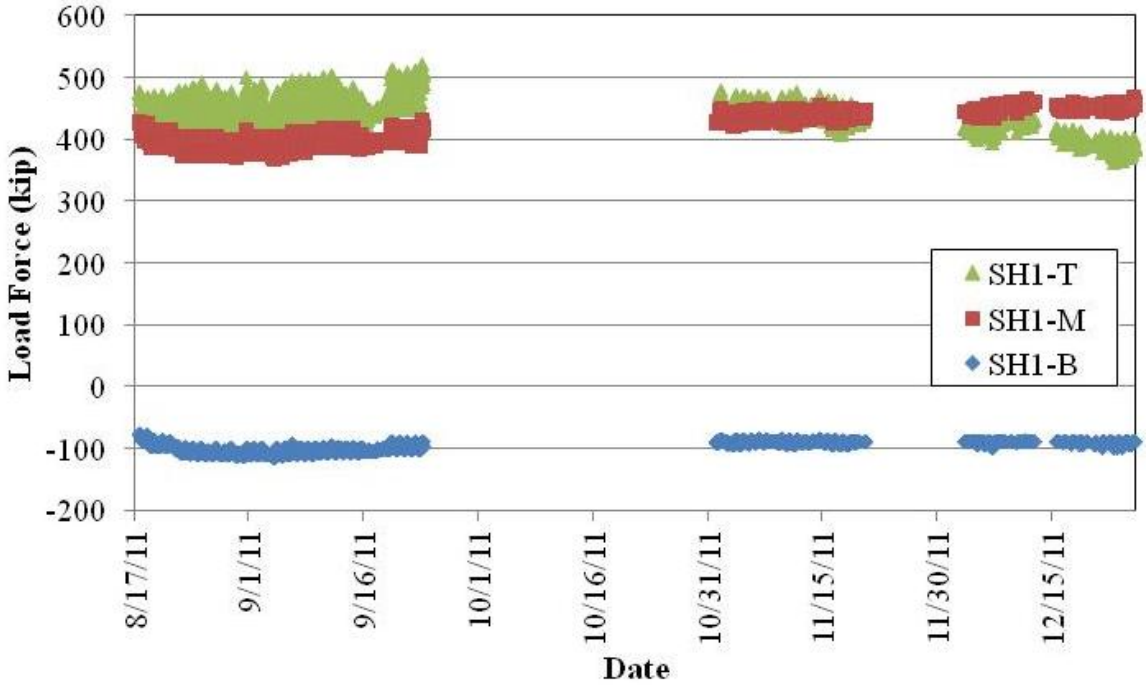

Figure 27. Time history of Shaft 1 load

Bending Strains

Although the change in magnitude of the load strain from August 2011 to December 2011 is similar for the top level East and West gages of Pier 10 drilled shafts, the direction of the changes are different. The top level East gages tend towards tension (see Figure 28), while the top level West gages trend more toward compression (see Figure 29). Figure 30 is a direct comparison of the load strain in top level East and West gages of Shaft 1. Similar plots for Shaft 2-4 reveal similar trends. The difference in load strain across the shaft indicates Shaft 1 is experiencing bending in the East-West (longitudinal) direction. The difference between the East and West load strains appear to follow a seasonal trend, as well as a daily trend similar to the temperature, implying that the bending in the top level gages is likely due to the thermal straining of the deck and girders supported by Pier 10, which is a fixed pier. The loads due to the thermal expansion and contraction of the superstructure are apparently transferred to the top of the drilled shafts through the columns.

Figures 31 and 32 are direct comparisons of the load strain in the East and West gages of Shaft 1 at the middle and bottom levels, respectively. Similar plots for Shafts 2-4 reveal

similar findings with slightly varying magnitudes of differential strains at each level. The difference in magnitude of load strain from the East to West side indicates Shaft 1 is in

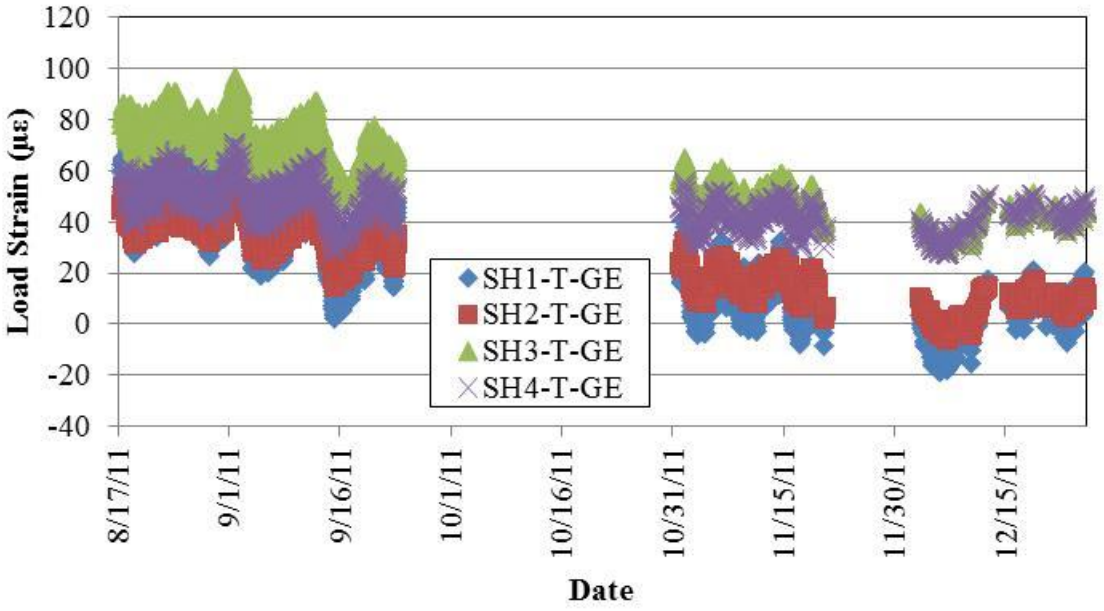

Figure 28. Time history of load strain in the East gages at the top of the shafts

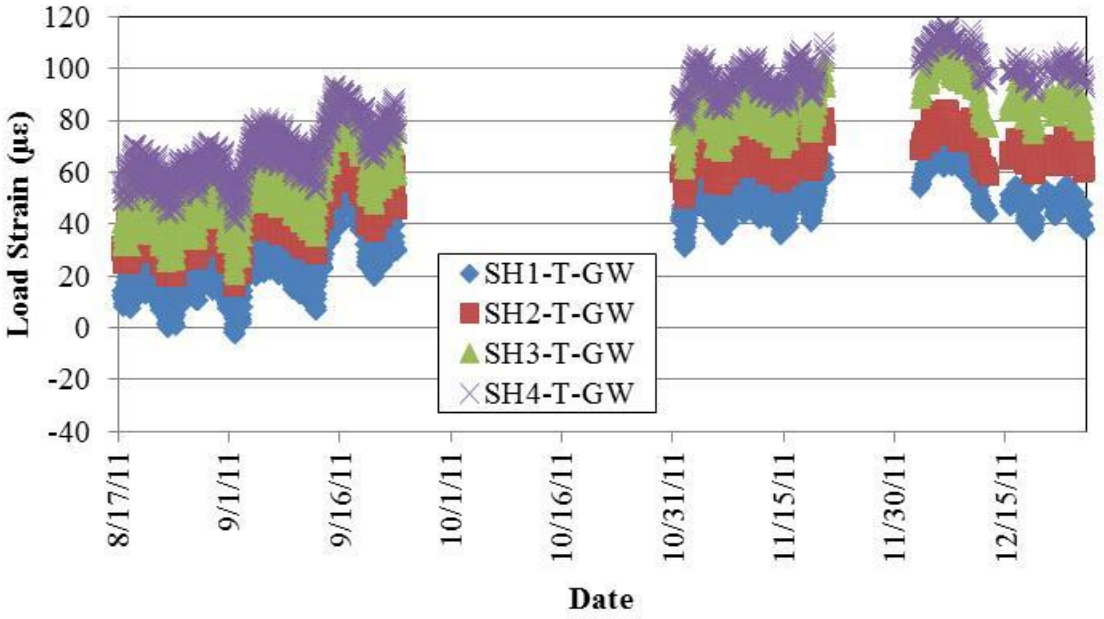

Figure 29. Time history of load strain in the West gages at the top of the shafts

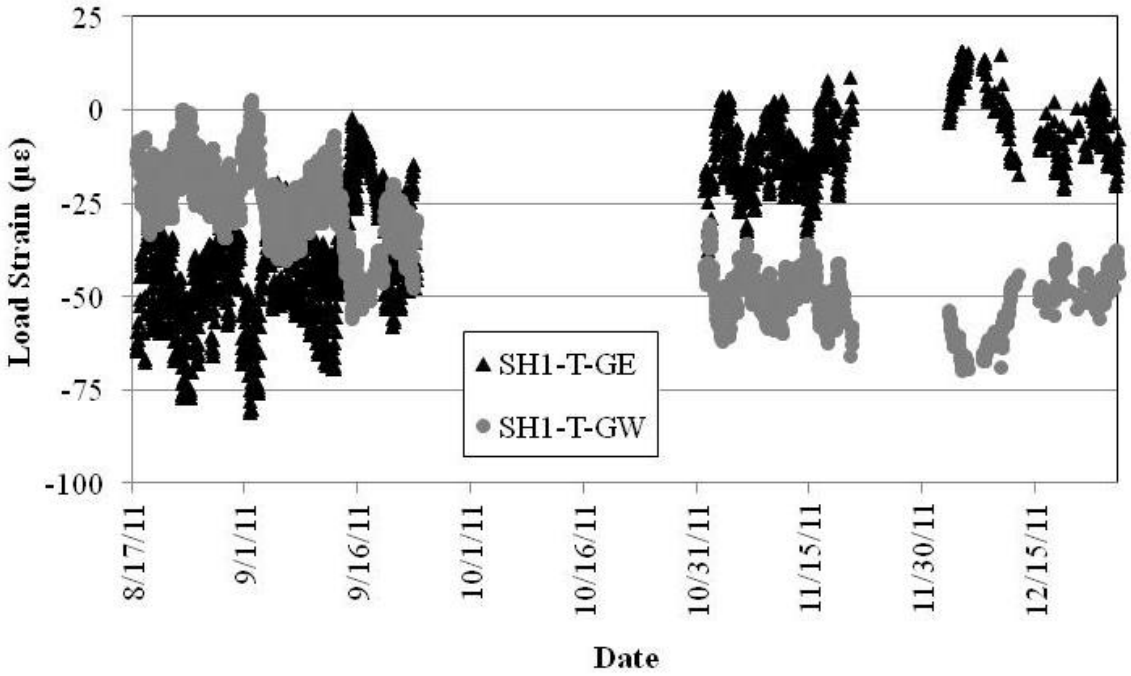

Figure 30. Load strain at the top of Shaft 1 for East and West gages, indicating bending about the North-South axis

bending at the middle and bottom levels as well, although likely not due to thermal straining of the deck and girders as for the top of the shaft as the difference in load strain across the diameter of the shaft is constant with time. The magnitude of bending, indicated by the difference in magnitude of load strain across the shaft, remains fairly constant at the middle and bottom levels of gages. The magnitude of bending is larger at the bottom of the shaft than at the middle, possible due to the grout not spreading evenly across the bottom of the shaft. The bending induced by thermal expansion and contraction of the superstructure experienced at the top level of gages in Shaft 1 dissipates before reaching the middle and bottom level of gages.

Figures 33 and 34 show that the load strain in the North and South top level gages appear to follow a slight seasonal trend. Directly comparing the load strain in the North and South gages at the top of Shaft 1 indicates that the magnitude of bending in the transverse direction of the bridge is much small than the longitudinal direction, due to the greater stiffness of the pier in the transverse direction.

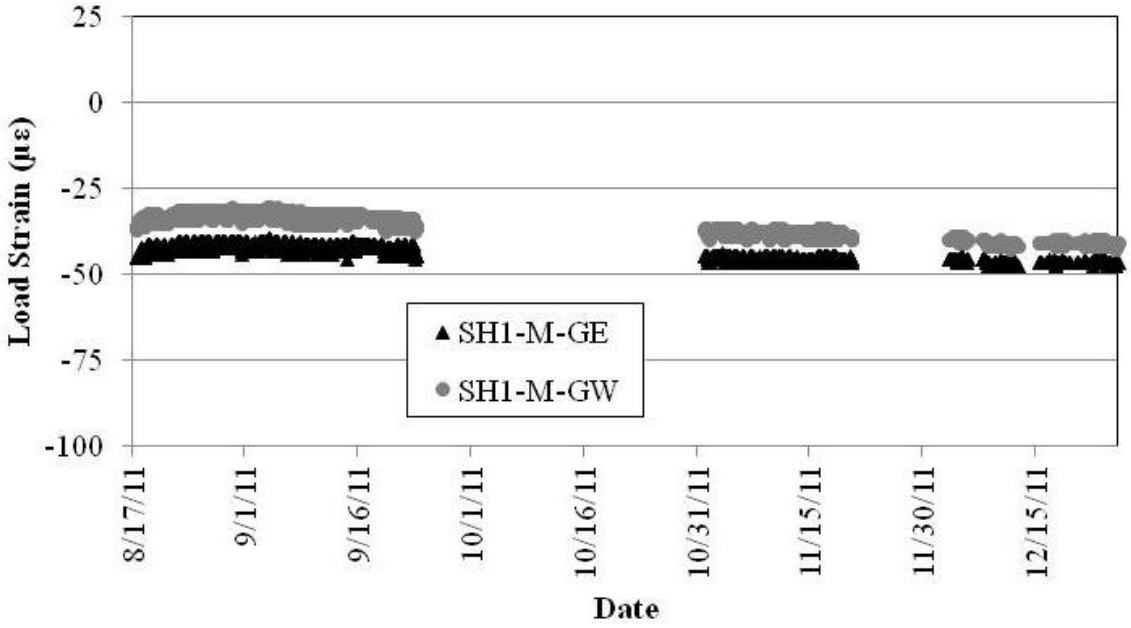

Figure 31. Load strain in the middle of Shaft 1 for East and West gages, indicating bending about the North-South axis

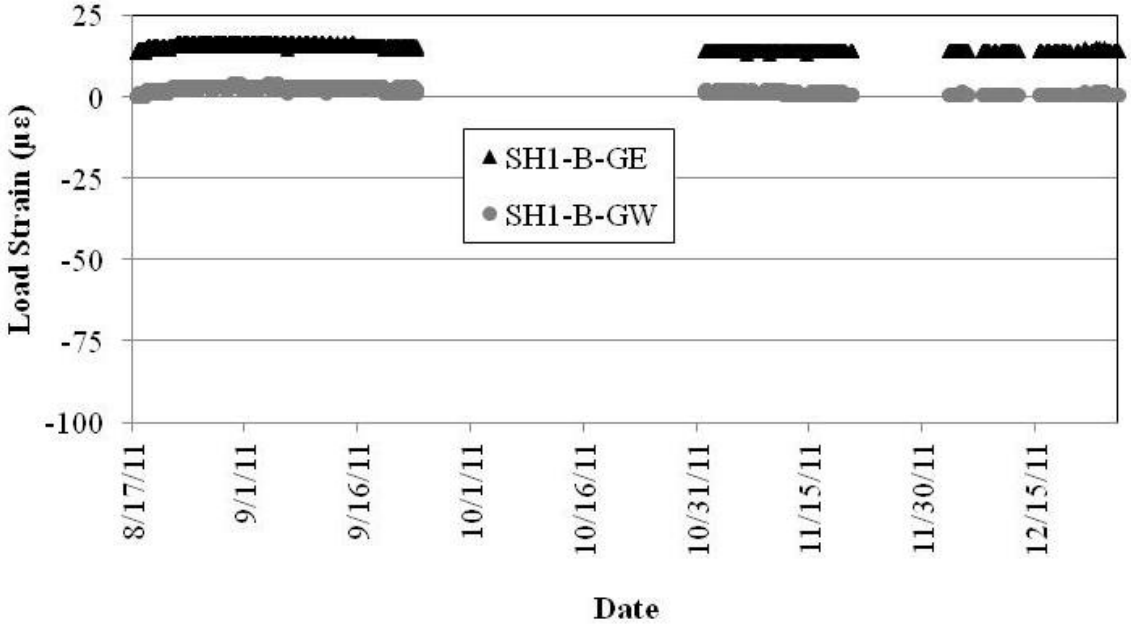

Figure 32. Load strain in the bottom of Shaft 1 for East and West gages, indicating bending about the North-South axis

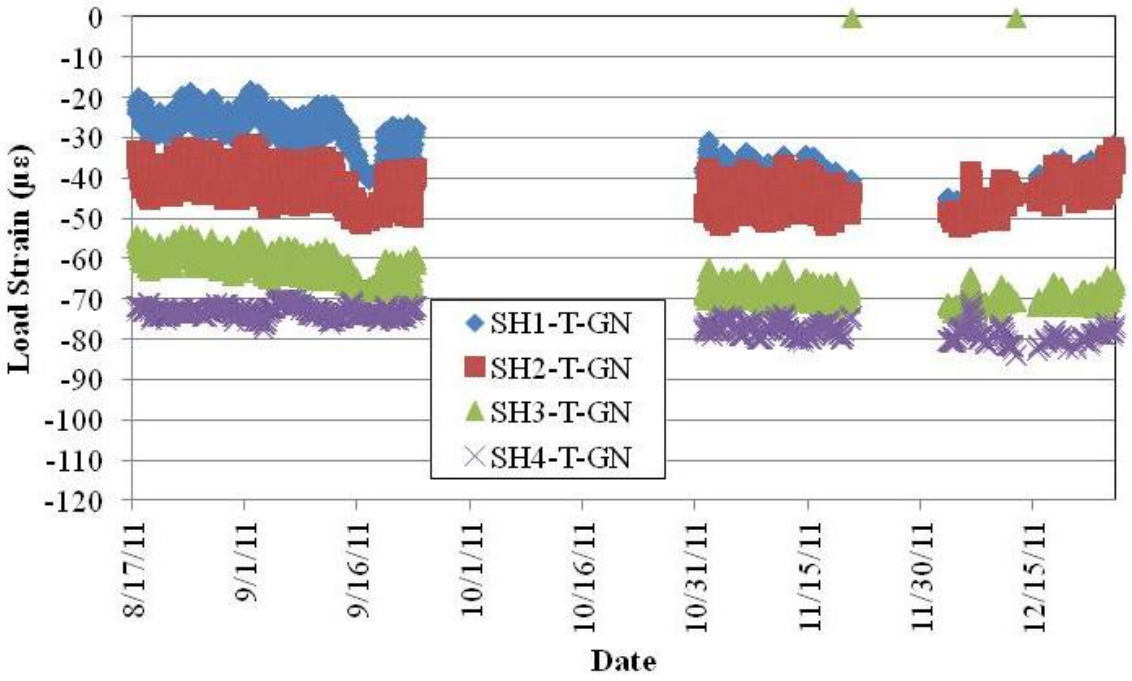

Figure 33. Time history of load strain in the North gages of the top of the shafts

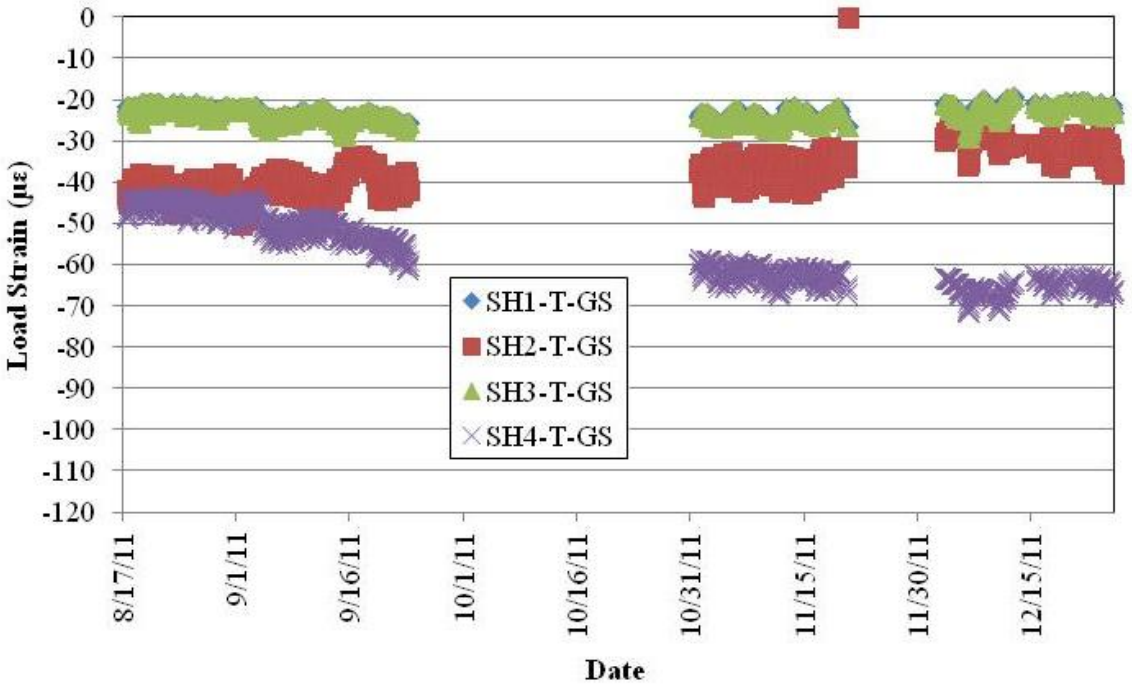

Figure 34. Time history of load strain in the South gages of the top of the shafts

Load Transfer

The axial load at each level of gages was calculated using the average of the working gages at the respective level at various points in time for Shafts 1 and 2. The variation of axial load with depth in Shaft 1 is shown in Figure 35 at each construction milestone and two points in time under the service loading. The load varies similarly with depth for Shaft 2. Figure 35 shows Shaft 1 to be mostly in compression throughout the Phase I construction of Pier 10. The Phase I – Column load reading (July 21, 2010) indicates that Shaft 1 was in tension when the columns were completed, this is likely due to the selected value of the coefficient of thermal expansion used for the concrete, as the load strain (and

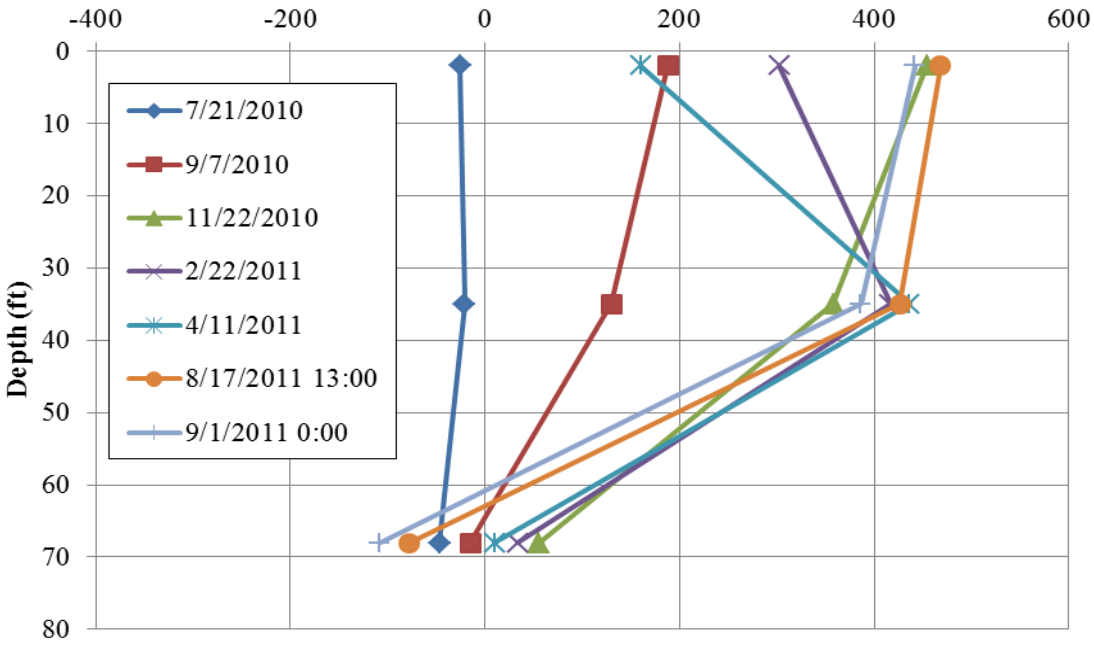

Figure 35. Force with depth for Shaft 1 during construction and service

therefore the load) is highly sensitive to the selection of the coefficient of thermal expansion. The negative force readings at the bottom of the shaft may indicate that the grot bulb is shrinking or the soil relaxing relative to the reference date fo July 9, 2010 (see Table 15). Shaft 1 was poured on June 8, 2010 and post-grouted on June 16, 23 day prior to the reference date. The axial load dissipates with depth as expected at all points in time except at the Cage Setting of Shafts 3 and 4 (February 22, 2011) and the Abutment LFCF pour (April 11, 2011) where the axial load increases from the top to middle level and decreases from the middle to bottom level. At the time of the Cage Setting of Shafts 3 and 4 the respective

excavations were open which may have impacted the loads seen by Shafts 1 and 2. At the time of the Abutment LFCF pour, the Phase II pier cap had been completed but the diaphragm, girders, and bridge deck had not yet been constructed. However, the Phase II pier cap was joined to the Phase I pier cap, and therefore would have influenced the loads on Shafts 1 and 2.

In addition to increasing the axial capacity of drilled shafts, post grouting can be used to verify the lower bound end bearing and side shear capacities of drilled shafts using the achieved grouting pressure and for the specified upward displacement. The shaft tip area of 19.64 ft^2 was multiplied by the maximum achieved grouting pressure to calculate the verified end bearing capacity. The difference of the resulting force at the tip and the shaft buoyant weight was divided by the shaft perimeter area to obtain the verified side shear capacity. Table 16 compares Pier 10 drilled shaft capacities calculated using this procedure to the maximum axial load experienced by the shafts. The Pier 10 drilled shafts have the same

Table 16. Comparison of Axial Service/Construction Load to Verified Drilled Shaft Capacity

Pier 10 Shaft	Maximum Achieved Grouting Pressure (psi)	Verified Capacity			Maximum Axial Service Load (kip)
		Side Shear (kip)	End Bearing (kip)	Total (kip)	
Shaft 1	653	1706	1846	3552	510
Shaft 2*	-	-	-	-	606
Shaft 3	420	1047	1188	2235	823
Shaft 4	460	1160	1301	2461	1002

*Grouting record not available

dimensions and therefore the verified side shear, end bearing, and total capacities are directly proportional to the maximum achieved grouting pressure. The maximum axial service load increase from 510 kips at Shaft 1 to 1002 kips at Shaft 4; this is likely due to the pedestrian walkway located on the North side (Shaft 4 side) of the bridge deck which tends to create a larger compressive force on the North side of the bridge than the South side of the bridge. Because Shaft 1 achieved the highest maximum grouting pressure and supports the smallest axial service load, it has the largest factor of safety of nearly seven on axial service load in

the reported time period. Conversely, Shaft 4 has the smallest factor of safety of about 2.5 on axial service load in the reported time period.

Construction Loads

As a means of comparing the loads for which a bridge foundation is designed to those actually imposed during construction, the monitoring system was treated as a scale to measure the axial load in the top of Shafts 1 and 2. A comparison of the Shaft 1 and Shaft 2 measured theoretical load during construction can be seen in Figures 36 and 37. The first step in determining the theoretical loads on the Pier 10 foundation system was to calculate the weight of each component of the bridge that was supported by Pier 10 during the first stage of construction.

The weight of each component was determined by multiplying the volume of the component by the weight of reinforced concrete, assumed to be 150 pounds per cubic foot. At the time of the Phase I Column load reading, the only load on the shafts was that of their respective columns. Each column was centered on a drilled shaft, therefore the theoretical load on each shaft was taken as the weight of the respective column. At the time of the Phase I Pier cap loading reading, the columns were connected by the pier cap, but the system was not symmetric. Therefore, the load on each shaft was determined by summing moments about the base of each column. The Phase I Diaphragm and bridge deck load reading was taken after the diaphragm was poured, the girders were placed, and the bridge deck was poured. The weight of the diaphragm was considered a uniformly distributed load applied directly to the pier cap. The weight of the bridge deck was first distributed to the girders and weight of the bridge deck and the self-weight of the girders were considered to be supported equally by Pier 10 and either Pier 9 or Pier 11 for the West or East span, respectively. Similar to the column-pier cap system, the column-pier cap-diaphragm-girder-bridge deck system was not symmetrical, therefore the load on each shaft was calculated using the summation of moments about the base of each column. It should be noted that the following components were not considered in determining the theoretical loads due to the lack of information about the loads;

- Steel and wood form-work and partial diaphragm reinforcing at the time of the Phase I Pier cap load reading,

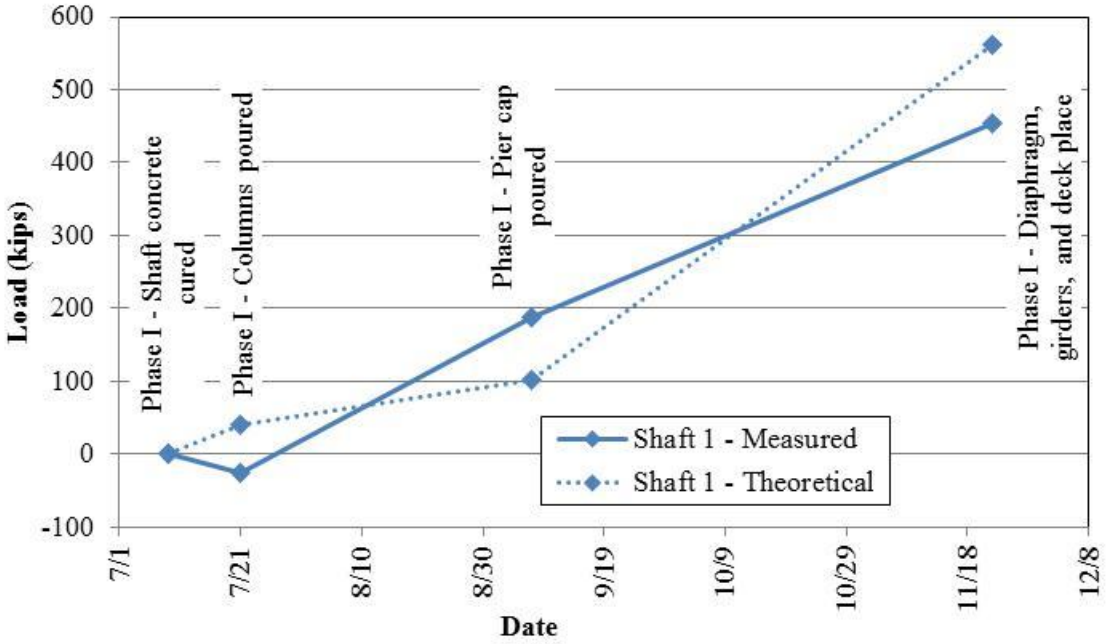

Figure 36. Comparison of Shaft 1 measured and theoretical load

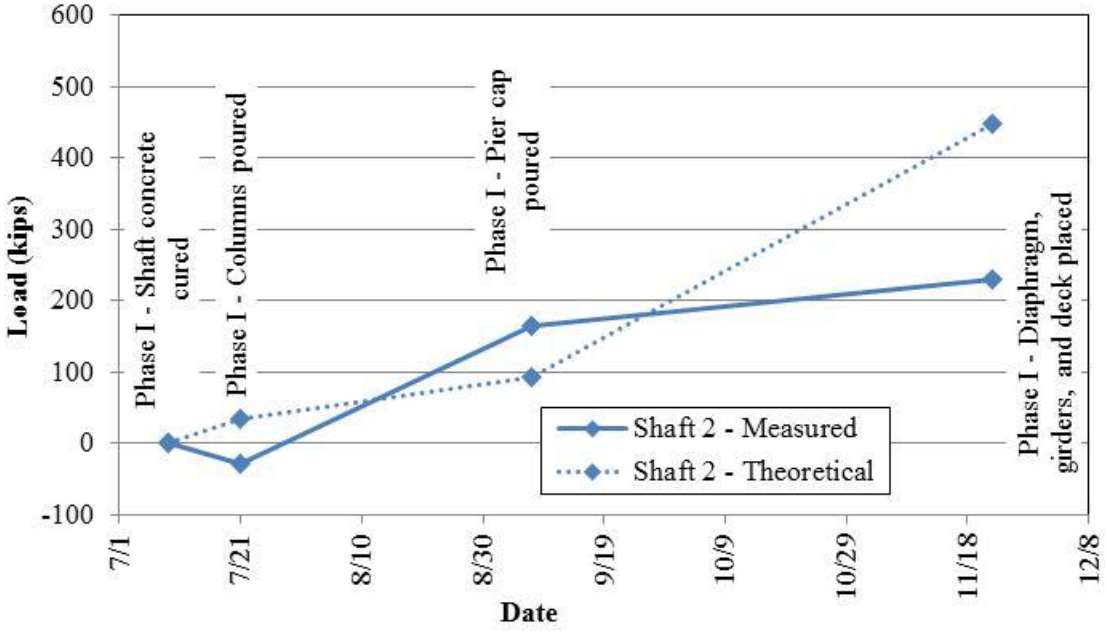

Figure 37. Comparison of Shaft 2 measured and theoretical load

- scaffolding attached to the South side of the Phase I bridge deck at the time of the Phase I Diaphragm and bridge deck load reading,
- metal light posts installed along the South side of the Phase I bridge deck at the time of the Phase I Diaphragm and bridge deck load reading, and
- minimal construction equipment and materials supported by the Phase I bridge deck at the time of the Phase I Diaphragm and bridge deck load reading.

The difference between measured and theoretical forces for Shafts 1 and 2 are listed in Table 17. The apparent tension in the measured axial force at the time of the column loads is likely due to the selection of the coefficient of thermal expansion as discussed previously, this may also in part explain the difference in the measured and theoretical load at all readings. The underestimate of approximately 85.1 kips and 71.7 kips in the loads in

Table 17. Difference in Measured and Theoretical Construction Loads

Date	Milestone	Measured – Theoretical (kip)	
		Shaft 1	Shaft 2
July 9, 2010	Phase I – Shaft concrete cured (no load)	0	0
July, 21, 2010	Phase I – Column load	-65.0	-63.4
September 7, 2010	Phase I – Pier cap load	85.1	71.7
November 22, 2010	Phase I – Diaphragm and bridge deck load	-107.0	-217.6

Shafts 1 and 2, respectively, at the time of the column construction reading can also be partially explained by the exclusion of the weight of steel and wood form work and a portion of the diaphragm reinforcing in the theoretical load due to a lack of information about the weights. The difference in the measured and theoretical load was similar for Shafts 1 and 2 at the time of the column construction and pier-cap construction readings, although this was not the case for the Phase I Diaphragm and bridge deck load reading. On the final comparison of the measured and theoretical load, the difference in Shaft 2 is more than twice the difference in Shaft 1. This difference can be partially attributed to the steel light posts installed along the South side of the Phase I bridge deck (the Shaft 1 side). The added weight on the South side of the Phase I bridge deck would be resisted by differential loads in the foundation system. The overturning moment due to the added weight of the steel light masts would

result in a compressive load in Shaft 1 and a tensile load in Shaft 2. Adding the overturning moment due to the added weight of the steel light masts to the rest of the weight supported by Shafts 1 and 2 would effectively result in a smaller compressive load in Shaft 2 as compared to Shaft 1. Other factors which contributed to the difference in measured and theoretical load include the estimation of the weight of concrete and the absence of an as-built plan set to estimate the volume of each bridge component.

The maximum construction axial load applied to the top of Shafts 1 and 2 was 454 kips and 230 kips, respectively, for both Phase I Diaphragm and bridge deck load readings measurements. The larger compressive force on Shaft 1 can be attributed to the steel light masts on the South side (Shaft 1 side) of the bridge. The maximum construction axial loads were 89% and 38% of the measured maximum service axial loads for Shafts 1 and 2, respectively.

Conclusions and Recommendations

Conclusions

As expected, the axial strain and axial load at the top of the shafts followed a seasonal trend while dissipating with depth. The seasonal trend of the axial strain and force can be attributed to the thermal expansion and contraction of the superstructure relative to the Pier 10 drilled shafts. The axial strain and force indicate that thes tip of post grouted drilled shafts may experience a reduction in compressive force, due to the grout bulb shrinking away from the tip of the drilled shaft.

Similar to the axial strain and force, bending about the centerline of Pier 10 (longitudinal bending), at the top of the shafts follows a seasonal trend as the top of the shaft is pushed and pulled by the thermal expansion and contraction of the superstructure. The bending in the Pier 10 drilled shafts dissipates with depth and there is minimal bending in the transverse direction. The base of some of the drilled shafts experienced small amounts of bending at the tip which is likely due to an uneven grout bulb forming at the tip of the drilled shaft.

The dissipation of load with depth did not appear to be influenced greatly by the post grouting with the exception of the tip of the drilled shaft being in tension. The rate at which the load dissipated with depth seemed only to be affected by the stiffness of the drilled shaft and the construction sequence.

Recommendations

Based on the conclusions drawn from the data presented herein, the following recommendations for current practice and future studies should be considered when designing and constructing post grouted drilled shafts:

- Long-term performance monitoring should be considered for post grouted drilled shafts with a goal of further understanding the bending forces and load transfer with time at the tip of post-grouted drilled shafts.
- For improved understanding of these types of forces, pressure transducers should be installed in conjunction with the post grouting apparatus to monitor the distribution of grout pressure at the tip and a sufficient number of gage levels should be used to determine the extent of the tensile reading axial forces.
- To gain a better understanding of the true magnitude of tip forces, shaft strains should be measured prior to and during post-grouting. Strains measured just before grouting should then be taken as the reference condition. As post-grouting on this project was performed within 8 to 10 days of pouring the shaft concrete, the validity of the vibrating wire sister bar strain gage measurements at such early stages of concrete curing should be studied.

CHAPTER 5. WORKS CITED

Mullins, G., Winters, D., and Dapp, S. 2006. Predicting End Bearing Capacity of Post-Grouted Drilled Shaft in Cohesionless Soils. *Journal of Geotechnical and Geoenvironmental Engineering, ASCE.* Volume 132. Issue 4. Pages 478-487, ISSN 1090-0241, DOI: 10.1016/(ASCE)1090-0241(2006)132:4(478).

CHAPTER 6. CONCLUSIONS & RECOMMENDATIONS

This chapter presents an overview of the technical merit and/or scientific value gained from these studies and recommendations based on these conclusions. The conclusions and recommendations are grouped into two categories; (1) those associated with integral abutment bridges and (2) those associated with post grouted drilled shafts.

APPROACH SLABS INTEGRAL WITH INTEGRAL ABUTMENT BRIDGES

The conclusions and recommendations in this section are drawn directly from the research presented in Chapter 3, based on the instrumentation and year-long monitoring of two integral abutment (I-A) bridges with precast approach slabs:

- The integral connection between the approach slabs and the bridge appear to function well with no observed distress and little relative longitudinal movement.
- The measured strains in the approach slabs indicate that a significant force exists at the expansion joint. This force approached a range of approximately 200 kips/ft.
- Notable frictional forces exist at the bottom of the approach slab.
- The minor visible distress could not be attributed to the fact that the approach slab is integrally connected to the bridge.

The following recommendations for current practice and future studies, which are based on the study of approach slabs tied to integral abutment bridges, should be considered when designing and constructing I-A bridges:

- Prevention of the “bump at the end of the bridge” should be considered a design goal for approach slabs.
- The force which develops at the expansion joint should be taken into consideration when designing both the approach slab and the bridge. A more robust abutment may transfer less of the expansion/contraction force to the approach slab and more to the abutment foundation, resulting in less force at the expansion joint. A second alternative would be to reduce or even eliminate the interaction of the abutment and soil with the use of a mechanically stabilized earth wall placed between the abutment and earth fill.

- The frictional interaction with the supporting soil should be taken into consideration during the design process.
- As good engineering practice dictates, these recommendations should undergo a comprehensive testing program and be validated with further studies. Future studies should also ensure that approach slabs are instrumented throughout their entire width in order to determine if a gradient exists in the forces across the slab.

POST GROUTED DRILLED SHAFTS

The conclusions and recommendations in this section are drawn directly from the research presented in Chapters 4 and 5. The following conclusions were drawn from the test shaft program and long-term monitoring of production post-grouted drilled shafts:

- Post grouting of drilled shafts can be used to verify a minimum capacity of drilled shafts as limited by the uplift criteria for post grouting.
- Improvement of drilled shaft end bearing resistance by post-grouting, is sensitive to the soil conditions. Soil with high fines content can be difficult to grout and the presence of a gravel seam near the tip of a drilled shaft can create an alternate path for the grout, rather than forming a bulb at the base of the shaft.
- Post grouting of the production shafts correlated to an average increase of 150 % in end bearing capacity and an average increase of 36% in total capacity.
- The groutability of soil is dependent on the achievement of a minimum grouting pressure. The test shaft did not achieve a sufficient grouting pressure to experience improved capacity. Although not all production shafts reached their design grouting pressure, they did achieve sufficient grouting pressure to improve their end bearing capacity.
- Long-term monitoring of the post-grouted drilled shafts revealed a reduction in end-bearing experienced at the base of the shafts. These reductions in end-bearing may be due to the grout bulb shrinking away from the tip of the shaft.
- The bending strains at the tip of the drilled shafts were not present in all shafts and were small in comparison to the bending strains and forces at the top of the shafts;

therefore the bending strains at the tip of the post-grouted drilled shafts may be due to an uneven grout bulb forming at the tip of the drilled shaft.

The following recommendations for current practice and future studies should be considered when designing and constructing post-grouted drilled shafts:

- Due to the uncertainty with subsurface work, the decision to utilize post grouting to increase drilled shaft capacity should be approached with caution and should be accompanied by a test shaft program. It is also recommended that a groutability study be completed on the soil in which a post-grouted drilled shaft will be tipped.
- Long-term performance monitoring should be considered for post-grouted drilled shafts with a goal of further understanding the bending strains and end-bearing at the tip. To achieve further understanding of these types of forces, pressure plates should be installed in conjunction with the post grouting apparatus to monitor the distribution of grout pressure and end-bearing stresses at the tip and a sufficient number of gage levels should be used to determine the distribution of axial forces.
- As good engineering practice dictates, these recommendations should undergo a comprehensive testing program and be validated with further studies.

SUMMARY OF CONCLUSIONS

The goals of this research, as stated in the introduction, were:

- Mediate the bump at the end of the bridge.
- Validate the use of post grouting to increase drilled shaft capacity.

Although this research did not fully mediate the bump at the end of the bridge, the findings of this research did reveal forces in the approach slabs of I-A bridges with connected approach slabs which should be considered in future design and construction of these bridges. Consideration of these forces in the design and construction of precast approach slabs which are integrally connected to integral abutment bridges could potentially lead to reduced maintenance costs associated with the bump at the end of the bridge. This research did validate that post grouting can be used to increase drilled shaft capacity, though the technique should be approached with caution and engineering judgment should be exercised. Increasing the end bearing resistance of drilled shafts through the use of post grouting can effectively

allow drilled shafts to be shortened without losing capacity or exceeding service displacement criteria, potentially leading to reduced costs for drilled shafts.

WORKS CITED

Akbulut, S. and A. Saglamer. 2002. Estimating the groutability of granular soils: a new approach. *Tunneling and Underground Space Technology*. Volume 17. Issue 4. Pages 371-380, ISSN 0886-7798, DOI: 10.1016/S08867798(02)0040-8.

American Association of State Highway and Transportation Officials (AASHTO). 1998. AASHTO LRFD Bridge Design Specification. Customary U.S. Units Second Edition.

Applied Foundation Testing (AFT). 2010. Broadway Viaduct Bridge Replacement Post Grout Report.

Bigelow, J., Faris, A., Greimann, L., Phares, B. 2008. Instrumentation and Monitoring of Integral Bridge Abutment-to-Approach Slab Connection. IHRB Projects TR-530 & TR-539, Iowa DOT Projects 05-197 & 05-219. Ames, IA, Institute for Transportation.

Burwell, EB. 1958. Cement and clay grouting of foundations. Practice of the corps of engineering. ASCE, Soil Mechanics and Foundation Division, Vol 84, No. SM1 Paper 1551.

CH2MHILL. 2007. Preliminary Geotechnical Recommendations for Broadway Bridge Viaduct Improvement Project Council Bluffs, Pottawattamie County, Iowa.

Coe, J. and S. Brandenberg, 2010. P-Wave Reflection Imaging of Submerge Soil Models Using Ultrasound. *Journal of Geotechnical and Geoenvironmental Engineering, ASCE.*

Dapp, S.D., Muchard, M., and Brown, D.A., 2010. "Experiences with Base Grouted drilled Shafts in the Southeastern United States," Proc. Of 10th International Conference on Deep Foundations, Amsterdam, Netherlands.

Farouz, E., Muchard, M., and Yang, K. (2010). Evaluation of Axial Capacity of Post Grouted Drilled Shafts, *Deep Foundations and In Situ Geotechnical Testing (GSP 205), Proc. GeoShanghai 2010*, ASCE, pp. 216-223.

Fernandez, A.L.,Pando, M.A., and King, P.G. (2007). Load Test Program to Validate Model for Post Grouted Drilled Shafts, *Contemporary Issues in Deep Foundations (GSP 158), Proc. Geo-Denver 2007*, 221, 32, ASCE, DOI:10.1061/40902(221)32.

Horvath, J. 2000. Integral-Abutment Bridges: Problems and Innovative Solutions Using EPS Geofoam and Other Geosynthetics. Manhattan College Research Report No. CE/GE-00-2. Bronx, New York.

Incecik, M. and Ceren, I. 1958. Cement grouting model tests. Bulletin of The Technical University of Istanbul, 48(2): 305-317.

Kunin, J., Alampalli, S. 1999. Integral Abutment Bridges: Current Practice in the United States and Canada. Transportation research and Development Bureau, New York State Department of Transportation. Federal Highway Administration (FHWA) Special Report 132.

Lenke, L. 2006. Settlement Issues – Bridge Approach Slabs (Final Report Phase 1). Transportation Engineering Research Program (TERP). Albuquerque, NM. Department of Civil Engineering.

LoadTest. 2010. Report on Drilled Shaft Load Testing (Osterberg Method) for Broadway Viaduct. May 2010.

Mistry, V.. 2005. Integral Abutment and Jointless Bridges. Federal Highway Administration (FHWA) Conference.

Mullins, G., Dapp, S., Frederick, E. and Wagner, V., 2001. Post Grouting Drilled Shaft Tips, Phase I. Florida Department of Transportation, Report FDOT BC165 v1.

Mullins, G. and Winters, D., 2004. Post Grouting Drilled Shaft Tips, Phase II. Florida Department of Transportation, Report FDOT BC165 v2.

Mullins, G., Winters, D., and Dapp, S. 2006. Predicting End Bearing Capacity of Post-Grouted Drilled Shaft in Cohesionless Soils. *Journal of Geotechnical and Geoenvironmental Engineering, ASCE.* Volume 132. Issue 4. Pages 478-487, ISSN 1090-0241, DOI: 10.1016/(ASCE)1090-0241(2006)132:4(478).

O'Neill, M.W. and Hassan, K.M., 1994. "Drilled Shafts: Effects of Construction on Performance and Design Criteria." Proceedings of the International Conference on Design and Construction of Deep Foundations, December 1994, Vol. 1, pp. 137-187.

Ruiz, M.E. and Pando, M.A. 2009. Load Transfer Mechanisms of Tip Post-Grouted Drilled Shafts in Sand, Contemporary Topics in Deep Foundations – Proc. 2009 Int. Foundation Congress and Equipment Expo, GSP No. 185, pp. 23-30, Elsevier, ISSN 08950563, DOI 10.1061/41021(335)3